

HIGH PRESSURE STATES IN CONDENSED MATTER:

- I. HIGH PRESSURE BEHAVIOR OF THE IRON-SULFUR SYSTEM WITH APPLICATIONS TO THE EARTH'S CORE
- II. EMPIRICAL EQUATION OF STATE FOR ORGANIC COMPOUNDS AT HIGH PRESSURES

Thesis by

William Wyatt Anderson

In Partial Fulfillment of the Requirements

for the Degree of

Doctor of Philosophy

California Institute of Technology

Pasadena, California

1990

(Submitted May 21, 1990)

## Acknowledgements.

This thesis represents the culmination of a long and busy educational career. To claim, however, that I have achieved this point by my own devices alone would be a great disservice to those who have supported, helped, cajoled, and inspired me in my search for knowledge.

It is difficult to know where to begin. Perhaps I should start with those whom I have come to know here at Caltech. I must thank my office mates, Bruce Betts and Mark Hofstadter (or is that Hoff?) for helping make occasional preemptive strikes on insanity, encountering Chuckwallas, Geckoes, and all sorts of other beasts along the way, and Walter Kiefer, who has suffered through this madness. Never was there (or, if the Earth is lucky, will there be) another office with quite the same level of volatility and hair-trigger reflex as ours.

The many other "planetoids" whom I have come to know are deserving of appreciation for participation in Bill Dinners and sticking together through all the miseries inflicted on the life of a graduate student at Caltech. To those who have gone ahead—Mike Summers, John Lunine, Dave Paige, Randy Kirk, Greg Ojakangas, Carol Polanskey, Ken Herkenhoff, Don Rudy, and Tim Dowling—congratulations on achieving escape velocity and thanks for the good times, advice, and encouragement. To those whom I will leave behind when I depart for the Real World—Rich (#1), Michelle, Don, Julie, Kathy, Joel, Bryan, Tomas, Laszlo, Steve, Rich (#2), Mark, Bruce, Kim, Toshiko, Elizabeth, Alden, David, Janusz, Stuart (#1), and Stuart (#2)—hang in there. Graduate school really is a survivable experience.

Special mention must go my fellow rock and mineral torture specialists, past and present: Phil Ihinger, Carol, Cathy Smither, Bob

Svendsen, Doug Schmitt, Greg Miller, Linda Rowan, and Tom Duffy. Sticking together and sharing ideas, advice, and general support has been a great help. However, none of us in the Experimental Geophysics Group could have done it without the capable help and guidance provided by Mike Long and Papo Gelle in the shock wave lab, and Sue Yamada, who somehow manages to keep the EGG from cracking and falling apart. You three have given invaluable moral support, as well as keeping everything running smoothly and efficiently.

To the faculty in the Division of Geological and Planetary Sciences: thanks for inspiring us to think big and test our limits. It's not hard to see why Caltech is tops in these fields. (It's also not hard to understand the statement made by Professor Stearns at Vanderbilt: "So you're going to the pressure cooker, eh?") Dr. Stevenson's insistence on the importance of PHYSICS has led to a new way of looking at many phenomena, while the Meteor Crater trips led by Dr. Shoemaker and Project Pahoehoe (complete with the demise of Philihuhu Paio) led by Dr. Sharp have provided much-needed opportunities to get out into the field, stretch my legs and do a little geology. My advisor in the production of this thesis, Dr. Ahrens, has put such a marvelous lab at the disposal of the students. We don't always see eye to eye on things, but working for Dr. Ahrens has given me a rich experience base from which to launch out on my own.

There are also some very special people whom I knew long before my association with Caltech and from whom I have continued to receive inspiration, guidance, and support. These include my professors at Vanderbilt and David Lipscomb. Professors Reesman and Stearns at Vanderbilt encouraged me to continue on to a Ph.D. and have kept in

touch and continued to show interest in my progress. They deserve special recognition for showing me just how low the stress level can be in advisor-advisee relations. Professors Langford, Johnston, Butler, and Srygley at Lipscomb gave me a foundation upon which to build my graduate education in the sciences and have shown me support throughout the duration of my college career. Mr. Chamberlain and Mr. Sullivan, at David Lipscomb High School, gave me a unique high school science experience which is as much responsible for my continued striving for greater achievement as anything else.

I've saved the best for last. An education is so much more than just classes and lab work. Some people have given me a complete education in itself—not the formal kind, but perhaps even more important. My wife, Toni, has given me the very best she has had to offer—her love, support, and comfort when the outlook seemed so bleak. Without her, I could not have done it. And, to what I'm convinced is the best family in the world: Mom, Dad, Jean, David; you gave me that early spark of fascination with and inquisitiveness about the things around me. And Jeff, Irene, and John Doss and Maggie Perry have given me some of my fondest memories to bolster me through difficult times. I wish that I could repay what all of them have meant to me. Unfortunately, I cannot. Jeff and Irene have left a hard life behind. And my father, who was so proud of the achievements of all his children and was willing to make deep sacrifices for us, lost his battle against cancer last year. Even as he lay in the hospital, though, he urged me to return to Caltech and finish my work. He wanted so much to be a part of my success and he still is, even though he is not here.

## Abstract

## Part I:

The earth's core is generally accepted to be composed primarily of iron, with an admixture of other elements. Because the outer core is observed not to transmit shear waves at seismic frequencies, it is known to be liquid or primarily liquid. A new equation of state is presented for liquid iron, in the form of parameters for the 4th order Birch-Murnaghan and Mie-Grüneisen equations of state. The parameters were constrained by a set of values for numerous properties compiled from the literature. A detailed theoretical model is used to constrain the  $P$ - $T$  behavior of the heat capacity, based on recent advances in the understanding of the interatomic potentials for transition metals. At the reference pressure of  $10^5$  Pa and temperature of 1811 K (the normal melting point of Fe), the parameters are:  $\rho = 7037$  kg/m<sup>3</sup>,  $K_{S0} = 110$  GPa,  $K_S' = 4.53$ ,  $K_S'' = -.0337$  GPa<sup>-1</sup>, and  $\gamma = 2.8$ , with  $\gamma \propto \rho^{-1.17}$ . Comparison of the properties predicted by this model with the earth model PREM indicates that the outer core is 8 to 10 % less dense than pure liquid Fe at the same conditions. The inner core is also found to be 3 to 5% less dense than pure liquid Fe, supporting the idea of a partially molten inner core. The density deficit of the outer core implies that the elements dissolved in the liquid Fe are predominantly of lower atomic weight than Fe. Of the candidate light elements favored by researchers, only sulfur readily dissolves into Fe at low pressure, which means that this element was almost certainly concentrated in the core at early times. New melting data are presented for FeS and FeS<sub>2</sub> which indicate that the FeS<sub>2</sub> is the S-bearing liquidus solid phase at

inner core pressures. Consideration of the requirement that the inner core boundary be observable by seismological means and the freezing behavior of solutions leads to the possibility that the outer core may contain a significant fraction of solid material. It is found that convection in the outer core is not hindered if the solid particles are entrained in the fluid flow. This model for a core of Fe and S admits temperatures in the range 3450 K to 4200 K at the top of the core. An all liquid Fe-S outer core would require a temperature of about 4900 K at the top of the core.

## Part II.

The abundance of uses for organic compounds in the modern world results in many applications in which these materials are subjected to high pressures. This leads to the desire to be able to describe the behavior of these materials under such conditions. Unfortunately, the number of compounds is much greater than the number of experimental data available for many of the important properties. In the past, one approach that has worked well is the calculation of appropriate properties by summing the contributions from the organic functional groups making up molecules of the compounds in question. A new set of group contributions for the molar volume, volume thermal expansivity, heat capacity, and the Rao function is presented for functional groups containing C, H, and O. This set is, in most cases, limited in application to low molecular liquids. A new technique for the calculation of the pressure derivative of the bulk modulus is also presented. Comparison with data indicates that the presented technique

works very well for most low molecular hydrocarbon liquids and somewhat less well for oxygen-bearing compounds. A similar comparison of previous results for polymers indicates that the existing tabulations of group contributions for this class of materials is in need of revision. There is also evidence that the Rao function contributions for polymers and low molecular compounds are somewhat different.

## Table of Contents

Acknowledgements	ii
Abstract	v
List of figures	x
List of Tables	xiii
I. HIGH PRESSURE BEHAVIOR OF THE IRON SULFUR SYSTEM WITH APPLICATION TO THE EARTH'S CORE	xv
Chapter 1. A Liquid Iron Equation of State for Geophysical Applications	1
1. Abstract	2
2. Introduction	4
3. Determination of the Liquid Fe Equation of State	6
4. Discussion and comparison with other equations of state	31
5. Comparison with the core	49
6. Conclusion	56
7. Acknowledgements	57
8. Appendix A	58
9. Appendix B	73
9. References	78
Chapter 2. Shock Temperatures in Iron Sulfides: Experimental Constraints on Phase Relations and Speciation in the System Fe-S at High Pressures	86
1. Abstract	87
2. Introduction	89
3. Experimental Techniques	90
4. Experimental results and data analysis	100
5. Phase relations in the system iron-sulfur system	128
6. Temperature and state of the outer core	158



7. Conclusion	166
8. References	168
II. EMPIRICAL EQUATION OF STATE FOR ORGANIC COMPOUNDS AT HIGH PRESSURES	177
Abstract	178
Introduction	180
The Model	181
1. Additive functional group contributions	182
(a) Molecular weight	182
(b) Molar volume	182
(c) Thermal expansivity	192
(d) Heat capacity	197
(e) Bulk modulus and the Rao function	206
2. Calculation of high pressure states	213
3. Calculation of shock Hugoniot curves	218
4. Comparison with experimental data	219
Conclusion	226
References	234

## List of Figures.

## Part I.

## Chapter 1.

1.	Density of liquid Fe as a function of temperature at 1 bar.	11
2.	Longitudinal sound speed in liquid iron at 1 bar.	16
3.	$U_S$ - $u_P$ Hugoniot for iron.	25
4.	Specific heat at constant volume for liquid iron as a function of temperature at four different densities.	32
5.	Temperatures along the liquid phase region of the principle Hugoniot.	36
6.	$U_S$ - $u_P$ Hugoniot in the liquid regime predicted for porous iron.	39
7.	$P$ - $V$ Hugoniot for Fe.	42
8.	Estimates of the thermodynamic Grüneisen parameter of liquid iron.	44
9.	a) Sound speeds predicted by the present model and that of Jeanloz (1970). b) Volume thermal expansion coefficients from our model and that of Jeanloz (1979)	47
10.	Temperatures along the isentropes used for comparison with PREM.	50
11.	a) Densities of liquid Fe along the isentropes, compared with PREM. b) Isentropic bulk moduli of liquid Fe along the isentropes, compared with PREM.	52
A1.	Interatomic potentials for liquid iron.	66
A2.	Radial distribution function for liquid Fe.	71
B1.	Assumed geometry of a porous material for this model.	74

## Chapter 2.

1.	Diagram of a typical shock temperature experiment.	92
2.	Scanning electron micrograph of a typical crystal boundary gap in a thin film sample.	94
3.	Measured interface temperatures as a function of pressure.	102

4.	Melting and Hugoniot temperatures derived from the nonporous experiments.	116
5.	Broadband photodiode signal from a typical experiment involving a porous sample.	120
6.	Typical spectrum and fit from a porous sample experiment.	122
7.	Energy increases from ambient conditions required to melt Fe and FeS.	126
8.	(a) The Fe melting curve of Williams et al. (1987), along with the melting datum from shot 650. (b) Our melting temperatures for FeS, along with the melting curve of Williams and Jeanloz (1990). (c) Our experimental melting temperatures for FeS <sub>2</sub> .	129
9.	Liquidi for pure closest-packed transition metals melting into solution with a s,p metal.	142
10.	Best fit liquidi for melting in compound-forming transition metal - s,p metal systems.	148
11.	Isobaric phase diagrams for the Fe-S system.	151
12.	Liquidus surface for the Fe-S system.	153
13.	Metastable FeS melting curve.	156
14.	Isobaric phase diagrams for the Fe-S system at the pressures of the core-mantle boundary and inner core boundary of the earth.	159
Part II.		
1.	Comparison of experimentally determined molar volumes with volumes predicted by the present model.	187
2.	(a) Schematic of a typical intermolecular potential. (b) Form assumed for the intermolecular potential in the discussion of thermal expansion.	193
3.	Comparison of experimental results for thermal expansivities with the predictions from our results.	200
4.	Comparison of experimental heat capacities with predictions based on our results.	204
5.	Pressure-volume projections of the shock Hugoniot curves of four organic liquids.	222

6. The predicted Hugoniot curves and experimental data shown in figure 2, but now projected on the particle velocity-shock velocity plane. 224
7. Predicted Hugoniot curve for benzene, with the data from Marsh (1980) 227
8. Pressure-volume projections of the predicted shock Hugoniot curves of four polymers. 229
9. Us-up projection of the curves and data presented in figure 5. 231

## List of Tables

## Part I.

## Chapter 1.

1. References for experimental data on liquid iron.	7
2. Sound speed data for liquid iron at 1 bar.	15
3. High pressure sound speeds and Grüneisen parameters from Brown and McQueen (1986).	22
4. Data for the liquid phase portion of the nonporous iron principle Hugoniot.	28
5. Final equation of state parameters for liquid iron.	34

## Chapter 2.

1. Shock Hugoniot parameters used in this study.	99
2. Experimental conditions and measured interface temperatures and emissivities.	101
3. Parameters for the calculation of the thermodynamic Grüneisen parameter.	112
4. Melting and Hugoniot temperatures determined from the interface temperatures presented in table 2.	115
5. Melting and Hugoniot temperature determined from the interface temperatures of porous samples presented in table 2.	125
6. Equation of state parameters used to obtain $P$ - $\rho$ - $T$ relations in this study.	133
7. The systems for which liquididi are presented in figure 9.	141
8. Data used to obtain the value of $K_{eq}$ for this study.	147

## Part II.

1. Group contributions to the molecular weight.	183
2. Group contributions to molar volumes.	189
3. Group perturbations to the molar volume thermal expansivities.	198
4. Group contributions to the molar heat capacities.	202

5. Group contributions to the Rao function and  $\delta c'$ . 208
6. Sound speeds and temperature derivatives for liquids. 214
7. Predicted and measured properties of compounds. 214

Part I.

HIGH PRESSURE BEHAVIOR OF THE IRON-SULFUR SYSTEM WITH APPLICATIONS TO  
THE EARTH'S CORE

Chapter 1.

A LIQUID IRON EQUATION OF STATE FOR GEOPHYSICAL APPLICATIONS

William W. Anderson and Thomas J. Ahrens

Division of Geological and Planetary Sciences, California Institute of  
Technology, Pasadena, CA 91125

For submission to Geophysical Journal International.



## ABSTRACT

A new equation of state for liquid iron, in the form of a 4th order Birch-Murnaghan and Mie-Grüneisen equations of state, is presented. The parameters are constrained by ultrasonic, thermal expansion, and enthalpy data for temperatures to over 2300 K at 1 bar ( $10^5$  Pa) and by shock wave compression and sound speed data up to 10 Mbar. The interatomic contribution to the specific heat is calculated by numerical solution of a modified hypernetted chain equation for the structure of a fluid with an interatomic potential that accurately depicts both the s- and d-electron contributions, For the electronic contribution, we use the results of Boness et al. (1987), modified for the difference in free electron density. This represents the most detailed specific heat model extant. The equation of state parameters, anchored at  $10^5$  Pa and 1811 K (the normal melting point of iron), are  $\rho_0 = 7037$  kg/m<sup>3</sup>,  $K_{S0} = 110$  GPa,  $K_S' = 4.53$ ,  $K_S'' = -.0337$  GPa<sup>-1</sup>, and  $\gamma_0 = 2.8$ . We find that  $\gamma \propto \rho^{-n}$  with  $n = 1.17$ . These parameters, combined with our expressions for  $c_v$ , define an equation of state that fits all the available data. Parameters, such as the pressure of a certain  $\rho$ - $T$  point, calculated with this equation of state should be accurate to within 2% at pressures below 1 Mbar for temperatures within a few thousand degrees of the reference isentrope, and to within 4% at core conditions. Comparison of the model for Fe with PREM indicates that the outer core is 8 to 10% less dense than pure liquid iron at the same pressure over the ranges of temperature estimates for the core and also that the inner core is 3 to 5% less dense than pure liquid iron at the expected conditions of the inner core ( $P = 330$  GPa,  $4000$  K  $< T < 8000$  K).

This density deficit points to an inner core that is probably partially molten, with an upper bound of 50% to the liquid mass fraction of the inner core.

## INTRODUCTION.

The earth's core is generally accepted to be composed primarily of iron, with lesser amounts of other elements. This hypothesis is based on the observed behavior of seismic waves in the core and constraints based on elemental cosmic abundances and the moment of inertia of the earth. Moreover, the outer core appears to be fluid, as shear waves do not propagate through that region of the earth.

Much recent research (i.e., Williams and Jeanloz, 1989; Knittle and Jeanloz, 1988; Anderson et al., 1989; Svendsen et al., 1989) has focussed on modelling the phase diagrams of the Fe-S and Fe-O systems and comparing properties of those systems as a function of temperature and pressure with those of the core in order to constrain the core composition. The comparison usually involves choosing a composition that satisfies the density of the outer core and, qualitatively, the density contrast at the inner core boundary (ICB), assuming that the ICB represents a point on the liquidus of the relevant system. The primary drawbacks with this approach are that the equations of state of candidate core phases and compositions generally have some poorly constrained parameters, and that the best established equations of state have been for solid phases, while it is the liquid region of the core for which properties are most well determined by observational data.

Previous attempts have not been made to develop an accurate thermodynamic description of the liquid phase of iron at the high temperatures and pressures relevant to the earth's interior, which is surprising, since this is the most relevant phase to the outer core. Jeanloz (1979) used the available shock wave data for both porous and

nonporous iron samples to develop a pressure-volume-temperature equation of state for iron. At the time of that study, many important data were lacking, which have since become available, allowing more accurate determination of some parameters. These new data include shock compression data in the liquid phase region of the shock Hugoniot and the high-quality sound speed data for iron under shock compression of Brown and McQueen (1986).

Stevenson (1980, 1981) applied theoretical arguments to develop a simple model of liquid Fe, but his model was not intended to be quantitatively accurate. Rather, he demonstrated the general trends of properties of liquid Fe at high pressures and characterized the general behavior of the earth's core. More recently, Anderson (1986) presented equations of state for the various phases of Fe. That work, however, concentrated on the solid phases and he presented only a partial set of properties for the liquid.

Most recently, Svendsen et al. (1989) present an equation of state for liquid iron, starting from an assumed functional form for the interatomic pair potential of Fe. They constrained the pair potential by assuming that the structure of a liquid is constant along the liquidus, by analogy with hard sphere fluids and with the Lindemann law for solids. They then used the melting curve of Fe from Williams et al. (1987) to determine the values of adjustable parameters in their equation of state. Since the primary goal of Svendsen et al. (1989) was to develop phase diagrams of Fe-bearing systems, however, they did not try to incorporate all of the available data for liquid Fe.

There are sufficient high-quality data available, from a number of sources, to make possible the development of a much more comprehensive

and robust equation of state (EOS) for the liquid phase of Fe. In the following section, we use published experimental data from studies performed at 1 bar to separately constrain the density and bulk modulus of liquid Fe. The classical portion of the specific heat is constrained using a highly realistic model for the atomic interactions in liquid transition metals. Because our development of the potential energy contribution to the specific heat is rather involved, we present a more detailed discussion of that portion of the model in Appendix A. The remaining portions of the EOS are constrained using high pressure data obtained from published shock wave studies.

The development of the equation of state is followed by a section in which we compare the properties of liquid Fe, as represented by our model, with other experimental data, which were not used to constrain our model, and with previous equations of state. Finally, we make comparisons with the Earth's core and draw conclusions concerning the properties of other elements in the core and the physical state of the core.

#### **DETERMINATION OF THE LIQUID IRON EQUATION OF STATE.**

References for the data that we used to constrain the properties of liquid Fe are presented in Table 1. Traditionally, equations of state used by geophysicists have been referenced to normal conditions (1 bar or 1 atmosphere, 298 K). We have broken with this tradition in that our equation of state for the liquid phase of Fe is referenced to the melting point of pure Fe at 1 bar ( $T_m = 1811$  K). This is because the

Table 1.

References for experimental data on liquid iron.

Property	Reference
Density at 1 bar	Drotning (1981) Basin et al. (1979) Ivakhmenko and Kashin (1976) Lucas (1972)
Thermodynamic potentials at 1 bar	Desai (1986)*
Sound speed at 1 bar	Tsu et al. (1985) Kurz and Lux (1969)
Sound speed and Grüneisen parameter at 1 bar	Brown and McQueen (1986)
Shock Hugoniot data	Al'tshuler et al. (1981) Marsh (1980)* Krupnikov et al. (1963) Al'tshuler et al. (1962) Al'tshuler et al. (1958)

\*Review paper or compendium.

properties of the liquid phase can be measured directly at the melting point, whereas the properties at 298 K are not. Hence, for the remainder of this paper the reference pressure and temperature are  $P_0 = 1$  bar (0.1 MPa) and  $T_0 = 1811$  K.

We chose to develop our model in the context of the Birch-Murnaghan equation of state for compression along a reference isentrope. In this equation of state, the pressure and internal energy on the reference isentrope, relative to the reference conditions, are given by

$$P_S = \frac{3}{2}K_{S0}(x^7 - x^5)[1 + \xi_1 - \xi_1 x^2 + \xi_2(x^2 - 1)^2] \quad (1)$$

$$E_S = \frac{9}{2}V_0K_{S0} \left[ (\xi_1 + 1) \left( \frac{x^4}{4} - \frac{x^2}{2} + \frac{1}{4} \right) - \xi_1 \left( \frac{x^6}{6} - \frac{x^4}{4} + \frac{1}{12} \right) + \xi_2 \left( \frac{x^8}{8} - \frac{x^6}{2} + \frac{3x^4}{4} - \frac{x^2}{2} + \frac{1}{8} \right) \right] \quad (2)$$

$$x = (\rho/\rho_0)^{1/3} \quad (3)$$

$$\xi_1 = 3(4 - K_S')/4 \quad (4)$$

$$\xi_2 = \frac{3}{8}K_{S0}K_S'' + \frac{3}{8}K_S'(K_S' - 7) + \frac{143}{24} \quad (5)$$

where  $K_{S0}$ ,  $K_S'$ , and  $K_S''$  are the reference value and the first and second pressure derivatives, respectively, of the isentropic bulk modulus, and  $V_0 (=1/\rho_0)$  is the specific volume at the reference conditions.

For transformation to points away from the reference isentrope, we use the Mie-Grüneisen equation of state:

$$\int_{T_1}^{T_2} c_v dT = \int_{P_1}^{P_2} \frac{V}{\gamma} dP \quad (6)$$

where  $\gamma$  is the thermodynamic Grüneisen parameter,

$$\gamma = V(\partial P / \partial E)_V \quad (7)$$

We chose these particular forms because they are commonly used in high pressure geophysics and are relatively simple to work with.

In the fitting process, we made use of the results of several different studies, performed at normal atmospheric pressure, which constrain some EOS parameters. Where such data were available, we chose to fit the appropriate parameters using only the low pressure data and hold those parameters constant during the fitting procedure using high pressure data.

Densities, sound speeds, and thermodynamic potentials are all well-known for liquid Fe at or near the melting point at 1 bar. Thus, we chose to fit the reference density, bulk modulus at the reference point, and the heat capacity at constant pressure and then use these parameters as *a priori* constants in the subsequent fitting process using high pressure data.

Numerous studies have been made of the density of liquid Fe at 1 bar (Drotning, 1981; Basin et al., 1979; Lucas, 1972; Ivakhnenko and Kashin, 1976). All of these studies place  $\rho_0$  in the range from 7015 to



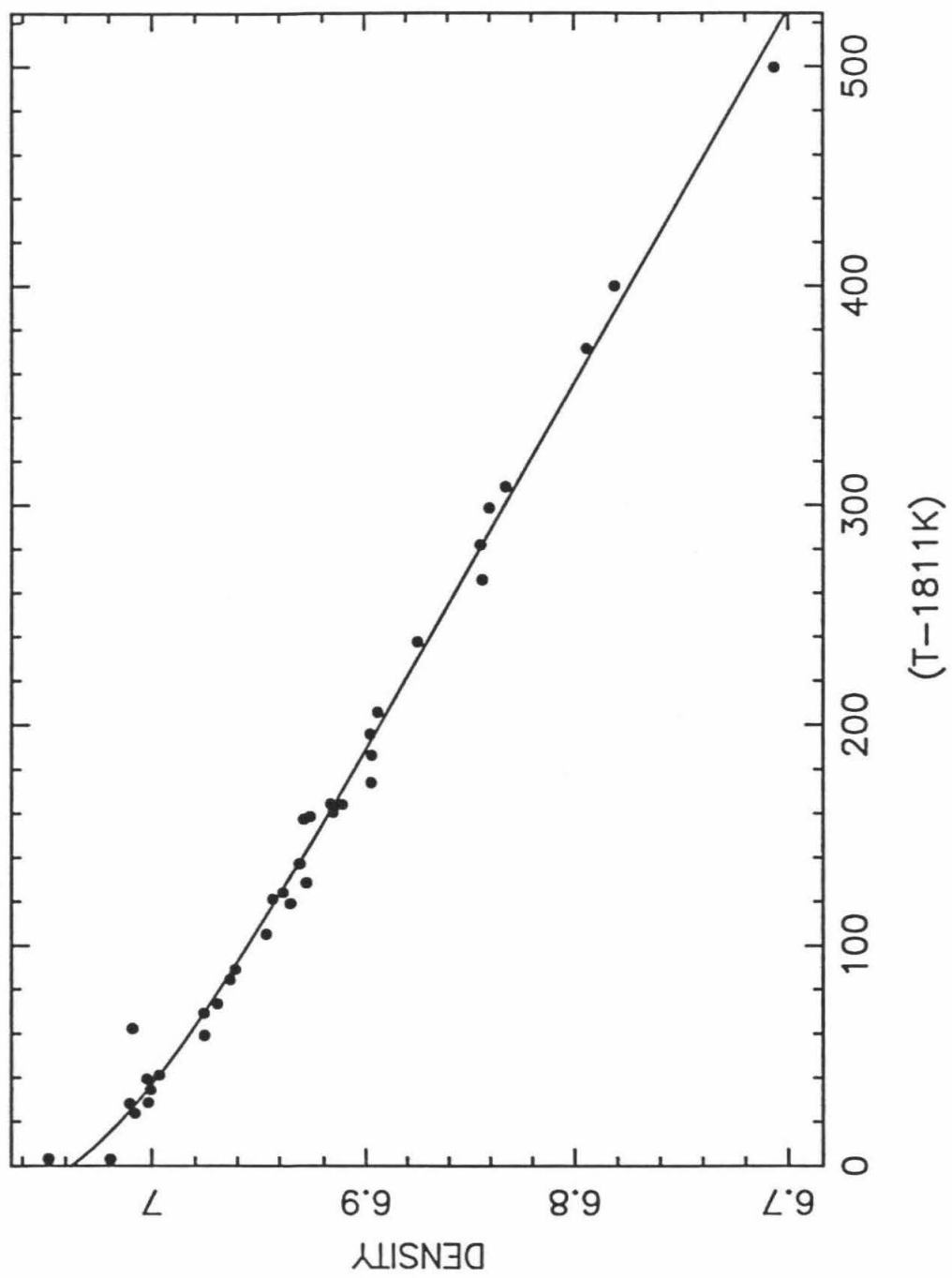
7150 kg/m<sup>3</sup>, with most recent results falling in the range from 7015 to 7070 kg/m<sup>3</sup>. One of the most thorough studies, and the most recent, is presented by Drotning (1981). His data extend to above 2300 K, spanning a range of about 400 K, twice that of any previous study. We combine his data with the results of Lucas (1972) and Ivakhnenko and Kashin (1976) for this study. Most other studies show anomalous behavior or systematic errors and have not been used here.

Normally,  $\rho$  is presented as a linear function of  $T$ , but Drotning's (1981) data show a very slight curvature within about 50 K of the melting point. This curvature becomes more apparent upon the addition of the other data. Since there is also some evidence that reactions may have occurred at the higher temperatures in Drotning's samples, we chose to try to capture the curvature in our fit. Hence, we fit the density data (figure 1) to the equation:

$$\rho = \rho^* + a(T - T_m) + \frac{b}{(T + T^* - T_m)^q} \quad (8)$$

with  $\rho^* = 7000$  kg/m<sup>3</sup>,  $a = -5.788 \times 10^{-4}$ ,  $b = .4327$ ,  $T^* = 30.88$  K, and  $q = .7126$ . This gives  $\rho_0 = 7037 \pm 12$  kg/m<sup>3</sup> and  $(d\rho/dT)_0 = -1.4452$  kg/m<sup>3</sup>·K. Although the formal error on  $d\rho/dT$  is fairly small, other factors such as the correctness of the functional form in equation (8) limit its validity. Also, Basin et al. (1979) and Drotning (1981) note that small concentrations of impurities in the samples can have a large effect on the temperature dependence of  $\rho$ . This may explain the variation by more than a factor of 2 in values of  $d\rho/dT$  quoted in the literature. Because

Figure 1. Density of liquid Fe as a function of temperature at 1 bar. The data are from Drotning (1981), Ivakhnenko and Kashin (1976), and Lucas (1972). The curve is our best fit.



of these uncertainties, we will not attempt to place any *a priori* constraints on the value of  $d\rho/dT$ .

Like  $\rho$ , the thermodynamic potentials of Fe have been extensively studied at atmospheric pressure. A recent review is presented by Desai (1986). The various authors whose work are reviewed all present  $C_p$  as being constant over the temperature range investigated. We have chosen to use Desai's (1986) preferred value of  $C_p = 46.362 \pm 3.0$  J/mol·K ( $c_p = 835 \pm 54$  J/kg·K) at 1 bar and 1811 K, but we did not require  $C_p$  to remain constant with increasing  $T$ . For later evaluation of shock wave data, we also need the quantity  $E_{tr}$ :

$$E_{tr} = E_{liq, 1 \text{ bar}, 1811 \text{ K}} - E_{\alpha, 1 \text{ bar}, 298 \text{ K}} \quad (9)$$

Although Desai (1986) does not present  $E_{tr}$ , he does present preferred values for the enthalpy difference between various temperatures and 298 K. We can obtain  $\Delta H_r$  from

$$\Delta H_r = \int_{298K}^T C_p dT + \Delta H_{\alpha \rightarrow \gamma} + \Delta H_{\gamma \rightarrow \delta} + \Delta H_{\delta \rightarrow liq} \quad (10)$$

and then get  $E_{tr}$ :

$$E_{tr} = \Delta H_r + P\Delta V \quad (11)$$

At one bar,  $P\Delta V$  is negligible and  $E_{tr} \approx \Delta H_r$ . Using values of  $C_p$  and  $\Delta H$  from Desai (1986), we get  $E_{tr} = 72641 \pm 658$  J/mol ( $1.3007 \pm .0118 \times 10^6$  J/kg).

In the calculations, we have used these values as stated here, although

the last two digits are not significant. This is done with all values obtained in the following discussion, to avoid the introduction of errors by numerous rounding operations and to identify the exact values used, for workers wishing to compare their results with ours.

$K_S$  may be obtained from the density and bulk sound speed via the equation

$$V_b = (K_S/\rho)^{1/2} \quad (12)$$

where  $V_b$  is the bulk sound speed. Since, in a liquid, the longitudinal sound speed  $V_p$  is identical to  $V_b$ , it is a readily measured quantity. Measurements of  $V_p$  as a function of  $T$  for liquid Fe at 1 bar have been presented by several authors. We combined the data of Kurz and Lux (1969) and Tsu et al. (1985) to cover a range of ~140 K (Table 2). These data are shown in figure 2 together with our straight-line fit. The use of a straight line fit of  $V_b$  as a function of  $T$  is in keeping with the convention established by previous investigators, (see, e.g., Kurz and Lux, 1969, Tsu et al., 1985). The recent work of Shaner et al. (1988) suggests that, for most liquid metals (but not all),  $V_b$  would be better represented as a straight line function of  $\rho$ . The data for Fe are too sparse to allow us to determine if this is true in the present case. In any event, our lack of precise knowledge of how  $\rho$  varies with  $T$  does not justify going to such detail for an extrapolation over only 23 K. The sign of the slope is as we expect from the work of Shaner et al. (1988), and many researchers find that  $q$  varies linearly with  $T$  near the melting point (Drotning, 1981; Basin et al., 1979; Lucas, 1972; Ivakhnenko and Kashin, 1976). Hence, our use of a straight line fit is justified and should in any case introduce only a negligible error into the value of  $V_{b0}$ . We find that at 1 bar and 1811 K,  $V_{b0} = 3954 \pm 24$  m/s with

Table 2.

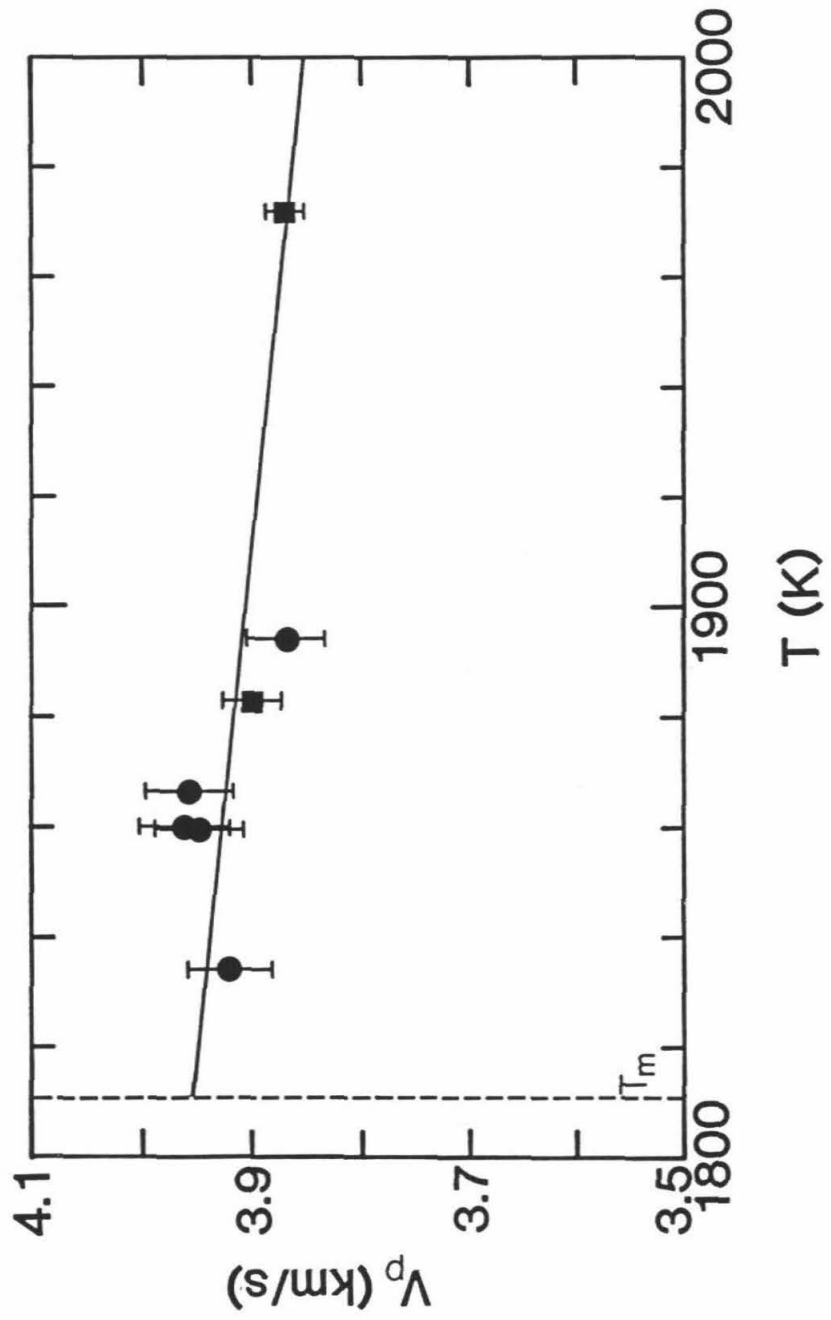
Sound speed data for liquid iron at 1 bar.

$T(K)$	$V_b(m/s)$	Reference
1972	3870±17	1
1883	3900±27	1
1834	3921±39	2
1859	3948±39	2
1860	3961±40	2
1867	3958±40	2
1894	3868±38	2

## References:

- 1) Kurz and Lux (1969)
- 2) Tsu et al. (1985)

Figure 2. Longitudinal sound speed in liquid iron at 1 bar. The squares represent the data of Kurz and Lux (1969) and the circles represent the data of Tsu et al. (1985). The line is the best fit straight line.





$dV_b/dT = -.539 \pm .208 \text{ m/s} \cdot \text{K}$ . This value of  $V_b$ , together with  $\rho_0$ , gives a value of  $K_{S0} = 110.02 \pm 1.34 \text{ GPa}$ .

We also chose to develop *a priori* expressions for the kinetic and potential energy terms of the specific heat at constant volume,  $c_v$ .

This quantity may be expressed as the sum

$$c_v = c_k + c_{\text{pot}} + c_e \quad (13)$$

where the subscripts  $k$ ,  $\text{pot}$ , and  $e$  represent the kinetic contribution due to the thermal motion of the ionic cores, the potential energy contribution due to interaction of the ionic cores, and the energy due to population of electronic states, respectively.

In the high temperature limit,  $c_k = 1.5R$ . Typically, this is valid if the temperature is well above the Debye temperature of the solid phase for the same material. We chose to use  $c_k = 1.5R$  here, although extrapolation to low temperatures (such as the development of a 0K isotherm) should be done using a  $c_k$  that obeys

$$\lim_{T \rightarrow 0} c_k = 0 \quad (14)$$

Appendix A gives a detailed discussion of our development of  $c_{\text{pot}}$ . In the case of a liquid of spherically symmetric atoms with an interatomic potential  $\varphi(r)$ , if the distribution of atoms around a central atom is described by a radial distribution function  $g(r)$ , then the specific energy  $E_{\text{pot}}$  due to interaction of the atoms through the interatomic potential is given by

$$E_{\text{pot}} = 2\pi n \int_0^{\infty} \varphi(r) g(r) r^2 dr \quad (15)$$

where  $n$  is the number density of the atoms. This integral is differentiated with respect to temperature to give  $c_{\text{pot}}$ . To solve the integral in equation (15), we need to know  $\varphi(r)$  and  $g(r)$  as functions of  $\rho$  and  $T$ . For  $\varphi(r)$ , we followed Wills and Harrison (1983) and Hausleitner and Hafner (1988) in separating  $\varphi(r)$  into its component d- and s-electron parts and used the expressions of Hausleitner and Hafner (1988) for the d-electron contributions. For the s-electron part, we used the analytic expression developed by Hafner and Heine (1986) for the s,p-metal pseudopotential with an empty core. The properties of the electron gas were taken from Ichimaru and Utsumi (1981).

We used the resulting  $\varphi(r)$  in a type of modified hypernetted chain (MHNC) equation to obtain  $g(r)$ . We then evaluated equation (15) numerically over the density range from 5000 to 13000 kg/m<sup>3</sup> and a temperature range from 1600 to 28000 K and fit the resulting energies with an analytic expression. Upon differentiation with respect to temperature at constant volume, this  $E_{\text{pot}}$  yielded an expression for  $c_{\text{pot}}$ , namely:

$$c_{\text{pot}} = \frac{\theta}{\theta+T} (1.5R + \Delta T + \Xi T^2 + \Upsilon T^3) \quad (16)$$

$$\theta(\text{K}) = 372.21 + 6.1653 \times 10^{-3} \rho + 1.9008 \times 10^{-6} \rho^2 - 7.014 \times 10^{-11} \rho^3 \quad (17)$$

$$\Lambda(\text{J/kg}\cdot\text{K}^2) = 6.2534\rho^{-1.252} + 5187.8\theta^{-1}\rho^{-.395} \quad (18)$$

$$\Xi(\text{J/kg}\cdot\text{K}^3) = -4.132 \times 10^{-6} - 337.5\theta^{-1}\rho^{-1.201} \quad (19)$$

$$\Upsilon(\text{J/kg}\cdot\text{K}^4) = 9.0151 \times 10^{-4}\theta^{-1}\rho^{-.931} \quad (20)$$

for  $\rho$  in  $\text{kg/m}^3$ . The original expression for the energy from which this  $c_{\text{pot}}$  is obtained is

$$E_{\text{pot}} = \int_0^T c_{\text{pot}} dT' \quad (21)$$

$$E_{\text{pot}} = \theta \left[ (1.5R - \Lambda\theta + \Xi\theta^2 - \Upsilon\theta^3) \ln(1 + T/\theta) + \Lambda T + \frac{1}{3} \Upsilon T^3 + \frac{1}{2} (\Xi - \Upsilon\theta) (T^2 - \theta T) \right] \quad (22)$$

This is a rather involved expression, but a simpler form would not accurately describe the numerical results. Generally,  $c_{\text{pot}}$  is assumed to be the high temperature limit for a classical solid, namely  $c_{\text{pot}} = 1.5R$ . We found, however, that  $c_{\text{pot}} < 1.5R$  over most of the range of densities and temperature investigated. This is in agreement with the results found by Stevenson (1980).

There is some justification for assuming that the functional form of  $c_e$  should be about the same for all phases of Fe at high pressure, whether solid or liquid (Boness et al., 1986). Hausleitner and Hafner (1988) note, however, that liquid transition metals seem to show more s-d hybridization than the corresponding solid phases. They find apparent

s-electron densities of about 1.5 electrons per atom, rather than the commonly assumed value of 1 electron per atom for the solid. It is therefore unlikely that the electronic specific heat determined for a solid can be applied directly to the liquid. In fact, we chose to use the  $c_e$  of Boness et al. (1986) for  $\epsilon$ -Fe, but allowed a multiplicative scaling factor for the density to account for the increased s-electron density. We would expect this scaling factor to have a value of about 1.5, but chose to allow it to vary in the fitting process. We should caution the reader at this point to note that our development is for an electrically conducting liquid. Metals such as Fe are usually insulators in the gas phase, so our expressions for  $c_v$  are not valid for the gas phase of the subcritical fluid.

We now discuss the high pressure data that we used to constrain the remaining parameters. Among the high pressure data relevant to liquid Fe are the sound speeds and Grüneisen parameters of Brown and McQueen (1986). We present these results in Table 3, but our numbers are different from those actually stated by Brown and McQueen (1986). In the experiments described, they did not directly measure the velocities of the shock waves in the samples. Rather, they used measured impactor velocities (for impact-generated shock waves) and detonation wave velocities (for explosively generated shock waves) in conjunction with a previously determined shock Hugoniot for Fe to obtain an impedance-match solution for the shock conditions. For Fe, they used a single Hugoniot curve, described in the shock velocity-particle velocity ( $U_s$ - $u_p$ ) plane by

$$U_s = C_0 + su_p \quad (23)$$

Table 3.

High pressure sound speeds and Grüneisen parameters from Brown and McQueen (1986). Both their original values and our reanalyzed values based on their data are presented. The original values presented by Brown and McQueen (1986) are enclosed in parentheses. Our error analyses are based in part on the results of Al'tshuler et al. (1981).

$\rho(\text{kg/m}^3)$	$P(\text{GPa})$	$V_b(\text{m/s})$	$\gamma$
12618±65 (12540±110)	277.4±18.4 (275±8)	9565±82 (9620±70)	1.398±.110 (1.564±.123)
13001±36 (12920±40)	331.5±9.4 (333±2)	10015±87 (10190±40)	1.387±.055 (1.580±.065)
13404±36 (13280±40)	397.1±10.2 (400±2)	10648±86 (10910±40)	1.296±.052 (1.506±.060)

with  $C_0 = 3955$  m/s and  $s = 1.580$ , to describe the entire Hugoniot, including the  $\epsilon$  and  $\gamma$  solid phases regions, the liquid phase region, and the mixed phase regions. The pressure and density were obtained using continuity and conservation relations:

$$P = \rho_{00}U_s u_p \quad (24)$$

$$\rho = \rho_{00}U_s / (U_s - u_p) \quad (25)$$

where  $\rho_{00}$  is the initial density of the unshocked sample used in the experiment.

Brown and McQueen (1986) determined the sound speed in the shocked iron by measuring the distance travelled by a shock wave through a sample before being overtaken by an elastic release wave. The longitudinal sound speed was obtained via

$$R^* = \rho V_p / \rho_{00}U_s \quad (26)$$

where

$$R^* = (R_T + 1) / (R_T - 1) \quad (27)$$

Here,  $R_T$  relates the distance travelled by the shock wave before being overtaken to the thickness of the impactor that generated the shock wave. The quantity  $(\partial E / \partial P)_V$  is also obtained:

$$(\partial E/\partial P)_V = \frac{U' \eta^2}{\rho_{00}} [1 + U' \eta + R^* (U' \eta - 1)]^{-1} \quad (28)$$

where  $\eta = u_p/U_s$  and  $U' = dU_s/du_p$ .

While the data in which we are interested represent the liquid phase region of the principal Hugoniot, the values of  $C_0$  and  $s$  used by Brown and McQueen (1986) were determined from data representing only the solid phase region. From the comparison with shock wave data in figure 3, we can see that this results in a value of  $U'$  larger than is justified by the data from the liquid phase region of the Hugoniot. We fit the data with a quadratic expression (also in figure 3),

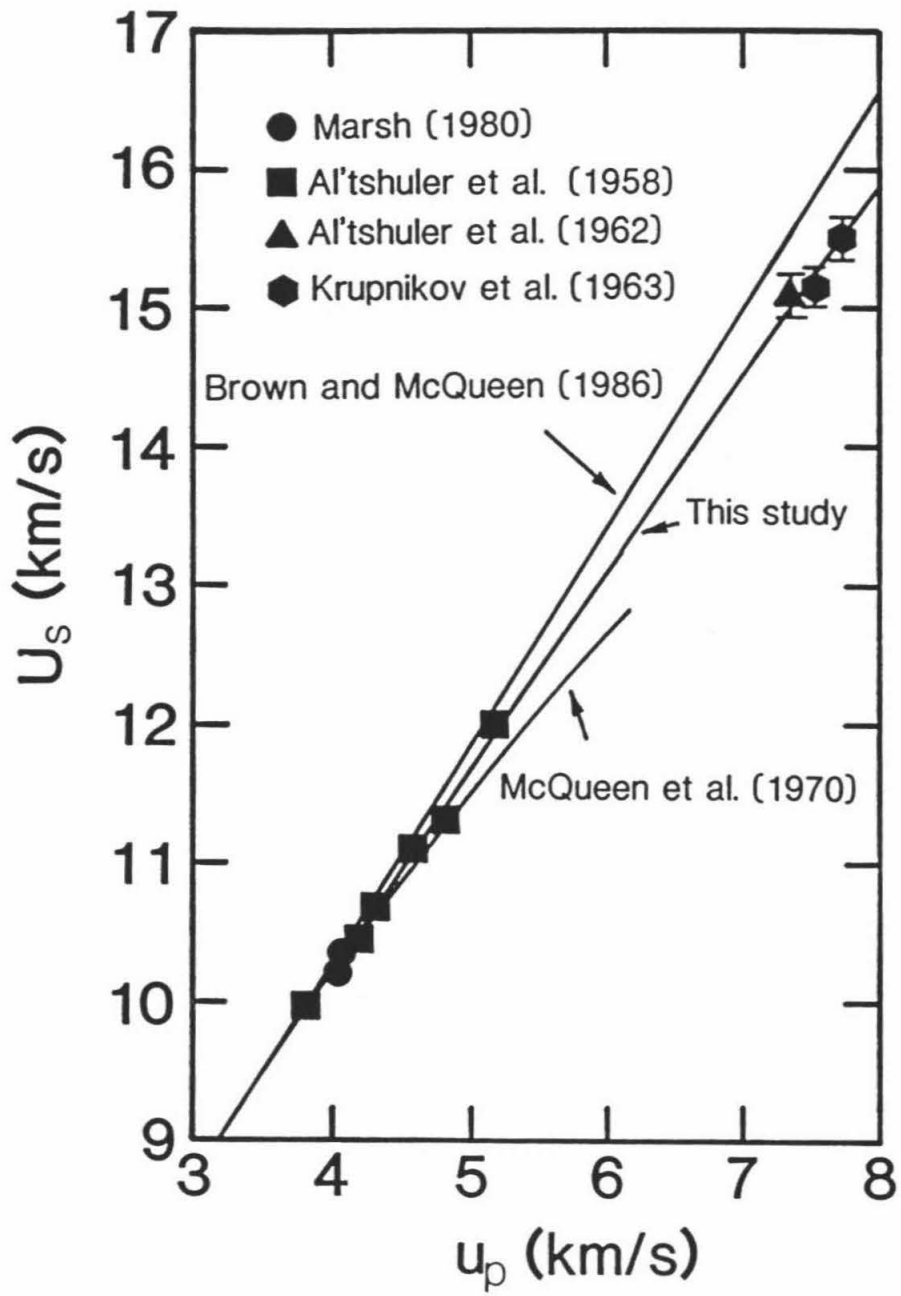
$$U_s = C_0 + s u_p + s' u_p^2 \quad (29)$$

with  $C_0 = 3919 \pm 1048$  m/s,  $s = 1.638 \pm .388$ , and  $s' = -1.76(\pm 3.35) \times 10^{-5}$  s/m.

Although the formal errors quoted are rather large, they are the result of the highly correlated nature of these parameters and the large extrapolation required to obtain  $C_0$  from the intercept at  $u_p = 0$ . This is more apparent if we fit the  $U_s - u_p$  Hugoniot in a transformed coordinate  $u_p^* = u_p - u_{p0}$ . For  $u_{p0} = 3500$  m/s,  $C_0^* = 9438 \pm 108$  m/s,  $s^* = 1.515 \pm .155$ , and  $s'^* = -1.76(\pm 3.35) \times 10^{-5}$  s/m. This fit and the fit in  $u_p$  are entirely equivalent. We can see that our fit gives uncertainties of about 1% in  $U_s$  and 10% in  $U'$ . We have reevaluated the results quoted by Brown and McQueen (1986) using this new expression for the liquid phase region of the principal Hugoniot. We find only slight differences (1-3%) in  $\rho$ ,  $P$ , and  $V_p$ , but a substantial change in  $\gamma$  (about 15%),

Figure 3.  $U_s$ - $u_p$  Hugoniot for iron, with experimental data for the liquid phase region of the Hugoniot. The Hugoniot of McQueen et al. (1970) was used by Jeanloz (1979). The Hugoniot used in this study was fit to only the liquid phase region data.





because of the extreme sensitivity of equation (28) to the value of  $U'$ . Our results also cast into doubt the common assumption that the thermodynamic properties of liquid and solid Fe at high pressures are about the same.

With the values of  $\gamma$  and  $V_p$  obtained here, we assumed that the thermodynamic Grüneisen parameter  $\gamma$  is described by the functional form

$$\gamma = \gamma_0(\rho_0/\rho)^n \quad (30)$$

This is a common assumption for solids and can also be shown to be valid for a hard sphere fluid with a constant specific heat. We cannot be certain, however, that  $\gamma$  does not show an explicit temperature dependence, only that the available data do not provide a basis for evaluating the temperature dependence. Mulargia (1977) argues that  $\gamma$  should have a temperature dependence, based on the presence of temperature-dependent terms in the vibrational and electronic specific heats. There are slight differences between Mulargia's (1977) definition of  $\gamma$  and the present usage. Hence, we have chosen to constrain other parameters (namely  $\alpha$  and the pressure derivatives of  $K_S$ ) through our functional form for  $\gamma$ .

We followed an iterative route to adjust the final parameters in the model. As the first step in an iteration, we estimated the value of  $\gamma_0$  for  $\rho_0 = 7037 \text{ kg/m}^3$  and performed a least squares fit of  $n$  using the values of  $\gamma$  derived from the data of Brown and McQueen (1986) (Table 3). With these estimates of  $\gamma_0$  and  $n$ , we used the shock compression data in Table 4 with equations (1)-(6) to obtain least squares fits of  $K_S'$  and  $K_S''$  from the pressure as a function of volume on a shock Hugoniot curve:

Table 4.

Data for the liquid phase portion of the nonporous iron principle Hugoniot.

$\rho_0$ (kg/m <sup>3</sup> )	$U_s$ (m/s)	$u_p$ (m/s)	$\rho_H$ (kg/m <sup>3</sup> )	$P_H$ (GPa)	Reference
7851	10200±102	4050±41	13021±177	324.3±6.1	1
7851	10350±104	4070±41	12939±173	330.7±6.2	1
7850	17740±176	9700±24	17317±566	1351±97	2
7850	9980±100	3830±24	12740±112	300±6.2	3
7850	10450±105	4200±42	13130±125	344±7.2	3
7850	10670±107	4320±43	13190±127	362±7.5	3
7850	11100±111	4590±46	13380±133	400±8.3	3
7850	11320±113	4830±48	13690±144	429±8.9	3
7850	12000±120	5170±52	13790±148	487±10.1	3
7850	15500±155	7710±77	15622±547	938±33	4
7850	15150±152	7520±75	15582±545	894±32	4
7850	15100±151	7340±73	15284±535	870±32	5

## References:

- 1) Marsh (1980)
- 2) Al'tshuler et al. (1981)
- 3) Al'tshuler et al. (1958)
- 4) Krupnikov et al. (1963)
- 5) Al'tsuler et al. (1962)

$$P_H = (E_S - VP_S / \gamma + E_{tr}) / [(V_{00} - V) / 2 - V / \gamma] \quad (31)$$

We also determined  $c_V$  at the reference point from the equation

$$c_P = c_V(1 + \alpha\gamma T) \quad (32)$$

with  $\alpha$  obtained from  $\gamma = \alpha K_S / \rho C_P$ . From equation (13), with  $c_V$  and since we already know  $c_K$  and  $c_{pot}$ , we could thus determine  $c_e$  at the reference point and so obtain the density scaling required for the application of the results of Boness et al. (1986).

Once we had obtained test values for all the parameters in the equation of state, we compared sound speeds predicted by those parameters with the results of Brown and McQueen (1986), listed in Table 3. The standard  $\chi^2$  statistic was calculated for the sound speed and a new iteration was begun with a better estimate of  $\gamma_0$  as an attempt to improve the fit. The procedure was continued until a minimum in  $\chi^2$  was reached, at which point we adopted the current parameters as the final model. The final results are  $\gamma_0 = 2.8 \pm 0.2$ ,  $n = 1.17 \pm 0.13$ ,  $K_S' = 4.531$ , and  $K_S'' = -.0337 \text{ GPa}^{-1}$ . The density scaling for the electronic specific heat gives 1.53 electrons per atom, close to the expected value of 1.5 from the work of Hausleitner and Hafner (1988). We chose to describe  $c_e$  by a single analytic expression applicable at all temperatures and densities, namely:

$$c_e = a \tanh^{3/2}(T/\theta) + AT / (1+T) + XT + YT^2 \quad (33)$$

where  $a = 407.63 \text{ J/kg}\cdot\text{K}$  and

$$\theta(K) = .01271\rho^{1.434} \quad (34)$$

$$A(J/kg \cdot K) = .002965\rho - 24.8 \quad (35)$$

$$X(J/kg \cdot K^2) = 5.112 \times 10^{-7}\rho - .008339 \quad (36)$$

$$Y(J/kg \cdot K^3) = 8.218 \times 10^{-11}\rho - 6.867 \times 10^{-15}\rho^2 \quad (37)$$

for  $\rho$  in  $\text{kg/m}^3$ . The electronic energy obtained upon integration from 0 K to temperature  $T$  is given by

$$E_e = \int_0^T c_e dT' \quad (38)$$

$$E_e = 1/2XT^2 + 1/3YT^3 + A[T - \ln(1+T)] \\ + a\theta \left[ \frac{1}{2} \ln \left( \frac{1+z}{1-z} \right) + \tan^{-1}(z) - 2z \right] \quad (39)$$

$$z = \tanh^{1/2}(T/\theta) \quad (40)$$

While it provides a satisfactory description of the results of Boness et al. (1986) (which we have transformed to higher electron densities), our expression for  $c_e$  has no special physical significance. Rather, it was chosen to give a single analytic expression applicable over the whole range of temperatures and densities treated.

In figure 4, we show the values of  $c_v$  given by our model over a range of temperatures and densities. We find that, except at temperatures that lie below the pure Fe melting curve,  $c_v > 3R$ . We do find, however, that the high s-electron density and the generally lower values of  $c_{pot}$  result in values of  $c_v$  that are lower than estimates for the solid phases that include  $c_e$ . The upper limit to  $c_v$  for the liquid is about  $4.6R$ . In contrast, some estimates for the solid are as high as  $6R$  for very high temperatures. We feel that our estimate will provide a much better  $c_v$  for use in assessing the heat content of the liquid portion of the core.

#### DISCUSSION AND COMPARISON WITH OTHER EQUATIONS OF STATE

Table 5 lists our final parameters for the equation of state of liquid Fe. This model should be valid for densities ranging from 5000 to 15000 kg/m<sup>3</sup> and temperatures below 25000 K. In practice, we advise caution in applying this EOS to densities below about 6500 kg/m<sup>3</sup>. The model appears to behave as if it has a critical point, below which there is a gaseous phase occupying a certain portion of  $\rho$ - $T$  space. However, since the specific heat in our model is not valid for gaseous Fe, the model produces numbers that are erroneous for high temperatures at densities below about 6300 kg/m<sup>3</sup>. The apparent "critical point" in the model is also probably not at the  $P$ - $T$  point of the true critical point of Fe (~10 kbar and 9000 K, Young and Alder, 1971). The model is only valid for the supercritical fluid and the liquid branch of the subcritical fluid.

Figure 4. Specific heat at constant volume for liquid iron as a function of temperature at four different densities.

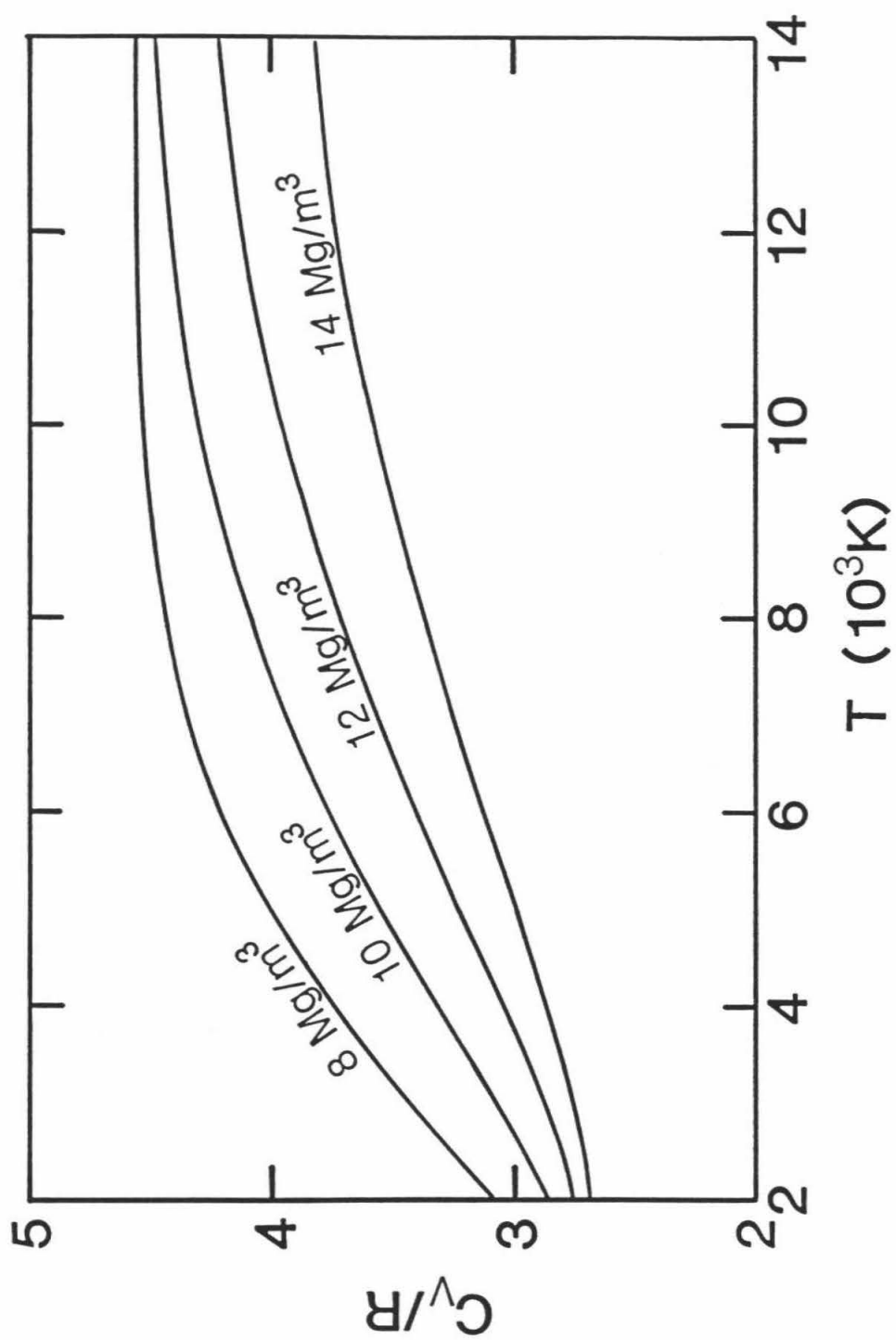




Table 5

Final equation of state parameters for liquid iron

$$P_0 = 1 \text{ bar}$$

$$T_0 = 1811 \text{ K}$$

$$\rho_0 = 7037 \text{ kg/m}^3$$

$$K_{S0} = 110.02 \text{ GPa}$$

$$K_S' = 4.531$$

$$K_S'' = -.0337 \text{ GPa}^{-1}$$

$$E_0 - E_{\alpha, 1\text{bar}, 298\text{K}} = 1.3007 \times 10^6 \text{ J/kg}$$

$$\gamma_0 = 2.80$$

$$\gamma = \gamma_0 (\rho_0 / \rho)^{1.173}$$

$$c_V = c_k + c_{\text{pot}} + c_e$$

$$c_k = 1.5R$$

for  $\rho$  in  $\text{kg/m}^3$ :

$$c_{\text{pot}} = \frac{\theta}{\theta + T} (1.5R + \Lambda T + \Xi T^2 + \Upsilon T^3)$$

$$\theta (\text{K}) = 372.21 + 6.1653 \times 10^{-3} \rho + 1.9008 \times 10^{-6} \rho^2 - 7.014 \times 10^{-11} \rho^3$$

$$\Lambda (\text{J/kg} \cdot \text{K}^2) = 6.2534 \rho^{-1.252} + 5187.8 \theta^{-1} \rho^{-.395}$$

$$\Xi (\text{J/kg} \cdot \text{K}^3) = -4.132 \times 10^{-6} - 337.5 \theta^{-1} \rho^{-1.201}$$

$$\Upsilon (\text{J/kg} \cdot \text{K}^4) = 9.0151 \times 10^{-4} \theta^{-1} \rho^{-.931}$$

$$c_e = a \tanh^{3/2}(T/\theta) + AT/(1+T) + XT + YT^2$$

$$a = 407.63 \text{ J/kg} \cdot \text{K}$$

$$\theta (\text{K}) = .01271 \rho^{1.434}$$

$$A (\text{J/kg} \cdot \text{K}) = .002965 \rho - 24.8$$

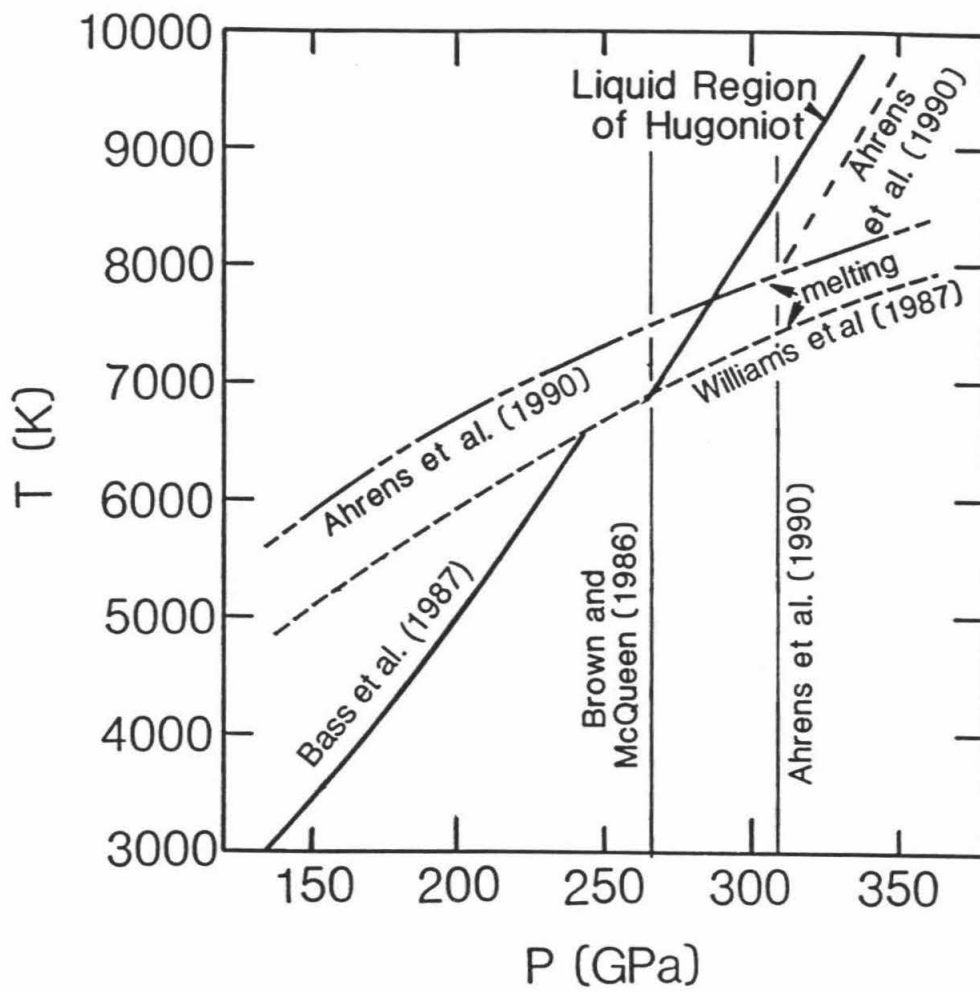
$$X (\text{J/kg} \cdot \text{K}^2) = 5.112 \times 10^{-7} \rho - .008339$$

$$Y (\text{J/kg} \cdot \text{K}^3) = 8.218 \times 10^{-11} \rho - 6.867 \times 10^{-15} \rho^2$$

Because of the variety of data types used in the development of this model, it is difficult to determine formal uncertainties in all the model parameters. In general, however, uncertainties in thermodynamic potentials calculated with this model should be less than 4% at core pressures and temperatures and 2% or less for pressures below 1 Mbar and temperatures within a few thousand Kelvin of the reference isentrope. This estimate is based on the uncertainties in the data, uncertainties in the parameters for which uncertainties are known, the goodness of fit of the model to the data, and the self-consistency shown by the different facets of the model in its final form.

Although we made as full use of the existing data as possible, two data sets are left, which were not taken into account during the fitting process and which can thus be used as independent tests of the model. The first of these is the temperature along the principal Hugoniot. While there is a great deal of uncertainty in the Hugoniot temperatures for the completely molten region, the existing data do constrain the melting curve fairly well (Williams et al., 1987; Ahrens et al., 1989). There is a range of estimates of the pressure at which the state represented by the Hugoniot becomes completely liquid. At that point, the principal Hugoniot temperature for the completely molten state is identical to the melting temperature. In figure 5, we present a predicted  $P$ - $T$  projection for the liquid portion of the principal Hugoniot and the measured solid phase portion. Also given are the experimentally constrained melting curves of Williams et al. (1987) and Ahrens et al. (1990). The vertical lines denote pressures at which the Hugoniot state has been estimated to enter the completely molten state by previous authors. This range is bounded on the lower side by the

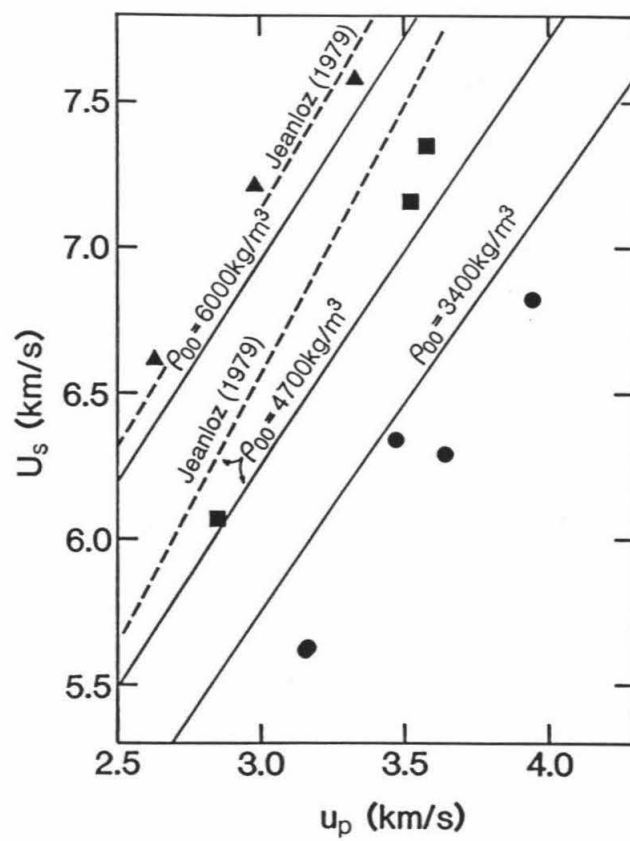
Figure 5. Temperatures along the the principal Hugoniot, compared with recent melting curves for iron constrained by experimental data. The liquid phase region of the principal Hugoniot is predicted from the present model, while the solid phase portion is based on the measurements of Bass et al. (1987). The vertical lines represent the upper and lower pressure limits for which completeion of melting on the Hugoniot has been inferred, based on the sound speed data of Brown and McQueen (1986) and the estimate of Ahrens et al. (1990). A successful liquid Fe equation of state should intersect the melting curve of Fe somewhere in the pressure range bounded by these limits. The present model satisfies this test for both proposed melting curves.



pressure at which the sound velocities of Brown and McQueen (1986) appear to leave the melting curve and enter the fully liquid state. The upper bound is the calculated estimate of Ahrens et al. (1990), which is based on the estimated latent heat of melting at high pressures. Agreement of our model with the data is indicated if the predicted Hugoniot curve intersects the melting curves within the pressure region bounded by these two curves. Our model satisfies this criterion for both proposed melting curves, indicating that our model is in agreement with the shock temperature data, to the level of uncertainty in the data.

The second data set with which we can test the model is the collection of Hugoniot data for porous Fe samples (Marsh, 1980). The model does not satisfactorily reproduce the shock wave data for porous samples of Fe when the traditional equations (i.e., equations (24), (25), and (31)) are used. Thouvenin (1964) has pointed out, however, that the propagation of a shock wave in a porous medium with voids larger than the thickness of the shock front is not a steady process and that the traditional equations should not be valid. He presents a model in which the propagation of a shock wave in such a material is the sum of shock propagation through the nonporous material with adiabatic expansion into the voids at the free surface velocity of the shocked material. The values of  $U_s$  and  $u_p$  become weighted averages of the nonporous equivalents and the free surface velocity. If we apply his model for the propagation of a shock wave through a porous medium, the agreement with the data is quite good for the regions of the Hugoniot curves in which our model applies (i.e., the region where the corresponding principal Hugoniot represents a completely liquid state, figure 6). The small amount of disagreement with the data is primarily

Figure 6.  $U_s$ - $u_p$  Hugoniot in the liquid regime predicted for porous iron using the method of Thouvenin (1964) and our equation of state. Lower  $u_p$  values represent incomplete melting and thus are not relevant to the completely liquid portion of the Hugoniot and thus are not presented. Also shown are experimental data from Marsh (1980) and the Hugoniot which result from using the equation of state of Jeanloz (1979) with the traditional continuum model of shock propagation. The circles represent initial densities of about 3400 kg/m<sup>3</sup>, squares represent initial densities of about 4700 kg/m<sup>3</sup>, and triangles represent initial densities of about 6000 kg/m<sup>3</sup>.



due to our assumption here that the free surface velocity of a shocked nonporous material will be precisely twice the particle velocity imparted by the shock wave.

We also wish to compare our equation of state with other models. We have already seen from figure 3 that our  $U_s$ - $u_p$  relation provides a better description of the liquid phase region of the principal Hugoniot than other available expressions. Our expression is very similar to that of Al'tshuler et al. (1981), except that their inclusion of data from the solid phase region of the Hugoniot forces a greater curvature in the Hugoniot. This greater curvature results in higher values of  $U_s$  for intermediate values of  $u_p$ . In the  $P$ - $V$  plane (Figure 7), the present model is in better agreement with the data than the other available expressions.

For the general behavior of liquid Fe, the only extant complete description is that of Jeanloz (1979). That model is a single  $P$ - $V$ - $T$  relationship that was developed to be applicable to all phases of Fe at high pressures under the assumption that the different phases are nearly indistinguishable, from a thermodynamic standpoint, at high pressures. Jeanloz's model was developed using the Hugoniot of McQueen et al. (1970) in conjunction with porous Hugoniot data to constrain the compressional properties and the Grüneisen parameter. He tied in the temperature with the assumption that  $c_p = 3R$ . Since there are now more and higher-quality Hugoniot and sound speed data available, and since our model differs from his on some points, we expect at the outset that there will be disagreement between his model and the present one.

We compare the Grüneisen parameters from our model with the results of Jeanloz (1979) and Brown and McQueen (1986) in Figure 8.



Figure 7. *P-V* Hugoniot for Fe, presented with experimental data. The symbols for the data are the same as in figure 3.

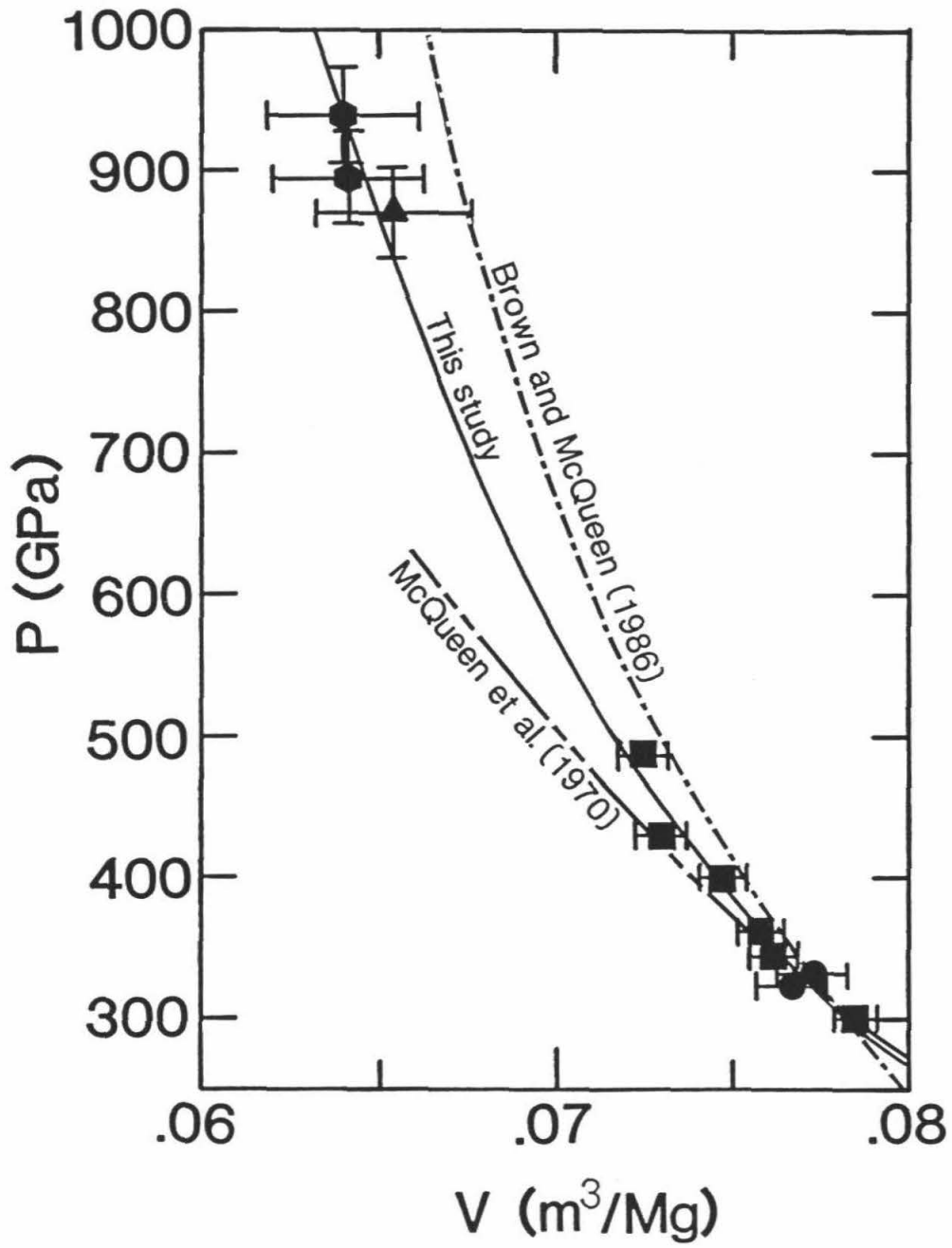
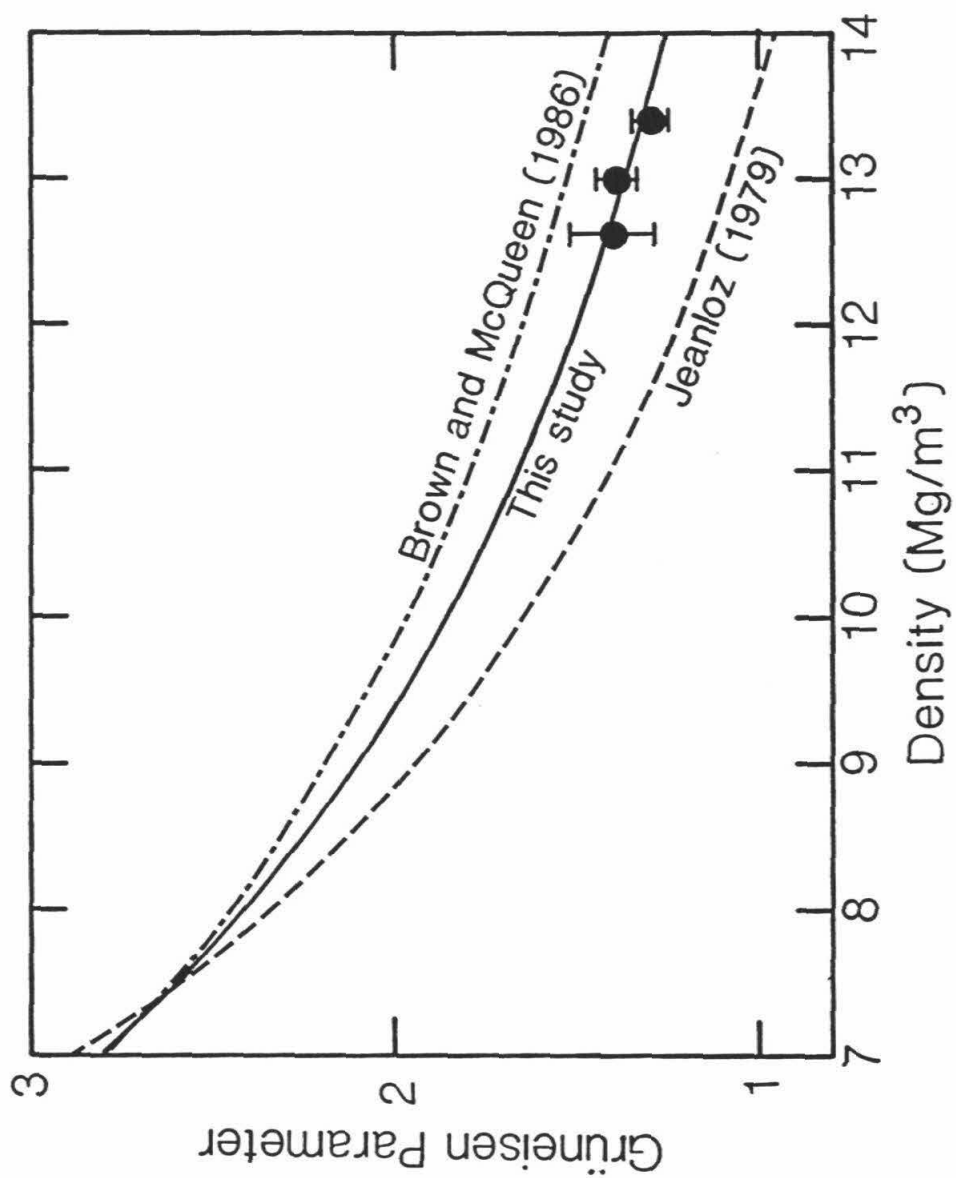


Figure 8. Estimates of the thermodynamic Grüneisen parameter of liquid Fe, presented with the reanalyzed data of Brown and McQueen (1986). The present study finds  $\gamma = \gamma_0(\rho/\rho_0)^{-1.173}$ .

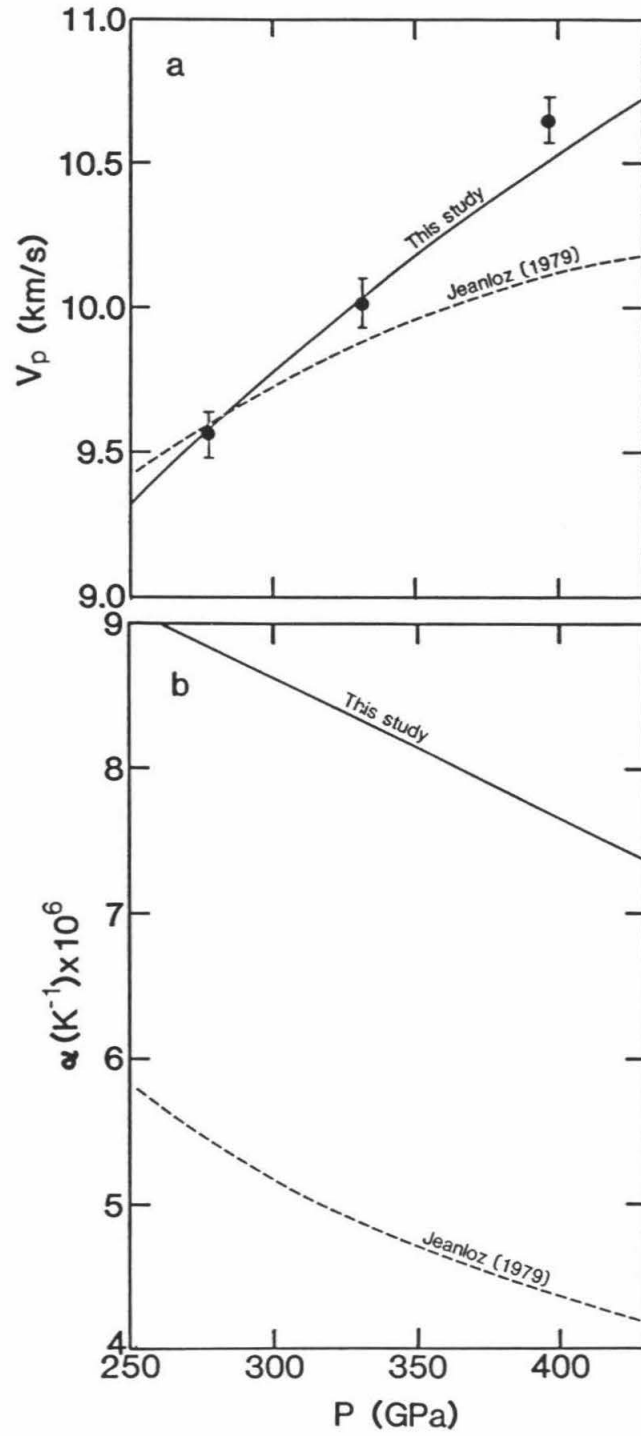


There is some disagreement (~30%) at high densities between our model and that of Jeanloz (1979), which is not surprising. The two models for  $\gamma$  agree quite well at low densities. Because our reevaluation of the experimental data for  $\gamma$  changed the values somewhat, the expression of Brown and McQueen (1986) now falls ~15% above the data. They also assumed that  $n=1$  in equation (30), while we allowed  $n$  to vary, with the result that our model  $\gamma$  has a stronger dependence than that of Brown and McQueen (1986). However our value of  $n=1.173$  indicates a weaker dependence than found by Jeanloz (1979) who obtained  $n=1.62$ .

Jeanloz (1979) also calculated  $K_S$  along the principal Hugoniot. Using equation (12) and the density along the McQueen et al. (1970) Hugoniot, we can obtain the values of  $V_b$  that correspond to the bulk moduli in Jeanloz's model. Comparison with the results of our model and the reanalyzed data of Brown and McQueen (1986) (figure 9a), shows that the use of the McQueen et al. (1970) Hugoniot results in higher values of  $V_b$  than our present fit would indicate. Jeanloz's (1979) model should give the proper results since it is simply a statement of thermodynamic identities, but the less suitable data available at the time that work was done gave rise to less accurate results.

Likewise, the volume thermal expansion coefficient,  $\alpha$  (figure 9b) in Jeanloz's (1979) model differs from the present model over the entire range shown. In this case, however, there are no data to test the relative merits of this result. The difference can be shown to be mainly a function of the relatively low specific heat Jeanloz assumed for the calculation, namely,  $c_p = 3R$  (with  $c_p > c_v$ ). Our higher specific heat, combined with the other differences between the two models,

Figure 9. a) Sound speeds predicted by the present model and that of Jeanloz (1979) using the Hugoniot of McQueen et al. (1970). Also shown are the reanalyzed data of Brown and McQueen (1986). Below 270 GPa, the Hugoniot does not represent a completely liquid state and thus cannot be compared with our model. b) Volume thermal expansion coefficients from our model and that of Jeanloz (1979).



results in our model giving a range of values for  $\alpha$  which is up to 75% larger than the estimates of Jeanloz (1979).

#### COMPARISON WITH THE CORE.

Our primary purpose in developing this equation of state was to aid in modelling the properties of the cores of the earth and planets. To investigate the constraints that our model places on the properties of the non-iron component of the Earth's core, we first compare our equation of state to an earth model. We use the Preliminary Reference Earth Model (PREM) of Dziewonski and Anderson (1981).

Since the fluid outer core is believed to be convecting and thus to have an adiabatic temperature gradient, the most appropriate comparison is between PREM and isentropes for liquid Fe. We have chosen to use four different isentropes, anchored at 3000, 4000, 5000, and 6000 K at the core-mantle boundary (CMB) pressure of 135.75 GPa. These are shown, labelled A, B, C, and D, respectively, in figure 10 together with the melting curve of pure Fe from Williams et al. (1987) and from Ahrens et al. (1990). A first point to note is that, as expected, the isentropes are all less steep than the melting curves, although the highest temperature curve is not greatly so. Thus, we find no support for the contention of Higgins and Kennedy (1971) that the core might freeze at shallower levels, rather than deeper.

We begin our comparison with PREM by examining the densities of liquid Fe and PREM (figure 11a). As is well known, the outer core



Figure 10. Temperatures along the isentropes used for comparison with PREM. Also shown for reference are the melting curves of Williams et al. (1987) and Ahrens et al. (1989).

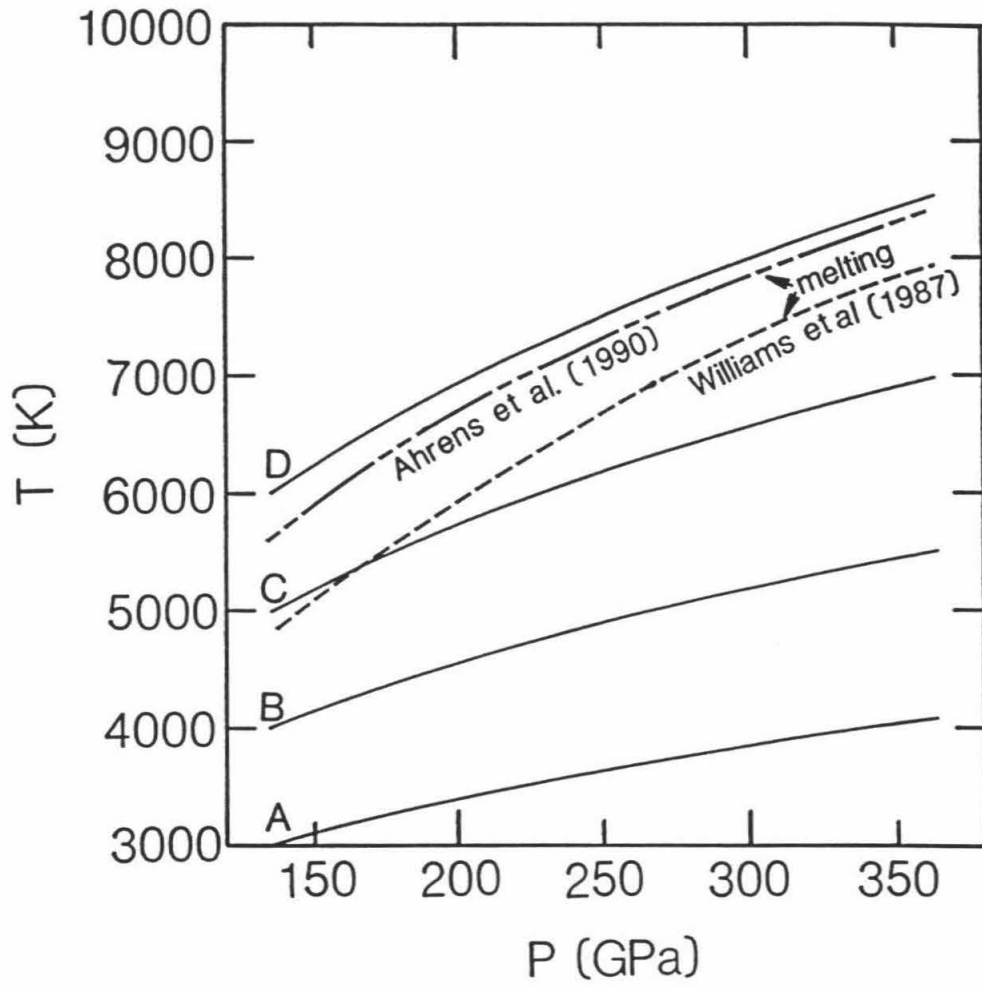
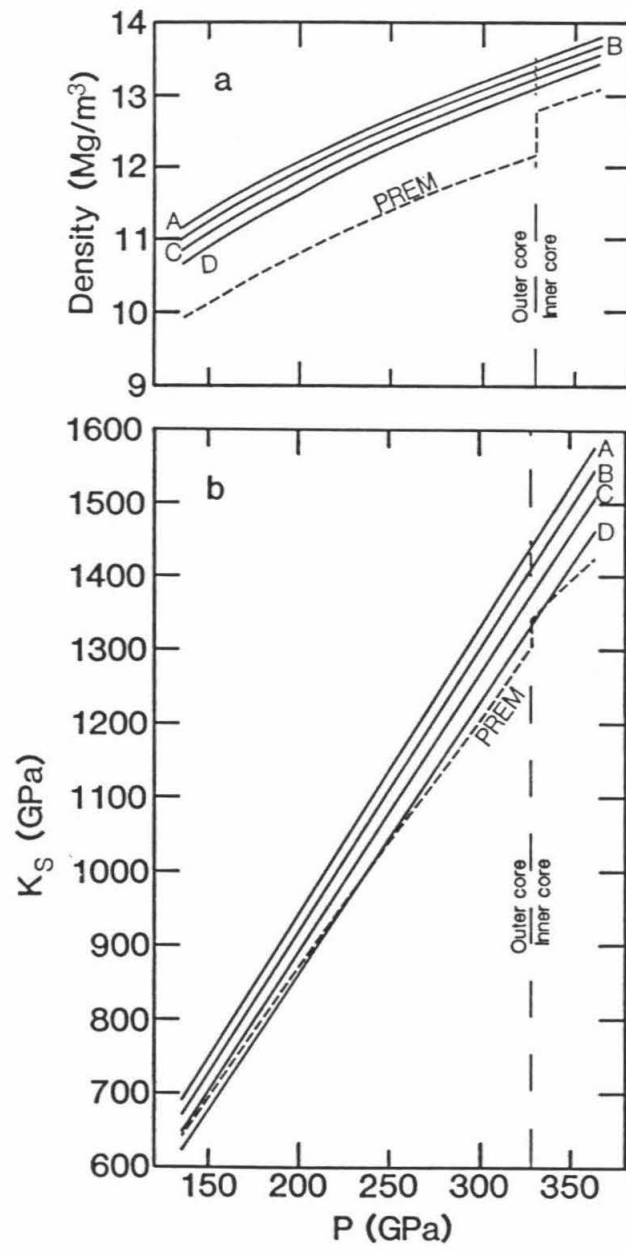


Figure 11. a) Densities of liquid Fe along the isentropes shown in figure 10, compared with the density of the core from PREM. b) Isentropic bulk moduli of liquid Fe along the isentropes, compared with PREM.



displays a density deficit relative to pure Fe. We find the value of that deficit to be from 8 to 10% for temperatures relevant to the core. We also note that the PREM inner core has a lower density than pure liquid Fe, by about 3 to 5%. This is only slightly larger than the estimated resolution of our model at these pressure-temperature conditions, but a similar result found by Jephcoat and Olsen (1987) gives us confidence that the effect we observe is real. There are several possible explanations for the inner core density deficit. First, the core may be at a much higher temperature than currently thought. This might be possible if a large quantity of oxygen is dissolved core and acts to raise the solidus and liquidus temperatures (Knittle and Jeanloz, 1988). Another possibility is that the solid phase in the inner core contains some amount of the light component responsible for the density deficit in the outer core (Jephcoat and Olson, 1986). A third alternative is that the inner core is not completely solid, but contains some fraction of melt (Fearn and Loper, 1981). Finally, the apparent density deficit might be simply due to the fact that the inner core density is poorly resolved in extant seismological earth models. Actually, any combination of these effects could explain the density discrepancy. Although we are currently unable to evaluate the relative merits of the different alternatives, we can at least place an upper limit on the fraction of the inner core that is liquid. Let us assume as a limiting case that the inner core liquid component is in good communication with the outer core and is therefore of the same composition as the outer core, and that the solid phase is pure Fe and has a density only slightly higher than that of pure liquid Fe. We can perform a mixing calculation at the inner core boundary,

where the density of the outer core liquid is known, with solid iron at the same conditions. We chose to estimate the density of solid Fe at the ICB conditions by the density of the liquid on isentrope A at 330 GPa (probably an overestimate because of the low temperature). We can estimate the density of solid Fe at the melting point to be about 1-2% higher than the density of the pure Fe liquid, based on a slope of  $dT_m/dP \approx 10 \text{ K/GPa}$  and assuming the entropy change on melting to be  $\Delta S_m \approx R$ . When we solve for the mixing ratio of these two densities, which will give the density of the PREM inner core at the ICB, we find an absolute upper limit on the mass fraction of liquid in the inner core of 50%. In reality, the liquid may be somewhat enriched in light elements relative to the outer core and the solid probably has a significant light element component itself. Both of these effects would tend to lower the estimated liquid fraction dramatically.

The other comparison that we would like to make is in the isentropic bulk modulus  $K_S$ . In figure 11b we see that  $K_S$  is only slightly higher for pure liquid Fe than for the core. Thus the non-iron component in the core is required to lower the bulk modulus of Fe by less than 1%, but must still lower the density of liquid Fe by close to 10%. There is some evidence that the effect of oxygen in Fe is to raise the bulk modulus, while the effect of sulfur is to lower it (see Jeanloz and Ahrens, 1980; Anderson et al., 1989). Since the presence of oxygen in the core is apparently unavoidable (Knittle et al. 1987), it seems likely that at least one more element, such as sulfur, will be required in order to develop a model composition that will successfully reproduce the properties of the outer core.

## CONCLUSION

Past models of the earth's core have been limited by the lack of a complete and accurate set of properties for liquid iron. The present equation of state is the first complete representation of the thermodynamic properties of liquid Fe at high pressures and provides a greater degree of self-consistency than previous simpler models that ignore electronic effects. The values of  $\rho_0 = 7037 \pm 12 \text{ kg/m}^3$  and  $K_{S0} = 110.02 \pm 1.34 \text{ GPa}$  at 1 bar ( $10^5 \text{ Pa}$ ) and 1811 K were constrained with the available experimental data obtained at 1 bar and did not require the use of high pressure data. Shock wave data were used to constrain the pressure derivatives of  $K_S$ :  $K_S' = 4.531$  and  $K_S'' = -.0337 \text{ GPa}^{-1}$ ; and the Grüneisen parameter:  $\gamma_0 = 2.80$ , and  $n = 1.173$  for  $\gamma \propto \rho^{-n}$ . Calculated properties from our model should be accurate to within 2% at low pressures and temperatures and 4% at core conditions. This model thus paves the way for more accurate calculations of the properties of candidate core compositions.

One major result of the present effort is the theoretical development of a realistic specific heat for a transition metal, which is valid for the supercritical fluid and for the liquid branch of the subcritical fluid. We find that, for temperatures greater than the melting point at a given pressure,  $3R \leq c_V \leq 4.6R$ .

Comparison of the properties displayed by our equation of state with those of PREM indicates that the non-iron component of the core must reduce the density of liquid Fe by 8 to 10%, while reducing the bulk modulus by only 1 to 2%. This may require at least two light elements in future compositional models. We also find that the inner

core is 3 to 5% less dense than pure liquid Fe. One likely explanation is that the inner core is not completely solid. The absolute upper limit to the mass fraction of liquid in the inner core is 50%, assuming a liquid of outer core composition and a pure Fe solid phase.

#### Acknowledgements.

We wish to thank D. Anderson and D. Stevenson for helpful discussions and suggestions concerning this work and to R. Jeanloz, E. Knittle, and Q. Williams for copies of their unpublished manuscripts. Support for this work was provided by the National Science Foundation. Contribution number 4803 of the Division of Geological and Planetary Sciences, California Institute of Technology.



## APPENDIX A. INTERATOMIC POTENTIAL CONTRIBUTION TO THE HEAT CAPACITY.

From equation (15), we have the potential internal energy of a liquid

$$E_{\text{pot}} = \int_0^{\infty} \varphi(r)g(r)r^2dr \quad (\text{A1})$$

The form of equation (A1) is deceptively simple. In reality, neither  $\varphi(r)$  nor  $g(r)$  is easily determined. Recently, Hausleitner and Hafner (1988) have presented a promising method of calculating the interatomic potentials of transition metals. Their work expands upon the earlier work of Wills and Harrison (1983), that uses a less accurate functional form for the s-electron contribution to  $\varphi(r)$ .

The development presented here is mostly that of Hausleitner and Hafner (1988) and Hafner and Heine (1986). While many of the equations presented are from these two studies, some of them have been simplified here. Our purpose in presenting this discussion in detail is to allow the reader to obtain a complete and coherent picture of the method we used to obtain a tractable expression for  $c_{\text{pot}}$ .

A note on the units used in this appendix is in order at this point. Because the energies and distances involved in discussions of interactions on the atomic level are quite small, it is customary to make a transformation to so-called "atomic units." Since the literature on atomic interactions is rather uniform in this respect, including Hausleitner and Hafner (1988) and Hafner and Heine (1986), and since the use of atomic units results in equations that are less awkward in presentation, we have chosen to adhere to this convention and so present

this discussion using atomic units. In this system, energies are expressed in Rydbergs ( $1 \text{ Ryd} = 2.1797 \times 10^{-18} \text{ J}$ ) and distances are in units of the Bohr radius of the hydrogen atom,  $a_0 = 5.29177 \times 10^{-11} \text{ m}$ .

We begin by noting that  $\varphi(r)$  can be separated into an s-electron part,  $\varphi_s(r)$ , and two d-band contributions: a bonding term,  $\varphi_b(r)$ , and a repulsive term  $\varphi_r(r)$  due to the shift of the d-band centers:

$$\varphi(r) = \varphi_s(r) + \varphi_b(r) + \varphi_r(r) \quad (\text{A2})$$

where (Hausleitner and Hafner, 1988)

$$\varphi_b(r) = -2Z_d(1-Z_d/10)(12/N_c)^{1/2}(28.06/\pi)R_d^3/r^5 \quad (\text{A3})$$

$$\varphi_r(r) = Z_d(450/\pi^2)R_d^6/r^8 \quad (\text{A4})$$

and (Hafner, 1987)

$$\varphi_s(r) = \frac{2Z_s^2}{r} \left[ 1 + 16 \int_0^\infty \frac{\chi(q)}{\varepsilon(q)} \cos^2(qR_c) \sin(qr) q^{-3} dq \right] \quad (\text{A5})$$

Here,  $Z_d$  is the number of electrons per atom in the d-band,  $Z_s$  is the number of s-electrons per atom,  $R_c$  is the radius of an empty core about which the s-electron term is built (Ashcroft, 1966),  $R_d$  is the d-state radius, and  $N_c$  is the nearest neighbor coordination number at the zero

point.  $\chi(q)$  and  $\epsilon(q)$  are the Lindhard susceptibility and dielectric screening function, respectively, of the electron gas (Hafner, 1987).

Hybridization between the d and s states is taken into account by varying the relative values of  $Z_s$  and  $Z_d$ . Hausleitner and Hafner (1988) give  $Z_s=1.5$  and  $Z_d=6.5$  for Fe in the liquid state. They also use  $N_c=8$ , since Fe is in the bcc  $\alpha$  phase at the zero point. They find that these values give accurate results for the entropy of liquid Fe at 1 bar, so we have chosen to use their values in our calculations.

Equations (A3) and (A4) are already analytic and may be used as they are. Equation (A5), however, is more difficult and, in general, nonanalytic. Hafner and Heine (1986) have developed an analytic approximation for equation (A5) which is quite accurate enough for our purposes. They give

$$\varphi_s(r) = \frac{Z_s^2}{r} [\frac{1}{4}H(r-2R_c) + \frac{1}{2}H(r) + \frac{1}{4}H(r+2R_c)] \quad (\text{A6})$$

where  $H(r)$  is the real space screening function and is broken down into a repulsive term  $H_{\text{rep}}(r)$  and an oscillatory term  $H_{\text{osc}}(r)$ :

$$H(r) = H_{\text{rep}}(r) + H_{\text{osc}}(r) \quad (\text{A7})$$

$H_{\text{rep}}(r)$  is further broken down:

$$H_{\text{rep}}(r) = H_{r1}(r) + H_{r2}(r) \quad (\text{A8})$$

$$H_{r1}(r) = e^{-Q_1 r} \quad (\text{A9})$$

$$H_{r2}(r) = \frac{-BQ_2^5 r}{8(2k_F)^4} e^{-Q_2 r} \left\{ \left[ -3 + \left( \frac{2k_F}{Q_2} \right)^2 \right] + \left[ 1 + \left( \frac{2k_F}{Q_2} \right) \right] Q_2 r \right\} \quad (\text{A10})$$

where

$$Q_1 = \kappa_{\text{TF}} [2\varepsilon(2k_F) - 1/\pi k_F]^{-1/2} \quad (\text{A11})$$

$$Q_2 = k_F \left[ \left( \frac{.1875B}{h(k_F) - h_{r1}(k_F) - h_{\text{osc}}(k_F)} \right)^{1/3} - 1 \right] \quad (\text{A12})$$

Here,  $k_F$  is the Fermi wavevector and  $\kappa_{\text{TF}} = (4k_F/\pi)^{1/2}$  is the Thomas-Fermi screening constant.  $H(r)$  and  $h(q)$  are related by

$$H(r) = 1 - \frac{2}{\pi} \int_0^\infty h(q) \frac{\sin qr}{q} dq \quad (\text{A13})$$

and  $h(q)$  is given by

$$h(q) = \frac{\kappa_{\text{TF}}^2 \chi_N(q)}{q\varepsilon(q)} \quad (\text{A14})$$

$\chi_N(q)$  is the Lindhard susceptibility normalized such that  $\chi_N(0) = 1$ .

Pettifor and Ward (1984) give the following approximation for  $\chi_N(q)$ :

$$\chi_N(q) = \frac{1}{2} + \frac{4k_F^2 - q^2}{8k_F q} \ln \left| \frac{q+2k_F}{q-2k_F} \right| \quad (\text{A15})$$

$\epsilon(q)$  is given by

$$\epsilon(q) = 1 + \frac{\kappa_{TF}^2}{q^2} (1-G(q)) \chi_N(q) \quad (\text{A16})$$

Ichimaru and Utsumi (1981) have modelled the local field correction  $G(q)$  for a strongly coupled electron liquid as

$$G(q) = 16ay^4 + 4by^2 + c + [16ay^4 + (4b+32a/3)y^2 - c] \times \frac{1-y}{2y} \ln \left| \frac{1+y}{1-y} \right| \quad (\text{A17})$$

where  $y = q/2k_F$ ,  $a = 0.029$ , and

$$b = \frac{9}{16}\Gamma - \frac{3}{64}(1-g(0)) - \frac{16}{15}a \quad (\text{A18})$$

$$c = \frac{-3}{4}\Gamma + \frac{9}{16}(1-g(0)) - \frac{16}{5}a \quad (\text{A19})$$

The constant  $\Gamma$  is given by (Pines and Nozières, 1966; Hafner and Heine, 1986)

$$\Gamma = \frac{1}{4} + .00634R_s \quad (\text{A20})$$

where  $R_s$  is the radius of a sphere containing, on average, one  $s$ -electron. The local field correction is related to the electron gas radial distribution function at the origin by

$$\lim_{q \rightarrow \infty} G(q) = 1 - g(0) \quad (\text{A21})$$

From values given by Ichimaru and Utsumi (1981), we find that  $g(0)$  is approximated by

$$g(0) \approx \frac{.558}{R_s + 1} \cdot 0055(R_s - 1) \quad (\text{A22})$$

The variable  $B$  in equations (A10) and (A12) is given by

$$B = \pi k_F (2\varepsilon(2k_F) - 1) + 4\gamma - 1 - \frac{13}{4\pi k_F} e^{-2} \quad (\text{A23})$$

The terms  $h_{r1}(q)$  and  $h_{osc}(q)$  are related to  $H_{r1}(r)$  and  $H_{osc}(r)$  by expressions equivalent to equation (A13) and are given by (Hafner and Heine, 1986)

$$h_{r1}(q) = (1 + q^2/Q_1^2)^{-1} \quad (\text{A24})$$

$$h_{\text{osc}}(q) = \frac{y}{2\pi k_F \varepsilon(2k_F)} [1 - 5.5(1-y)](1-y) \times \ln(1-y) \exp[-2(1-y)] \quad (\text{A25})$$

for  $0 \leq y < 1$ .

For the oscillatory part  $H_{\text{osc}}(r)$  of the real space screening function, Hafner and Heine (1986) give

$$H_{\text{osc}}(r) = \frac{2}{\pi^2 k_F \varepsilon(2k_F)} [\cos(2k_F r) (\text{Im}I_1(\mu) + 2\text{Im}I_2(\mu)) - 3.5\sin(2k_F r) \text{Re}I_2(\mu)] \quad (\text{A26})$$

where

$$I_1(\mu) = \mu^{-2}(1 - \gamma_e - \ln\mu) \quad (\text{A27})$$

$$I_2(\mu) = \mu^{-3}(3 - 2\gamma_e - 2\ln\mu) \quad (\text{A28})$$

$$\mu = 2 - 2ik_F r \quad (\text{A29})$$

where  $\gamma_e$  is Euler's constant.

Equations (A2)-(A28) provide the best estimate of  $\varphi(r)$  currently available for a transition metal. Hausleitner and Hafner (1988) use  $R_c = 1.37 a_0$  and  $R_d = 1.51 a_0$ .  $R_s$ , of course, depends on the density. The Fermi wavevector is given by (see Wallace, 1972)

$$k_F = 1.919158/R_s \quad (\text{A30})$$

Figure A1 shows the resulting  $\varphi(r)$  for three different densities of liquid Fe (note that there is no explicit temperature dependence). The potential well becomes deeper and the potential minimum moves to smaller radii as the density increases, reflecting increased importance of the d-band contributions at high densities.

Once we have  $\varphi(r)$ , we must determine the radial distribution function  $g(r)$  in order to evaluate the integral in equation (A1). The structure of a liquid is described by a set of integral equations relating the interatomic potential to the correlation of atomic positions. The basic equations may be found in a number of sources and can be stated as (Rosenfeld and Ashcroft, 1979)

$$h(r) = c(r) + n \int d\mathbf{r}' h(|\mathbf{r}-\mathbf{r}'|) c(\mathbf{r}') \quad (\text{A31})$$

$$c(r) = h(r) - \ln[g(r) \exp(-\varphi(r)/kT)] + B(r) \quad (\text{A32})$$

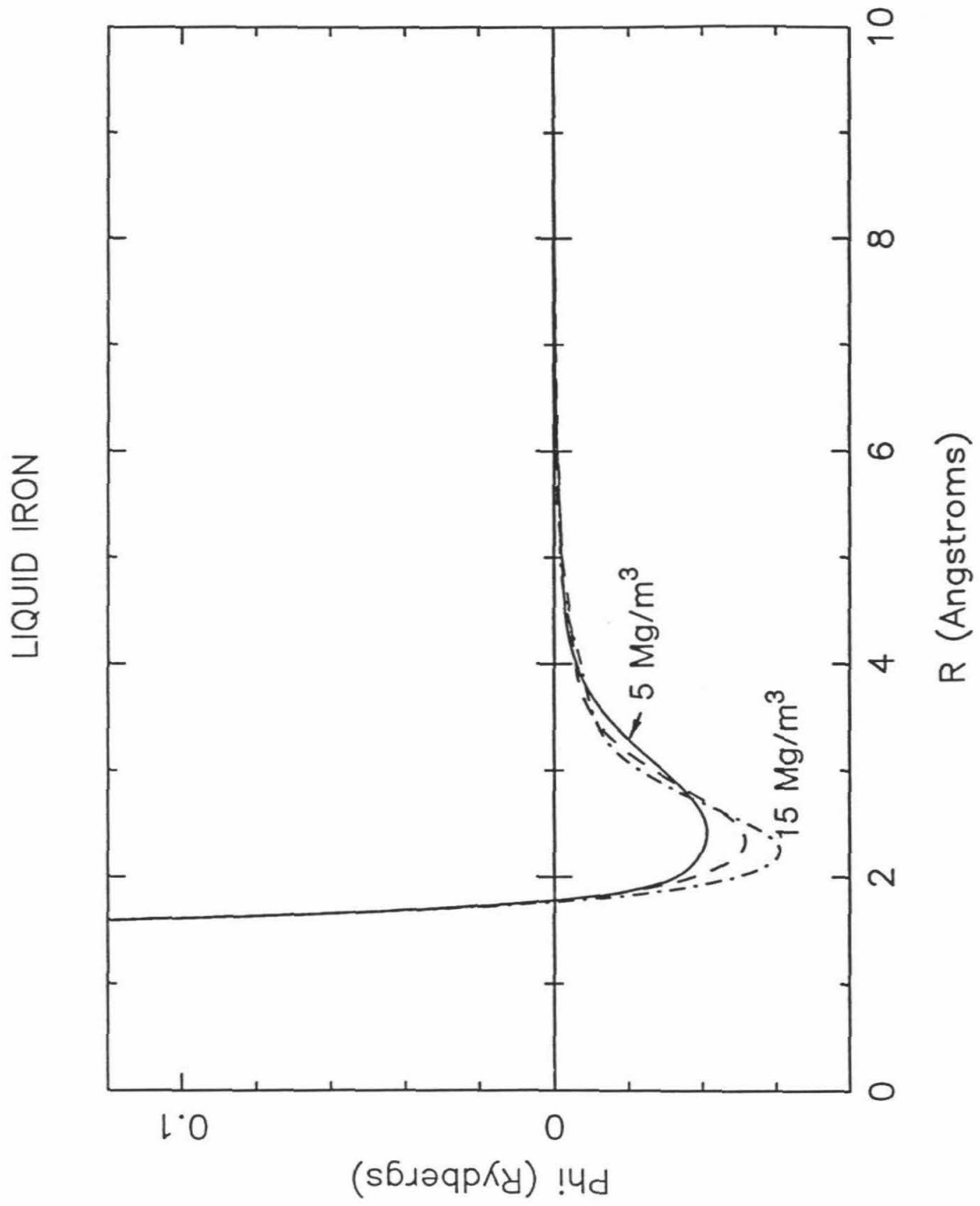
$$g(r) = 1 + h(r) \quad (\text{A33})$$

Equation (A31) is known as the Ornstein-Zernicke relation (Ornstein and Zernicke, 1914).

Equation (A32) provides a closure to the system. The variable  $B(r)$  is the sum of the so-called "bridge" functions in graphic analysis of two-point functions (see appendix 3.9 of Cole, 1967, for a brief discussion of graph theoretic analysis). A major difficulty in solving equations (A31)-(A33) is that  $B(r)$  is generally unknown. The usual approach is to assume a form for  $B(r)$  that can be determined *a priori*. There are numerous methods for approximating  $B(r)$ , the most simple of



Figure A1. Interatomic potentials for liquid iron at densities of 5000, 10000, and 15000 kg/m<sup>3</sup>. Increasing the density causes the d-band effects to be more important, resulting in a deeper potential well with the potential minimum at smaller radii.



which (and therefore one of the most widely used) is the Hypernetted Chain (HNC) equation:

$$g(r) = \exp(-\varphi(r)/kT)\exp(h(r)-c(r)) \quad (\text{A34})$$

where  $B$  is set to zero for all  $r$ . A second method, the Percus-Yevick (PY) equation, is simply a linearization of the HNC equation (Percus and Yevick, 1958):

$$g(r) = \exp(-\varphi(r)/kT)(1+h(r)-c(r)) \quad (\text{A35})$$

Both of these approaches, while very useful for certain applications, display marked deviations from the behavior of most real fluids and so are of limited utility for our purpose. There are other similar approaches, each of which is useful for some particular case, but none of which is good at describing a liquid transition metal.

Calculation of a realistic  $g(r)$  for liquid transition metals should, however, be readily accomplished by more careful estimates of  $B(r)$ . The two basic approaches are to solve for a  $B(r)$  which results in a thermodynamically self-consistent set of equations or to choose a  $B(r)$  that one has reason to believe is realistic for the case at hand. We have chosen the second of these two options, primarily because this approach is much simpler in practice. Rosenfeld and Ashcroft (1979), Lado et al. (1983), and Zerah and Hansen (1986) argued that  $B(r)$  is

basically the same set of functions for all potentials and that one can therefore simply use the  $B(r)$  for a hard sphere fluid, with the packing fraction  $\eta$  of the hard spheres used as an adjustable parameter to bring about self-consistency. They call this approach the Modified Hypernetted Chain (MHNC). We have used a variation of this approach. We found that when the HNC equation is used, we can reproduce the experimental radial distribution function of Waseda and Suzuki (1970) for liquid Fe at the correct density, but at the wrong temperature. We chose to take the difference between  $\varphi(r)/kT$  at the proper temperature (1893 K at  $6964.2 \text{ kg/m}^3$ ) and at the temperature (666.4 K) required to give the observed first peak height and position in  $g(r)$ , and use that difference to obtain  $B(r)$ .

We defined this difference to be  $B(r)$  at the experimental conditions, and then required  $B(r)$  to vary proportional to  $B(r)$  for the hard sphere fluid at the same radius relative to the Wigner-Seitz radius  $r_{ws} = (3/4\pi n)^{1/3}$  and at the same packing fraction. The packing fraction was obtained from the density and hard sphere radius (obtained via the usual condition  $r_{hs} = (r:\varphi(r) = \varphi_{\min} + 3kT/2)$ ). Use of this  $B$  resulted in solution for a fluid that behaved much like real liquid Fe.

We solved the MHNC equation for the quantity  $h(r)-c(r)$  as a function of  $r$ , using a modification of the approach suggested by Gillan (1979), but using the implementation of the Newton-Raphson method given by Press et al. (1986). A typical relatively low-temperature  $g(r)$  which results from our calculations is shown in figure A2. Energies were then obtained at a series of densities and temperatures by numerical evaluation of equation (A1). In order to obtain  $c_{\text{pot}}$ , we fit these

energies with an analytic function of  $T$  and  $\rho$ , which could then be differentiated to give  $c_{\text{pot}}$ . The final expression for  $c_{\text{pot}}$  is

$$c_{\text{pot}} = \frac{\theta}{\theta+T}(1.5R+\Lambda T+\Xi T^2+T T^3) \quad (\text{A36})$$

$$\theta(\text{K}) = 372.21+6.1653\times 10^{-3}\rho+1.9008\times 10^{-6}\rho^2-7.014\times 10^{-11}\rho^3 \quad (\text{A37})$$

$$\Lambda(\text{J/kg}\cdot\text{K}^2) = 6.2534\rho^{-1.252}+5187.8\theta^{-1}\rho^{-.395} \quad (\text{A38})$$

$$\Xi(\text{J/kg}\cdot\text{K}^3) = -4.132\times 10^{-6}-337.5\theta^{-1}\rho^{-1.201} \quad (\text{A39})$$

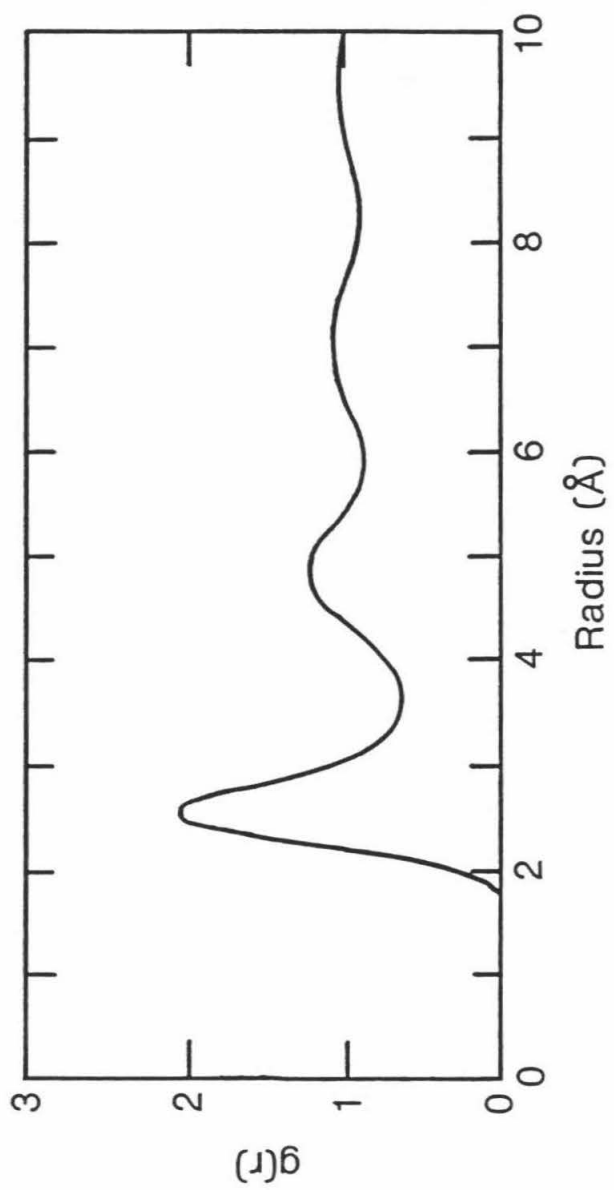
$$T(\text{J/kg}\cdot\text{K}^4) = 9.0151\times 10^{-4}\theta^{-1}\rho^{-.931} \quad (\text{A40})$$

for  $\rho$  in  $\text{kg/m}^3$ . The energy obtained upon integration from 0 K to some temperature  $T$  is

$$E_{\text{pot}} = \int_0^T c_{\text{pot}} dT \quad (\text{A41})$$

$$E_{\text{pot}} = \theta \left[ (1.5R-\Lambda\theta+\Xi\theta^2-T\theta^3)\ln(1+T/\theta)+\Lambda T \right. \\ \left. +\frac{1}{3}T T^3+\frac{1}{2}(\Xi-T\theta)(T^2-\theta T) \right] \quad (\text{A42})$$

Figure A2. Radial distribution function  $g(r)$  which results from our solution to the modified hypernetted chain equation for liquid Fe at a density of  $6000 \text{ kg/m}^3$  and a temperature of  $2100 \text{ K}$ .



APPENDIX B. THOUVENIN MODEL FOR SHOCK PROPAGATION IN A POROUS MEDIUM.

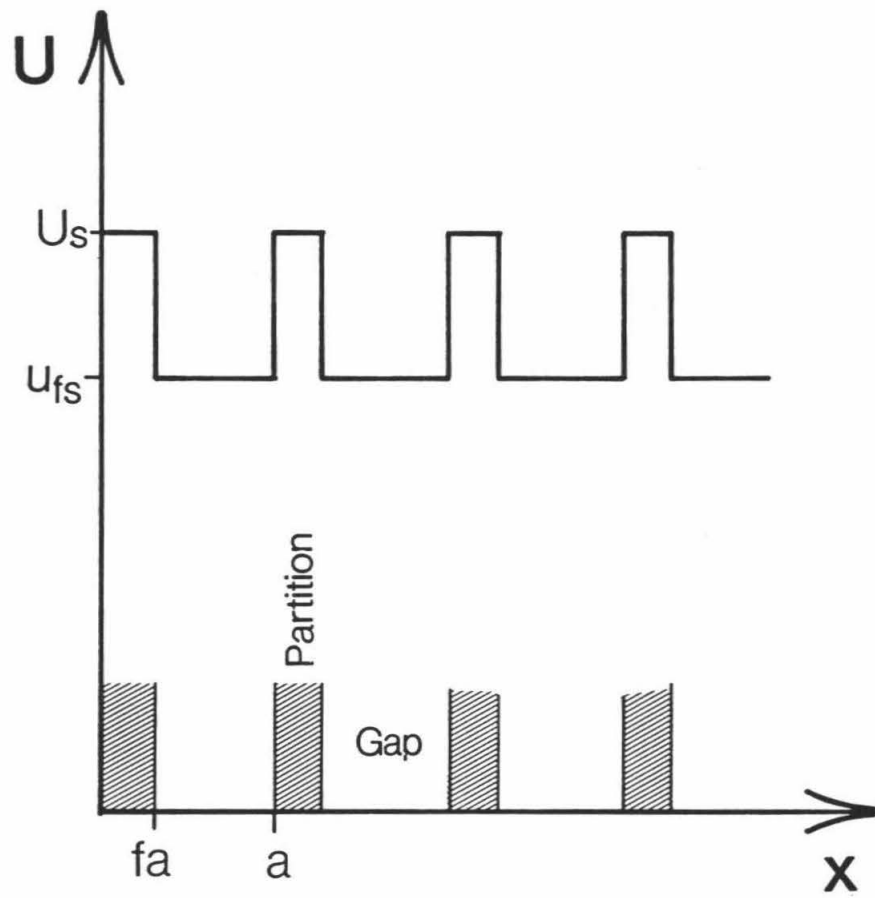
Most studies involving shock waves in porous media make, either implicitly or explicitly, the assumption that the medium may be treated as a continuum. For example, this approach was used by McQueen et al. (1970) and Jeanloz (1979) to obtain estimates of the thermodynamic Grüneisen parameter for iron. It should be obvious, however, that this assumption is usually seriously in error. Thouvenin (1964) noted this problem and developed a description of shock propagation in porous materials. We wish here to briefly recount and expand upon that development.

Let us first consider shock propagation in a uniform nonporous medium. The shock wave, travelling at a velocity  $U_s$ , will impart a velocity  $u_p$  to the material behind the shock wave. Upon arrival at a free surface, the shock wave is reflected as an isentropic release wave, travelling at the sound speed of the shock-compressed material, relative to the material. The release and consequent expansion of the material results in a velocity  $u_{fs}$  being imparted to the material at the free surface. If no phase changes involving large volume changes (i.e., vaporization) occur, then, in general,  $u_{fs} \approx 2u_p$ .

Now let us consider the propagation of a shock front in a porous material of bulk density  $\rho_{00} = f\rho_0$ , where  $\rho_0$  is the nonporous density of the material. It will help here if we think of the porous material as a series of partitions separated by intervening gaps (figure B1). Then as was pointed out by Thouvenin (1964), the shock front propagates at velocity  $U_s$  while in the partitions, but at velocity  $u_{fs}$  while



Figure B1. Assumed geometry of a porous material for this model, with the local propagation velocity  $U$  of the shock front.  $U = U_s$  in the solid material, but  $U = u_{fs}$  in the intervening gaps.



traversing a gap. The macroscopic phase velocity  $U_s^*$  of the shock front then becomes (Thouvenin, 1964):

$$U_s^* = [f/U_s + (1 - f)/u_{fs}]^{-1} \quad (\text{B1})$$

We can also develop an approximate expression for the equilibrium particle velocity,  $u_p^*$ , behind the shock front. Let us consider what happens when a partition which has been shocked and subsequently released (and is thus now travelling at velocity  $u_{fs}$  throughout) impacts the next partition. A nearly symmetrical pair of shock waves is generated, one propagating back into the previously shocked partition and one propagating into the new partition. If the new partition has a thickness  $fa$ , then the interface between the two partitions will have been in the shock-compressed state for a period of time  $t_1$  before the shock wave encounters the next free surface:

$$t_1 = fa/U_s \quad (\text{B2})$$

The reflected release wave then traverses the (now compressed ) partition in time  $t_2$ :

$$t_2 = fa(U_s - u_p)/U_s \cdot U_r \quad (\text{B3})$$

where  $U_r$  is the sound speed of the shocked material in the partition.

If, as a crude approximation, we take  $U_r \approx U_s$ , then the total time the interface is in the shock-compressed state is

$$\delta t = t_1 + t_2 = fa(2 - u_p/U_s)/U_s \quad (\text{B4})$$

Meanwhile, the time required for the shock front to traverse the total distance  $a$  is simply  $a/U_s^*$ . Finally, the time required for the shock wave generated by the next impact to reach the interface in question again given by equation (B2). Thus, the total fraction of time the interface is held in the shock-compressed state is

$$t^* = f(2 - u_p/U_s)/(U_s/U_s^* + f) \quad (\text{B5})$$

It should also be obvious from the fact that the initial shock wave is initiated at this point that the interface is the part of the system held at high pressure the longest. As such, it is this region which controls the equilibrium particle velocity, though the requirements of continuity and conservation of mass. To first order, this is thus

$$u_p^* = [t^*/u_p + (1 - t^*)/u_{fs}]^{-1} \quad (\text{B6})$$

or, under the assumption that  $u_{fs} = 2u_p$ ,

$$u_p^* = 2u_p/(t^* + 1) \quad (\text{B7})$$

## REFERENCES

- Ahrens, T. J., Tan, H., and Bass, J. D. (1990). Analysis of shock temperature data for iron. *High Press. Res.*, in press, 1990.
- Al'tshuler, L. V., Krupnikov, K. K., Ledenev, B. N., Zhuchikhin, V. I., and Brozchnik, M. I. (1958). Dynamic compressibility and equation of state of iron under high pressure. *Sov. Phys. JETP* 34(7): 606-619.
- Al'tshuler, L. V., Bakanova, A. A., and Trunin, R. F. (1962). Shock adiabats and zero isotherms of seven metals at high pressures. *Sov. Phys. JETP* 15:65-74.
- Al'tshuler, L. V., Bakanova, A. A., Dudoladov, I. P., Dynin, E. A., Trunin, R. F., and Chekin, B. S. (1981). Shock adiabatic curves of metals; new data, statistical analysis, and general laws. *J. Appl. Mech. Tech. Phys. Engl. Trans.* 22: 141-169.
- Anderson, O. L. (1986). Properties of iron at the Earth's core conditions. *Geophys. J. R. astr. Soc.* 84: 561-579.
- Anderson, W. W., Svendsen, B., and Ahrens, T. J. (1989). Phase relations in iron-rich systems and implications of the Earth's core. *Phys. Earth Plan. Inter.* 55: 208-220.

Ashcroft, N. W. (1966). Electron-ion pseudopotentials in metals. *Phys. Lett.* 23: 48-50.

Basin, A. S., Kolotov, Y. L., and Stankus, S. V. (1979). The density and thermal expansion of iron and ferrous alloys. *High Temp. High Press.* 11: 465-470.

Bass, J. D., Svendsen, B., and Ahrens, T. J. (1987). The temperatures of shock-compressed iron, in *High Pressure Research in Mineral Physics* (M. Manghni and Y. Syono, eds.), Terra, Tokyo, 393-402.

Boness, D. A., Brown, J. M., and McMahan, A. K. (1986). The electronic thermodynamics of iron under earth core conditions. *Phys. Earth Planet. Inter.* 42: 227-240.

Brown, J. M., and McQueen, R. G. (1986). Phase transitions, Grüneisen parameter, and elasticity for shocked iron between 77 GPa and 400 GPa. *J. Geophys. Res.* 91: 7485-7494.

Cole, G. H. A. (1967). *An Introduction to the Statistical Theory of Classical Simple Dense Fluids*. New York, Pergamon, 248pp.

Desai, P. D. (1986). Thermodynamic properties of iron and silicon. *J. Phys. Chem. Ref. Data* 15: 967-983.

Drotning, W. D. (1981). Thermal expansion of iron, cobalt, nickel, and copper at temperatures to 600K above melting. *High Temp. High Press.* 13: 441-458.

Dziewonski, A. M., and Anderson D. L. (1981). Preliminary reference Earth model. *Phys. Earth Planet. Inter.* 25: 297-356.

Fearn, D. R., Loper, D. E., and Roberts, P. H. (1981). Structure of the earth's inner core. *Nature* 292: 232-233.

Gillan, M. J. (1979). A new method of solving the liquid structure integral equations. *Mol. Phys.* 38: 1781-1794.

Hafner, J. (1987). *Hamiltonians to Phase Diagrams: The Electronic and Statistical-Mechanical Theory of sp-Bonded Metals.* New York, Springer-Verlag, 404 pp.

Hafner, J., and Heine, V. (1986). Theory of the atomic interactions in (s,p)-bonded metals. *J. Phys. F* 16: 1429-1458.

Hausleitner, C., and Hafner, J. (1988). Soft-sphere reference system in thermodynamic variational calculations. II: liquid transition metals. *J. Phys. F* 18: 1025-1036.

Higgins, G. H., and Kennedy, G. C. (1971). The adiabatic gradient and the melting point in the core of the Earth. *J. Geophys. Res.* 76: 1870-1878.

Ichimaru, S., and Utsumi, K. (1981). Analytic expression for the dielectric screening function of strongly coupled electron liquids at metallic and lower densities. *Phys. Rev. B* 24: 7385-7388.

Ivakhnenko, I. S., and Kashin, V. I. (1976). in *Zakonomernosti Vzaimodeistviya Zhidkogo Metalla s Gazami i Shlakami* (I. S. Kulikov, ed.). Moscow, Nauka, 135-142.

Jeanloz, R. (1979). Properties of iron at high pressures and the state of the core. *J. Geophys. Res.* 84: 6059-6069.

Jeanloz, R., and Ahrens, T. J. (1980). Equations of state of FeO and CaO. *Geophys. J. R. Astron. Soc.*, 62: 505-528.

Jephcoat, A. and Olson, P. (1987). Is the inner core of the earth pure iron? *Nature* 325: 332-335.

Knittle, E., Williams, Q., and Jeanloz, R. (1987). Reaction of core constituents with silicates and oxides: implications for the composition of the core-mantle boundary. *EOS* 68: 1210.

Knittle, E., and Jeanloz, R. (1989). The high-pressure phase diagram of  $\text{Fe}_{0.94}\text{O}$ : a possible constituent of the Earth's core. *J. Geophys. Res.*, submitted.



Krupnikov, K. K., Bakanova, A. A., Brazhnik, M. I., and Trunin, R. F. (1963). An investigation of the shock compressibility of titanium, molybdenum, tantalum and iron. *Sov. Phys. Dokl.* 8: 205-207.

Kurz, W., and Lux. B. (1969). Die Schallgeschwindigkeit von Eisen und Eisenlegierungen in festen und flüssigen Zustand. *High Temp. High Press.* 1: 387-399.

Lado, F., Foiles, S. M., and Ashcroft, N. W. (1983). Solution of the reference-hypernetted chain equation with minimization of free energy. *Phys. Rev. A* 28: 2374-2379.

Lucas, L. D. (1972). Densité de métaux à haute température (dans les états solide et liquide). *Mem. Sci. Rev. Met.* 69: 479-492.

Marsh, S. P. (1980). *LASL Shock Hugoniot Data*. Los Angeles, Univ. Cal. Press. 658pp.

McQueen, R. G., Marsh, S. P., Taylor, J. W., Fritz, J. N., and Carter, W. J. (1970). The equation of state of solids from shock wave studies. *in High Velocity Impact Phenomena* (R. Kinslow, ed.), 293-417.

Mulargia, F. (1977). Is the common definition of the Mie-Grüneisen equation of state inconsistent? *Geophys. Res. Lett.* 4: 590-592.

- Ornstein, L. S., and Zernicke, F. (1914). Accidental deviations of density and opalescence at the critical point of a single substance. Proc. Acad. Sci. Amst. 17: 793.
- Percus, J. K., and Yevick, G. L. (1958). Analysis of classical statistical mechanics by means of collective coordinates. Phys. Rev. 110: 1-13.
- Pettifor, D. G., and Ward, M. A. (1984). An analytic pair potential for simple metals. Solid State Commun. 49: 291-294.
- Pines, D., and Nozières, P. (1966). Theory of Quantum Liquids, v. 1: Normal Fermi Liquids. New York, Benjamin, 355 pp.
- Press, W. H., Flannery, B. P., Teukolsky, S. A., and Vetterling, W. T. (1986). Numerical Recipes. New York, Cambridge Univ. Press, 818 pp.
- Rosenfeld, Y., and Ashcroft, N. W. (1979). Theory of simple classical fluids: universality in the short-range structure. Phys. Rev. A 20: 1208-1235.
- Shaner, J. W., Hixson, R. S., Winkler, M. A., Boness, D. A., and Brown, J. M. (1988). Birch's law for fluid metals. in Shock Waves in Condensed Matters 1987 (S. C. Schmidt and N. C. Holmes, eds.), Elsevier, New York, 135-135.

Stevenson, D. J. (1980). Applications of liquid state theory to the earth's core. *Phys. Earth Planet. Inter.* 22: 42-52.

Stevenson, D. J. (1981). Models of the earth's core. *Science* 214: 611-619.

Svendsen B., Anderson, W. W., Ahrens, T. J., and Bass, J. D. (1989). Ideal Fe-FeS and Fe-FeO phase relations and the earth's core. *Phys. Earth Planet. Inter.* 55: 154-186.

Thouvenin, J. (1964). Action d'une onde de choc sur un solide poreux. *Compt. Rend.* 258: 3461-3464.

Tsu, Y., Takano, K., and Shiraishi, Y. (1985). The velocities of ultrasound in molten iron, cobalt, and nickel (in Japanese). *Bull. Res. Inst. Min. Dress. Met. Tohoku Univ.* 41: 1-8.

Wallace, D. C. (1972). *Thermodynamics of Crystals*. New York, Wiley, 484 pp.

Waseda, Y., and Suzuki, K. (1970). Atomic distribution and magnetic moment in liquid iron by neutron diffraction. *Phys. Stat. Sol.* 39: 669-675.

Williams, Q., Jeanloz, R., Bass, J., Svendsen, B., and Ahrens, T. J. (1987). The melting curve of iron to 250 gigapascals: a constraint on the temperature at Earth's center. *Science* 236: 181-182.

Williams, Q., and Jeanloz, R. (1989). Melting relations in the iron-sulfur system at ultra-high pressures: implications for the thermal state of the Earth. *J. Geophys. Res.*, submitted.

Wills, J. M., and Harrison, W. A. (1983). Interionic interactions in transition metals. *Phys. Rev. B* 28: 4363-4373.

Young, D. A., and Alder, B. J. (1971). Critical point of metals from the van der Waals model. *Phys. Rev. A* 3: 364-371.

Zerah, G., and Hansen, J. P. (1986). Self-consistent integral equations for fluid pair distribution functions: another attempt. *J. Chem. Phys.* 84: 2336-2343.

Chapter 2

SHOCK TEMPERATURES IN IRON SULFIDES: EXPERIMENTAL CONSTRAINTS ON PHASE  
RELATIONS AND SPECIATION IN THE SYSTEM FE-S AT HIGH PRESSURES

William W. Anderson and Thomas J. Ahrens

Division of Geological and Planetary Sciences, California Institute of  
Technology, Pasadena, CA 91125.

For submission to Journal of Geophysical Research.

**ABSTRACT.**

We have performed a series of experiments to measure the temperatures of Fe, FeS, and FeS<sub>2</sub> under shock compression to 240 GPa, and have constrained the melting curves of the latter two materials to 180 and 230 GPa, respectively. Our melting data for FeS agree with previous data obtained under static compression to 100 GPa. The resultant melting curve for FeS exhibits a very small slope ( $< 10$  K/GPa) for pressures above 100 GPa and falls at substantially lower temperatures than the melting curve of FeS<sub>2</sub> in the pressure range relevant to the earth's core. Application of a model phase diagram calculation, based on the phase relationships of transition metal - s,p metal systems at 1 bar, to the present data leads us to conclude that FeS begins to undergo peritectic decomposition at pressures slightly above 100 GPa at a temperature of  $\sim 3600$  K and that the sulfide phase in equilibrium with the eutectic liquid is FeS<sub>2</sub> above 170 GPa. We also find, based on a critical comparison of the liquidus behavior of the analog systems, that a significant quantity of the s,p metal (metallized sulfur in the present case) in the liquid phase is associated with atoms of the transition metal in a binary species. Assuming a completely liquid Fe-S outer core with the inner core boundary falling on the liquidus for the bulk outer core composition, the temperature at the top of the core is about 4700 K. Models for the freezing behavior of solutions, combined with the requirement that the core support shear waves below the inner core boundary, may not be compatible with the notion of a completely liquid outer core, however. For a model that allows suspended solid particles in the outer core, the adiabatic

temperature gradient must be steeper than for the completely liquid case, allowing a temperature drop across the core of up to 350 K more than the value of 1600-1700 K for the all liquid case. This effect, combined with a lower temperature for the inner core boundary admitted by a partially solid outer core, allows temperatures at the top of the outer core in the range from 3400 K to 4200 K, compared with the completely liquid value of 4700 K. Examination of the effects of a slurry on convective stability indicate that convection is not hindered in the outer core if the solid particles are sufficiently small to be entrained in the liquid flow.

## INTRODUCTION.

Sulfur has long been believed to be a light component of the predominantly iron core of the earth because of its cosmic abundance and its ability to dissolve readily into liquid iron, even at low pressure (Mason, 1966; Usselman, 1975a,b; Brett and Bell, 1969). Although arguments against a significant sulfur content in the core have been made on the basis of depletions of less volatile lithophile elements in mantle xenoliths (Ringwood, 1977; Ringwood and Kesson, 1977), such arguments ignore the complexity of the evolution of the earth and the processes involved, such as elemental partitioning and the effects of magmas with densities greater than coexisting crystals (Morgan and Anders, 1980; Rigden et al., 1984; Knittle and Jeanloz, 1989). As most models of core formation such as that of Stevenson (1981) would make the inclusion of any sulfur present almost unavoidable because of its solubility in liquid Fe and its effect on the melting temperature of Fe, an understanding of the phase relations and material properties in the Fe-S system is vitally important to questions of the formation and evolution of the core. This fact is reflected in the numerous studies of properties exhibited by the Fe-S system. Until recently, however, modelling of phase relationships in the Fe-S system under core conditions has been based on low-pressure data, often involving extrapolations over more than an order of magnitude in pressure (Usselman, 1975a,b; Anderson et al., 1987), as the only information for relevant pressures were indirect or nonexistent (Brown et al., 1984).

Fortunately this situation has begun to change. Recently, direct measurements have been obtained for the  $P$ - $T$  dependence of the melting of



pure Fe (Williams et al., 1987; Bass et al., 1987; Tan and Ahrens, 1990; Ahrens et al., 1990) and two different compositions in the Fe-S system (Williams and Jeanloz, 1990). The Fe results, in particular, made use of data from a judicious combination of experimental techniques to extend the range of measurements to over 200 GPa, well above the core-mantle boundary (CMB) pressure of 136 GPa (Dziewonski and Anderson, 1981).

In the present series of experiments, we have extended the measurements of melting of FeS to core pressures and obtained melting data for FeS<sub>2</sub> to over 200 GPa. We also obtain Fe melting data that are comparable to previous measurements made under static compression. Combination of the present data with the results of previous studies and comparison with suitable analogs allows us to obtain the first reliable estimates of the phase diagram of the Fe-S system at pressures relevant to the earth's core.

#### **EXPERIMENTAL TECHNIQUES.**

The basic experimental techniques used in the present study have been discussed elsewhere (Lyzenga, 1980; Kondo and Ahrens, 1983; Boslough, 1984; Schmitt et al., 1986; Bass et al., 1987; Tan and Ahrens, 1990; Ahrens et al., 1990), but will be briefly reiterated here. A sample of FeS or FeS<sub>2</sub> was sandwiched between a metal driver plate (baseplate) and a transparent window, in contact with both, to form a target assembly. The target assembly was placed in an evacuated chamber and impacted by a gun-accelerated projectile consisting of a

polycarbonate sabot and a metal flyer plate (figure 1). The impact of the flyer onto the baseplate generated a planar shock wave that propagated through the driver and sample and into the window. Thermal radiation from the sample-window interface was directed by an expendable mirror into a four-color pyrometer and the resulting signals were recorded on oscilloscopes and a 100 Mhz sample frequency digital recorder (Bass et al., 1987).

Most of the samples were optically thick films, which were vapor-deposited on the windows (Bass et al., 1987). The films were examined visually under high magnification, using both optical and electron microscopy, for gross morphology, thickness, and optical opacity. The compositions were also determined via quantitative energy dispersive x-ray spectroscopy and x-ray fluorescence spectroscopy. To the resolutions of these techniques with the thin films, the compositions were found to be stoichiometric FeS and FeS<sub>2</sub>. The thickness of the films was generally on the order of 1  $\mu\text{m}$ , as determined by direct measurement of the broken films viewed edge-on with the electron microscope. Attempts were made to detect porosity at  $\mu\text{m}$  scales by morphologic studies and optical searches under high magnification for regions of light transmission. No random porosity was detected, although the films, which consisted of thin single crystal domains several mm across, did show gaps at the crystal boundaries (figure 2). Care was taken to exclude these gaps from the visible portion of the sample during the experiments. Searches for porosity at submicron scales using backscattered electron images were fruitless (figure 2).

The sample for shot LGG217 was a single crystal slab of natural pyrite, 2.633 mm thick, with an archimedian density of  $4.945 \pm 0.002 \text{ Mg/m}^3$ .

Figure 1. Diagram of a typical shock temperature experiment (top view). The configuration shown is for the four channel pyrometer, which uses a series of beamsplitters to direct radiation from the sample-window interface into the four detectors.

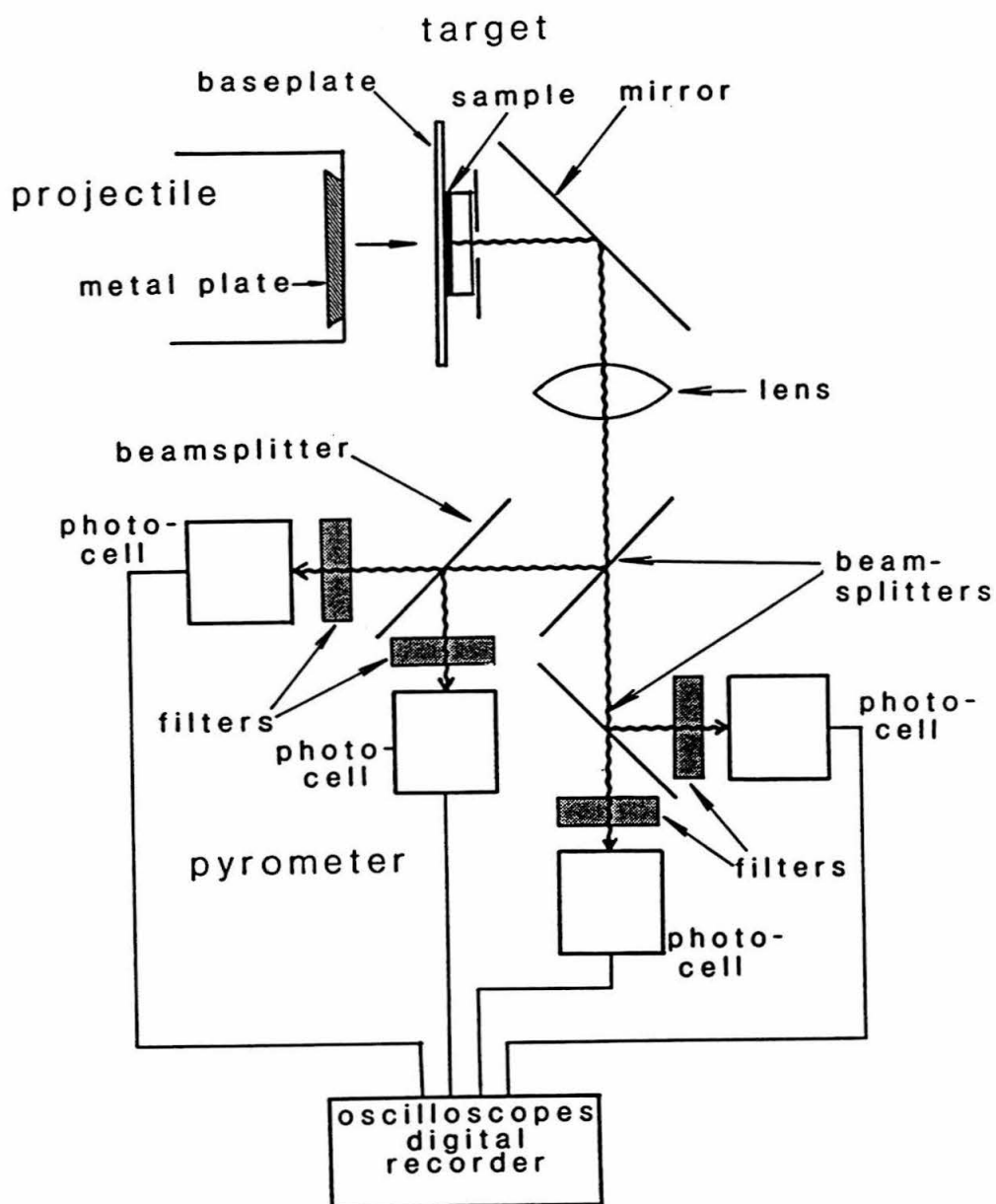
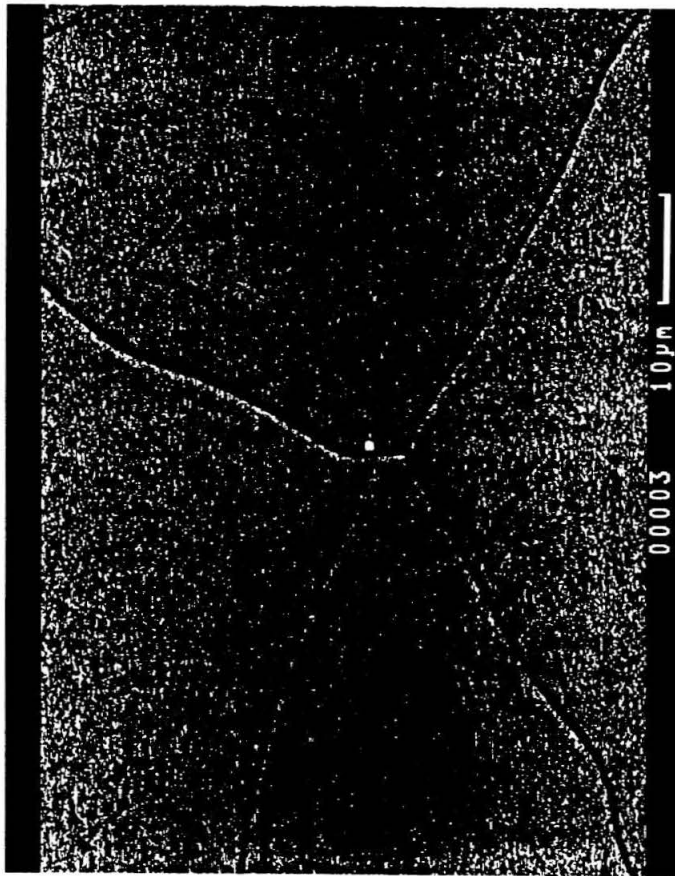


Figure 2. Scanning electron micrograph of a typical crystal boundary gap in a thin film sample, imaged with backscattered electrons to show differences in atomic number. The  $\text{Al}_2\text{O}_3$  window shows through the gaps as black. Although some slight variation in thickness is detectable within the domains, in bands parallel to the boundaries, there is no evidence for small scale porosity. The mottling in the image is due to the electron counting statistics.



The slab was ground flat to a thickness of 2.633 mm, and the surface contacting the window was polished and tested, using the window as an optical flat under Na light, until the sample surface visible during the experiments deviated by less than  $\sim .25 \mu\text{m}$  from the shape of the window surface, based on interference fringes observed at the interface when it is viewed through the window.

The raw signals from the experiments were converted to temperatures by minimization of the function

$$\chi^2 = \sum_i \left[ \left( V_{\text{obs},i} - \theta_i A_s \int_0^\infty I(\lambda, T) R_i(\lambda) d\lambda \right) / \sigma_{\text{obs},i} \right]^2 \quad (1)$$

where  $V_{\text{obs},i}$  is the observed voltage from the  $i$ 'th pyrometer channel,  $R_i(\lambda)$  is the spectral response of channel  $i$ ,  $\theta_i$  is the solid angle subtended by the active surface of the detector for channel  $i$ , as viewed from the emitting surface of the sample-window interface,  $A_s$  is the visible area of the emitting surface, and  $I(\lambda, T)$  is the graybody Planck function:

$$I(\lambda, T) = \frac{2\epsilon c_1}{\lambda^5 [\exp(c_2/\lambda T) - 1]} \quad (2)$$

Here,  $\epsilon$  is the emissivity,  $\lambda$  is the wavelength,  $T$  is the temperature,  $c_1 = 5.9544 \times 10^{-17} \text{ Wm}^2/\text{sr}$ , and  $c_2 = 1.4388 \times 10^{-2} \text{ mK}$ . The values of  $R_i(\lambda)$  used include the effects of the optical components in the system and Fresnel reflection at the rear surface of the window (Born and Wolf, 1980,

chapter 1). It should be noted that the internal (Fresnel) reflection of both  $\text{Al}_2\text{O}_3$  and  $\text{LiF}$  is negligible at the wavelengths of interest (determined from data provided by the manufacturer). During the fitting process, generally, both  $\epsilon$  and  $T$  were allowed to vary. With the thin films, the earliest usable timestep (determined from the rise time of the electronics and the limitations of the recording equipment) was used, generally 10 ns after arrival of the shock wave at the sample-window interface. This was done to avoid complications arising from conduction from the sample-baseplate interface, which occurs on a timescale of  $\sim 50$  ns for a  $1\ \mu\text{m}$  thick film with a thermal conductivity similar to that of Fe. In cases where only one pyrometer channel gave usable data, or where the data indicated that sample time deviations from different channels were unacceptable, one-channel fits were performed using an enforced  $\epsilon$  established from other experiments on the same sample composition.

The pressures achieved during the experiments were determined from the measured impact velocities of the projectiles using the impedance matching technique (see Ahrens, 1987, for a recent review). This technique requires the knowledge of the shock Hugoniot curves of the materials in the target and flyer plate. These are expressed in the form

$$U_s = C_0 + su_p \quad (3)$$

where  $U_s$  and  $u_p$  are the shock wave velocity and particle velocity, respectively, in the reference frame of the unshocked material. The



corresponding pressure and density of the shocked material are calculated, assuming the shock wave is steady, via (Rice et al., 1958):

$$P_H = \rho_0 U_s u_p \quad (4)$$

$$\rho_H = \rho_0 U_s (U_s - u_p)^{-1} \quad (5)$$

where  $P_H$  and  $\rho_H$  are the Hugoniot pressure and density and  $\rho_0$  is the initial density. Table 1 contains a list of the values of  $\rho_0$ ,  $C_0$ , and  $s$  used for this study.

Because of impedance mismatch between the sample and window, the final state of the sample represents either release or compression from the initial shock state. The path followed to the final state from the initial shock state is approximately isentropic in either case and involves pressure changes of a few percent at most.

The experimental details for four experiments, numbers 650, 722, 723, and 724, were somewhat different from those described in the preceding paragraphs. The samples for these shots were powders, were placed into metal confining rings and compressed to ~30% porosity. The powder for shot 723 was natural pyrrhotite of composition  $Fe_{.88}S$  (Ahrens, 1979; Brown et al., 1984; Anderson and Ahrens, 1986), while the other three were Fe with a nominal purity of 99.9%. In these experiments, we made use of a 500 channel optical multichannel analyzer

Table 1.

Shock Hugoniot parameters used in this study.

Material	$\rho_0$ (Mg/m <sup>3</sup> )	$C_0$ (km/s)	$s$	Reference
W	19.235	4.040	1.23	1
Ta	16.656	3.430	1.19	1
Fe	7.850	3.955	1.58	2
Al	2.712	5.380	1.34	1
Cu	8.930	3.940	1.489	1
FeS(1)	4.829	2.947	1.578	3
(s)		3.865	1.351	3
FeS <sub>2</sub>	5.011	5.478	1.401	4
Al <sub>2</sub> O <sub>3</sub>	3.977	8.724	0.975	1
LiF	2.640	5.148	1.353	5

---

References: (1) Marsh (1980), (2) Brown and McQueen (1986), (3) Brown et al. (1984), (4) Ahrens and Jeanloz (1987), (5) Carter (1973).

with a grating spectrometer (Kondo and Ahrens, 1983; Schmitt et al., 1986), rather than the pyrometer. This detector system gave time-integrated spectra, rather than time-resolved signals, but we did determine the time dependence of the total luminance by using a beamsplitter to divert some of the light from the experiment to a photodiode and recording the resulting signal with the digital recorder and oscilloscopes.

The treatment of the data for the porous samples was also somewhat different. Instead of the full Planck graybody, we used a linearized version to improve computation time. This will be discussed further later. The pressures in the windows in these experiments were determined directly from shock velocities in the windows, which were measured by a series of Hugoniot shorting pins (Brown et al., 1984) and the time-resolved signal from the broadband photodiode.

#### EXPERIMENTAL RESULTS AND DATA ANALYSIS.

Table 2 presents the results from the experiments. The interface temperatures,  $T_I$ , as a function of final pressure,  $P_F$ , are presented graphically in figure 3. To obtain temperatures that are useful from the standpoint of determining material properties and phase relationships, we apply the techniques developed by Urtiew and Grover (1974), Grover and Urtiew (1974), and Tan and Ahrens (1990) to the data analysis. Specifically, the observed temperature at the sample-window interface is related to either the melting temperature or the final release (or compression) state temperature by a series of expressions based on the thermal diffusion equation (see also Carslaw and Jaeger, 1959).

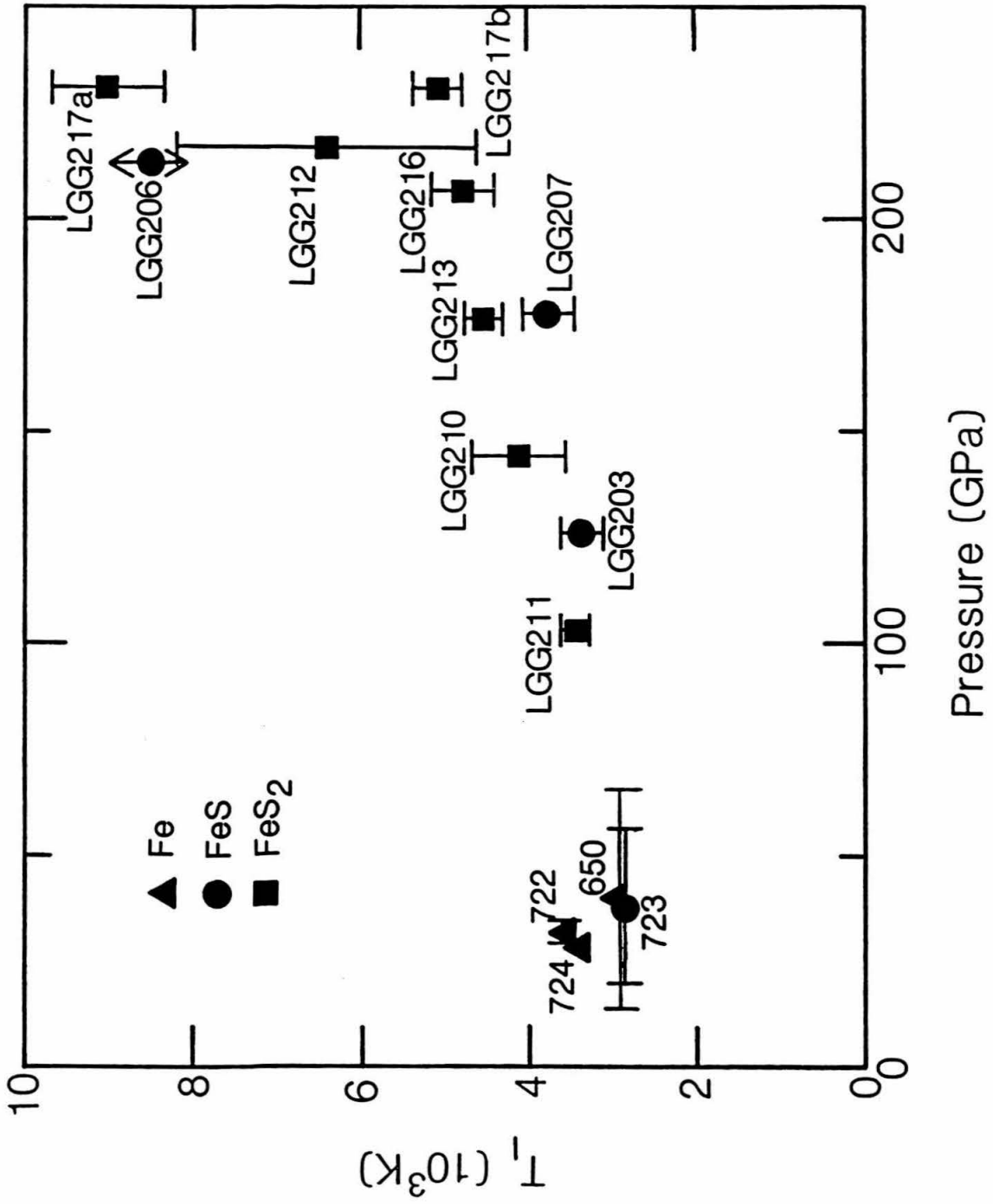
Table 2.

Experimental conditions and measured interface temperatures ( $T_I$ ) and emissivities ( $\epsilon$ ).

Experiment	Driver Matl.	Flyer Matl.	Sample Matl.	Window Matl.	Impact Velocity (km/s)	$T_I$ (K)	$\epsilon$
650	Fe	W	Fe	Al <sub>2</sub> O <sub>3</sub>	1.469	2918±34	.400±.051
722	Fe	W	Fe	LiF	2.240	3565±38	1.31±.090
723	Fe	W	Fe <sub>.88</sub> S	LiF	1.944	2852±34	.291±.011
724	Fe	W	Fe	LiF	1.963	3389±31	.842±.053
LGG203	Fe	Fe	FeS	Al <sub>2</sub> O <sub>3</sub>	4.157±.004	3355±215	.2885*
LGG206	Fe	Fe	FeS	Al <sub>2</sub> O <sub>3</sub>	6.203±.003	8498±5200	.2885*
LGG207	Fe	Fe	FeS	Al <sub>2</sub> O <sub>3</sub>	5.404±.020	3751±301	.247±.135
LGG210	Fe	Fe	FeS <sub>2</sub>	Al <sub>2</sub> O <sub>3</sub>	5.2959±.0021	4097±281	.403±.155
LGG211	Al	Fe	FeS <sub>2</sub>	Al <sub>2</sub> O <sub>3</sub>	6.2284±.0054	3452±191	.257±.074
LGG212	Cu	Fe	FeS <sub>2</sub>	Al <sub>2</sub> O <sub>3</sub>	6.2624±.0007	6379±1818	.041±046
LGG213	Ta	Fe	FeS <sub>2</sub>	Al <sub>2</sub> O <sub>3</sub>	5.3808±.0113	4518±221	.346±080
LGG216	Ta	Ta	FeS <sub>2</sub>	Al <sub>2</sub> O <sub>3</sub>	6.1771±.0024	4773±371	.585±187
LGG217	Ta	Ta	FeS <sub>2</sub>	Al <sub>2</sub> O <sub>3</sub>	6.649±.186	9002±651	.321±069
						5049±278	.697±.156

\* Emissivity constrained by other experiments on the same composition.

Figure 3. Measured interface temperatures,  $T_I$ , as a function of the final (observed) pressure state. The circles denote FeS, while the squares denote FeS<sub>2</sub>.



Let us first begin by examining the interface temperatures depicted in figure 3. Both FeS and FeS<sub>2</sub> data show a series of points falling on trends of very slowly increasing temperature with increasing pressure. The highest-pressure points in both cases fall well above these trends and, for FeS<sub>2</sub>, the lowest-pressure datum falls slightly below the trend. This is exactly what we would expect if the intermediate data represented a phase transition with a large latent heat (Tan and Ahrens, 1990). Based on the work of Brown et al. (1984) for FeS, and Ahrens and Jeanloz (1987) for FeS<sub>2</sub>, we conclude that those intermediate points indicate melting behavior in the sulfide samples. Points off the trend represent final states that are either completely solid (low pressure) or liquid (high pressure), and can thus be used to obtain Hugoniot temperatures in those phases.

We use the techniques of Tan and Ahrens (1990) to obtain melting temperatures or Hugoniot temperatures, as appropriate, from the interface temperatures. The particular expression we must use for the analysis is dependent upon the processes active during the experiment. These are discussed fully by Tan and Ahrens (1990).

Briefly, we begin by noting that the final state of the sample may be in the completely solid, completely liquid, or partially molten states, depending on the actual temperature of the sample relative to its melting temperature. The window temperature, however, is expected to fall well below the window melting curve. The higher compressibilities of the samples than the window material chosen for most of the experiments (Al<sub>2</sub>O<sub>3</sub>) also result in much higher temperatures in the sample than in the window. This being the case, conductive transfer of heat from the sample to the window will occur and the

observed interface temperature will be a consequence of the resulting conductive temperature profile. We can treat the conduction problem as 1-dimensional because we used a mask to exclude all but the center of the sample-window interface from observation.

The simplest case, which we will call Model 0, occurs when no phase changes occur because of heat transfer between the sample and the window and the final state of the sample does not fall into the mixed phase region of partial melting. The interface temperature is then given by (Urtiew and Grover, 1974; Grover and Urtiew, 1974):

$$T_I = T_s - (T_s - T_w)/(1 + \alpha) \quad (6)$$

$$\alpha = (K_s \rho_s c_s / K_w \rho_w c_w)^{1/2} \quad (7)$$

where  $K$  and  $c$  are the thermal conductivity and specific heat, respectively, and the subscripts  $s$  and  $w$  refer to the sample and window.

Model I includes the complication of a freezing front propagating into the sample from the interface, due to conduction of heat into the window (Tan and Ahrens, 1990):

$$T_I = T_w + \alpha(T_{m,s} - T_w)/(\alpha - \text{erf}\mu) \quad (8)$$

where  $T_{m,s}$  is the sample melting temperature and  $\mu$  is related to the propagation rate of the freezing front. Making the simplifying



assumption that the molten and solid sample have similar properties,  $\mu$  is the root of the equation

$$\frac{T_s - T_{ms}}{1 + \operatorname{erf}\mu} e^{-\mu^2} - \frac{\alpha^2(T_{ms} - T_w)}{\alpha - \operatorname{erf}\mu} e^{-\mu^2} - \frac{\pi^{\frac{1}{2}}}{c_s} \chi_s \Delta H_{ms} \mu = 0 \quad (9)$$

Now  $\chi_s$  is the fraction of sample melted prior to any conduction-induced freezing and  $\Delta H_{ms}$  is the enthalpy of melting of the sample. Under conditions when  $0 < \chi_s < 1$ , then  $T_s = T_{ms}$  and the first term in equation (9) vanishes. There is a range of cases in which  $\chi_s = 1$ , but for which this model applies because sufficient heat has been conducted into the window to induce freezing in the sample.

Model II looks at the reverse problem from Model I, namely that conduction-induced melting occurs in the window, but no phase change occurs in the sample. In this case, (Tan and Ahrens, 1990):

$$T_I = T_s - (T_s - T_{mw}) / (1 + \alpha \operatorname{erf}\lambda) \quad (10)$$

where  $T_{mw}$  is the melting temperature of the window and  $\lambda$ , which is analogous to  $\mu$  in Model I, describes the rate of advance of the melting front in the window. Assuming similar properties between the liquid and solid window material,  $\lambda$  is the root of

$$\frac{\alpha(T_s - T_{mw})}{1 + \alpha \operatorname{erf} \lambda} e^{-\lambda^2} - \frac{T_{mw} - T_w}{1 - \operatorname{erf} \lambda} e^{-\lambda^2} - \frac{\pi^{\frac{1}{2}}}{c_w} \Delta H_{mw} \lambda = 0 \quad (11)$$

Here,  $\Delta H_{mw}$  is the enthalpy of melting of the window material.

Model III combines the complications introduced in Models I and II, namely both melting in the window and freezing in the sample occur simultaneously. Here, (Tan and Ahrens, 1990):

$$T_I = T_{ms} + (T_{ms} - T_{mw}) \operatorname{erf} \mu / (\alpha \operatorname{erf} \lambda - \operatorname{erf} \mu) \quad (12)$$

where  $\mu$  and  $\lambda$  are the roots of the simultaneous equations

$$\frac{\alpha(T_{ms} - T_{mw})}{\alpha \operatorname{erf} \lambda - \operatorname{erf} \mu} e^{-\lambda^2} - \frac{T_{mw} - T_w}{1 - \operatorname{erf} \lambda} e^{-\lambda^2} - \frac{\pi^{\frac{1}{2}}}{c_w} \Delta H_{mw} \lambda = 0 \quad (13)$$

$$\frac{T_s - T_{mw}}{1 + \operatorname{erf} \mu} e^{-\mu^2} - \frac{T_{ms} - T_{mw}}{\alpha \operatorname{erf} \lambda - \operatorname{erf} \mu} e^{-\mu^2} - \frac{\pi^{\frac{1}{2}}}{c_s} \Delta H_{ms} \chi_s \mu = 0 \quad (14)$$

The particular cases that apply are easily distinguished upon examination of the total data set. The forms of equations (6)-(14) indicate that  $T_I$  will be most sensitive to the thermal state of the

material with the greater thermal conductivity, which is the sample in all the present cases. The shallow trends in the data for  $T_I$  thus reflect similar trends in the temperature of the sample. Specifically, these points represent cases where conductive freezing of the sample occurs. Whether melting occurs in the window is simply determined by comparison of  $T_I$  with  $T_{mw}$ , where  $T_I \geq T_{mw}$  indicates melting of the window. In the solutions for  $T_s$  and  $T_{ms}$ , the equations are rearranged (Tan and Ahrens, 1990):

Model 0:

$$T_s = T_I + (T_I - T_w)/\alpha \quad (15)$$

Model I:

$$T_{ms} = T_w + (T_I - T_w)(\alpha - \operatorname{erf}\mu)/\alpha \quad (\chi_s < 1) \quad (16)$$

with  $\mu$  being the root of equation (9), and

$$T_{ms} \approx T_I/.975 \quad (\chi_s = 1) \quad (17)$$

Model II:

$$T_s = T_I + (T_I - T_{mw})/\alpha \operatorname{erf}\lambda \quad (18)$$

with  $\lambda$  being the root of equation (11).

Model III:

$$T_{ms} = T_I + (T_{mw} - T_I)\text{erf}\mu/\alpha\text{erf}\lambda \quad (\chi_s < 1) \quad (19)$$

where  $\lambda$  for Model III is given by the root of

$$\frac{T_I - T_{mw}}{\text{erf}\lambda} e^{-\lambda^2} - \frac{T_{mw} - T_w}{1 - \text{erf}\lambda} e^{-\lambda^2} - \frac{\pi^{\frac{1}{2}} \Delta H_{mw} \lambda}{c_w} = 0 \quad (20)$$

and  $\mu$  is given approximately by the root of

$$\frac{T_I - T_{mw}}{\alpha\text{erf}\lambda} e^{-\mu^2} + \frac{\pi^{\frac{1}{2}} \Delta S_{ms} \chi_s \mu [T_I - (T_I - T_{mw})\text{erf}\mu/\alpha\text{erf}\lambda]}{c_s} = 0 \quad (21)$$

Now, we have replaced  $\Delta H_{ms}$  by  $T_{ms} \Delta S_{ms}$  where  $\Delta S_{ms}$  is the entropy change of the sample upon melting. Finally, for Model III where  $\chi_s=1$ ,

$$T_{ms} \approx T_I / .975 \quad (22)$$

It should be noted that equations (18), (19), and (21) are different from what should be the equivalent expressions of Tan and Ahrens (1990). This is due to typographical errors in the final version of the Tan and Ahrens (1990) paper.

In order to perform the calculations, we need estimates for the properties of the materials involved. For the windows, we adopt the methods discussed by Bass et al. (1987) for the calculation of the thermal properties. At the pressures obtained in the nonporous experiments, sulfur is metallic ( $P > 50$  GPa, Dunn and Bundy, 1977). Thus, the thermal conductivities of the samples may be estimated via the Wiedemann-Franz relation (Kittel, 1966):

$$K = L\sigma T \quad (23)$$

where  $L$  is the Lorentz number ( $L \approx 2.45 \times 10^{-8} \text{ W}\Omega/\text{K}^2$  for most metals) and  $\sigma$  is the electrical conductivity. There are no experimental data for  $\sigma$  in the iron sulfides under the conditions of interest. In order to estimate  $\sigma$ , we chose to develop approximate values for the expression presented by Tan and Ahrens (1990):

$$\sigma_H = T_0(a + bP_H)/T_H \quad (24)$$

where  $T_0 = 298$  K and the subscript H refers to the Hugoniot shock compression state. For pure iron,  $a = 2.743 \times 10^7$  mho/m and  $b = 1.1698 \times 10^6$  mho/m $\cdot$ GPa (Bass et al., 1987). The value of  $\sigma$  in the final state is related to the value on the Hugoniot curve via (Mott and Jones, 1959):

$$\frac{\sigma_r}{\sigma_H} = \frac{(\theta_r/\theta_H)^2}{T_r/T_H} \quad (25)$$

where  $\theta$  is the Debye temperature and the subscript r denotes the final reshock or release state. If we assume that  $\theta$  is related to the value at ambient conditions,  $\theta_0$ , via

$$\theta = \theta_0 \exp \left[ \int_{V_0}^V (\gamma_L/V') dV' \right] \quad (26)$$

where  $\gamma_L$  is the lattice Grüneisen parameter, then we get (Tan and Ahrens, 1990):

$$K = LT_0(a + bP_H) \exp \left[ -2 \int_{V_H}^{V_r} (\gamma_L/V') dV' \right] \quad (27)$$

We assume for this calculation that  $\gamma_L$  is approximately the same as the thermodynamic Grüneisen parameter,  $\gamma$ , and use the parameters listed in table 3 for  $\gamma$  in the form

$$\gamma = \gamma_0(\rho/\rho_0)^n \quad (28)$$

Since sulfur is metallic above ~50 GPa (Dunn and Bundy, 1977), we will assume that  $a$  and  $b$  for pure S are the same as for Fe. Since the samples contain both Fe and S, we must apply Nordheim's rule (Fink and Christiansen, 1982) to estimate the excess resistivity. This rule

Table 3.

Parameters for the calculation of the thermodynamic Grüneisen parameter.

Material	$\gamma_0$	$\rho_0(\text{kg/m}^3)$	n	Reference
FeS	1.54	5340	-1	1
FeS <sub>2</sub>	1.56	5011	-1	2

---

References: (1) Brown et al. (1984); (2) Ahrens and Jeanloz (1987).

states that the residual resistivity of a solution of two metals is given by

$$\rho_r = Cx(1 - x) \quad (29)$$

where  $C$  is a constant and  $x$  is the atomic fraction of one of the species. Intermediate phases and ordered solutions lower the resistivity from that given by this relation, so we expect in the present case that the resistivities we calculate will be upper limits. For most alloys,  $C$  falls in the range  $5 \times 10^{-7}$  to  $5 \times 10^{-6} \Omega\text{m}$  (Fink and Christiansen, 1982), so we have chosen to use the average of these two values. Furthermore, we apply this only to the zero-pressure conductivity,  $a$ . We thus find  $a = 6.193 \times 10^6$  mho/m for FeS and  $a = 6.781 \times 10^6$  mho/m for FeS<sub>2</sub>. For  $b$ , we retain the Fe value of  $1.1698 \times 10^6$  mho/m•GPa.

For  $\Delta S_{\text{ms}}$ , we use a value of  $k_B$  per atom. We assume  $c_s \approx 4.5k_B$  per atom, based on the results of Anderson and Ahrens (1990) for liquid Fe.

In cases where Models I and III apply, we also need to estimate  $\chi_s$ , the fraction of the sample initially melted by the shock and release or reshock processes. We do this by estimating the points in pressure at which the solid and liquid Hugoniot intersect the melting curve, based on both our experimental data and the results of equation of state studies, and then interpolating linearly in pressure along the melting curve from  $\chi_s = 0$  at the intersection with the solid Hugoniot to  $\chi_s = 1$  at the intersection with the liquid Hugoniot. Estimated corrections are applied to these values, based on the results from our data and the previous results for Fe (Bass et al., 1987; Ahrens et al., 1990).



Finally, any points falling above the pressure at which  $\chi_s = 1$  were assumed to have  $\chi_s = 1$ .

Let us first consider the experiments involving nonporous samples. When the data are evaluated with equations (15)-(29), the temperatures listed in table 4 and shown in figure 4 result. As comparison with the values of  $T_I$  in table 2 indicates, the corrections from  $T_I$  are generally small ( $\leq 10\%$ ) compared to the magnitude of  $T_I$  itself, so that detailed knowledge of the exact values of the properties incorporated into the calculations is unnecessary. We will discuss the melting curves in Figure 4 at some length later in this paper. The Hugoniot temperature curves presented are based on the models of Brown et al. (1984) and Ahrens and Jeanloz (1987) for the solid phase regions. The liquid phase Hugoniot temperatures are based on the present temperature data and, in the case of FeS, the observation of Brown et al. (1984) that melting on the FeS Hugoniot seems to be complete in the vicinity of 150 GPa. The liquid Hugoniot temperature curve for FeS<sub>2</sub> was constrained to approach the slope of the solid phase curve at low temperatures. The temperature offsets between the solid and liquid Hugoniot states indicate that the entropy of melting is about 30% of the specific heat in both FeS and FeS<sub>2</sub>. The actual number is about 28% for FeS and 32% for FeS<sub>2</sub>. If  $C_V$  is on the order of  $4.5k_B$  per atom then the molar entropies of fusion for FeS and FeS<sub>2</sub> are about  $2.52R$  and  $4.32R$ , respectively, with  $R$  being the ideal gas constant. It should be noted that these numbers are fairly uncertain and very model-dependent, so caution should be used in applying them.

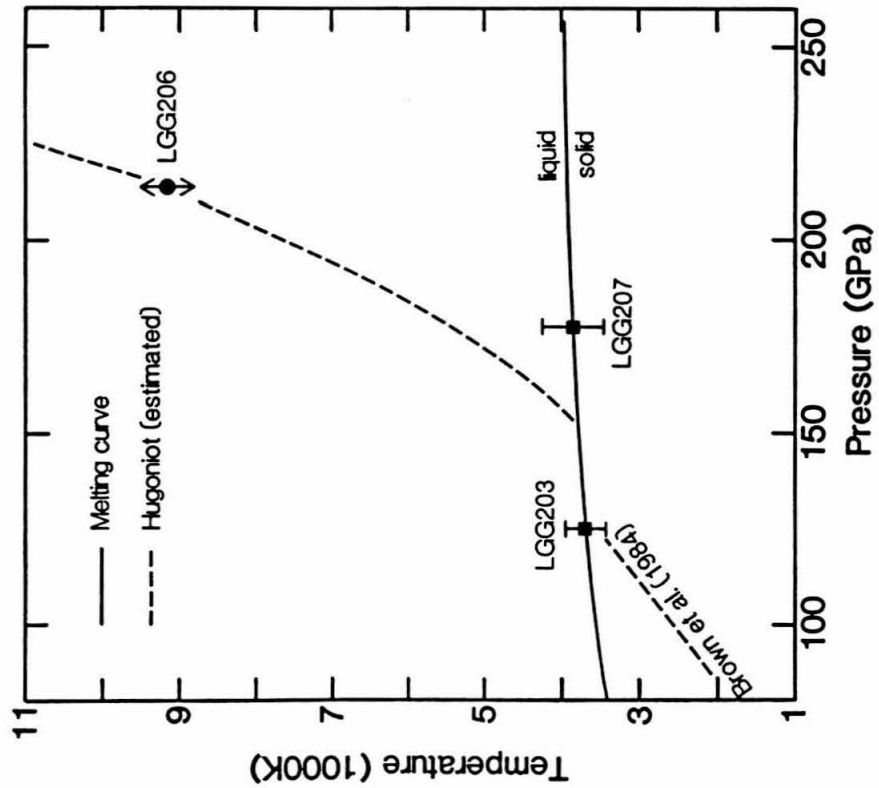
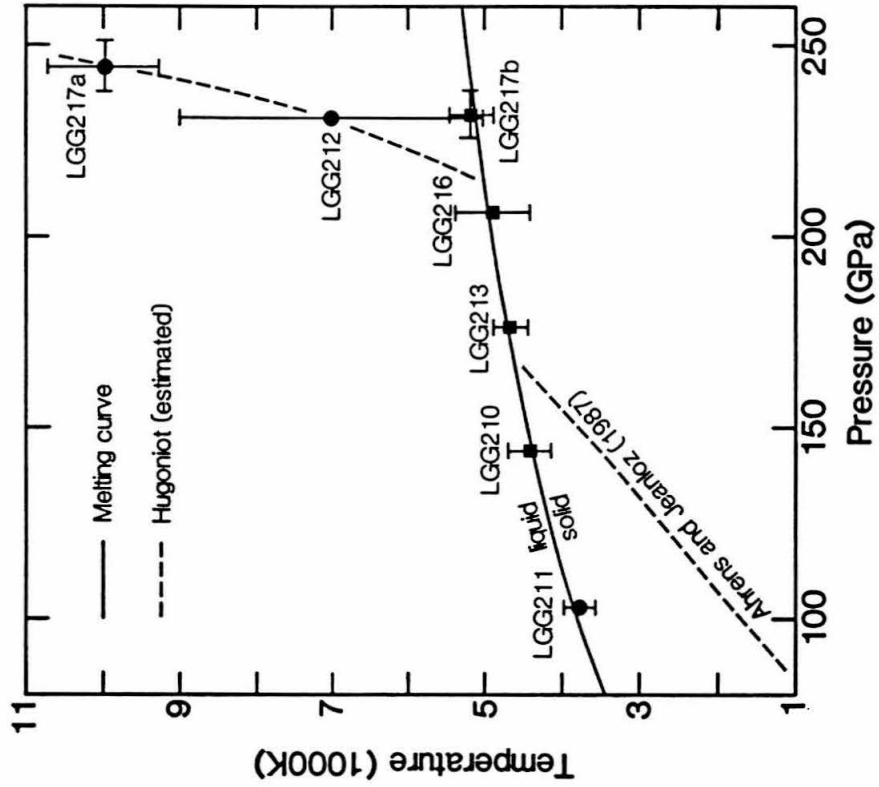
Concerns might be raised about the uncertainties of the film densities in this type of experiment. While the densities of the films

Table 4.

Melting and Hugoniot temperatures determined from the interface temperatures presented in table 2 for nonporous samples. The pressures given are relevant to the stated temperatures.

Experiment	Sample	Pressure (GPa)	Hugoniot Temperature (K)	Melting Temperature (K)	Model
LGG203	FeS	125.0±.1		3694±267	I
LGG206	FeS	213.6±.1	9151±5200		II
LGG207	FeS	177.4±.6		3847±397	I
LGG210	FeS <sub>2</sub>	144.0±.1		4406±281	I
LGG211	FeS <sub>2</sub>	102.8±.1	3777±200		0
LGG212	FeS <sub>2</sub>	216.6±.03	7006±1997		
LGG213	FeS <sub>2</sub>	176.4±.4		4518±221	I
LGG216	FeS <sub>2</sub>	206.4±.1		4895±493	III
LGG217	FeS <sub>2</sub>	244.2±6.8	9980±722		II
		231.8±6.5		5178±285	III

Figure 4. Melting and Hugoniot temperatures derived from the experiments on nonporous samples and from the models of Brown et al. (1984) and Ahrens and Jeanloz (1987). The circles represent points inferred to be in the single-phase regions of the Hugoniot and the squares represent points falling on the melting curve.



are not directly measured, experience with Fe (Bass et al., 1987; Ahrens et al., 1990) indicates that this is not a problem. In any case the results for the melting of the samples are unaffected. This is because of the nature of the final state that we observe. In the present experiments, the thin film samples are on the order of 1  $\mu\text{m}$  thick. The timescale for a shock wave or release wave to traverse the sample is generally  $\sim 1$  ns. This means that, by the time the first datum is obtained  $\sim 10$  ns after arrival of the shock wave at the sample-window interface, reverberation of the shock and release waves has brought the sample to a pressure more characteristic of the Hugoniot impedance match between the driver and the window, i.e., the pressure of the observed state is essentially independent of the properties of the sample. This, combined with the fact that we are observing a temperature that is buffered by a large latent heat, allows us to know with certainty both the temperature and the pressure of the state we are observing. Since this state is on the melting curve, we have a measurement of the melting curve, unaffected by uncertainties in the initial density of the sample. This may be the reason that some of the  $\text{FeS}_2$  data fall on the melting curve at pressures significantly lower than the intersection of the Hugoniot with the melting curve. Part of this may be due to uncertainties in the calculated solid phase Hugoniot temperatures. Because the liquid Hugoniot temperature obtained from experiment LGG212 is consistent with that obtained from LGG217 with a thick slab of known density, we infer that the sample densities are sufficiently close to the ideal crystal density that the thermal consequences of any density deficit are negligible. Hence, we conclude that the Hugoniot state

temperatures presented in table 4 and figure 4 are reliable to the extent that the measurement uncertainties allow.

The data obtained from initially porous samples must be handled somewhat differently from the rest. The spectral resolution of the detector system used is much better, but uncertainties are introduced by the fact that the resulting spectra represent averages over a ~300 ns sampling period. Since a finite time, on the order of 50-100 ns, is required for thermal equilibrium to be established between grain interiors and exteriors based on the temporal behavior of the light emitted at the powder-window interface (figure 5), the spectra tend to show some excess power at the shorter wavelengths. There is also some evidence for contamination from the window, possibly due to shear bands (Schmitt and Ahrens, 1983), in the spectra (figure 6). During the fitting of a graybody temperature and emissivity to the spectra, we have opted to use a linearized version of equation (2), namely,

$$I(\lambda, T) = \frac{2\epsilon c_1}{\lambda^5 \exp(c_2/\lambda T)} \quad (30)$$

This expression, in addition to being more computationally efficient to use in the analysis of the data from the 500 channels in these experiments, consistently gave temperatures that were ~50-100 K lower and therefore less sensitive to the short-wavelength portion of the spectrum and to the signal contamination.

Figure 5. Broadband photodiode signal from a typical experiment involving a porous sample (shot 723). The peak results from the initially strongly heated grain surfaces and decays as the grain interiors equilibrate thermally with the grain surfaces. Point "a" marks the arrival of the shock wave at the powder-window interface; "b" denotes the decay of the signal due to thermal equilibration of the grain interiors; "c" denotes the plateau signifying thermal equilibrium; and "d" marks the arrival of the shock wave at the window free surface.

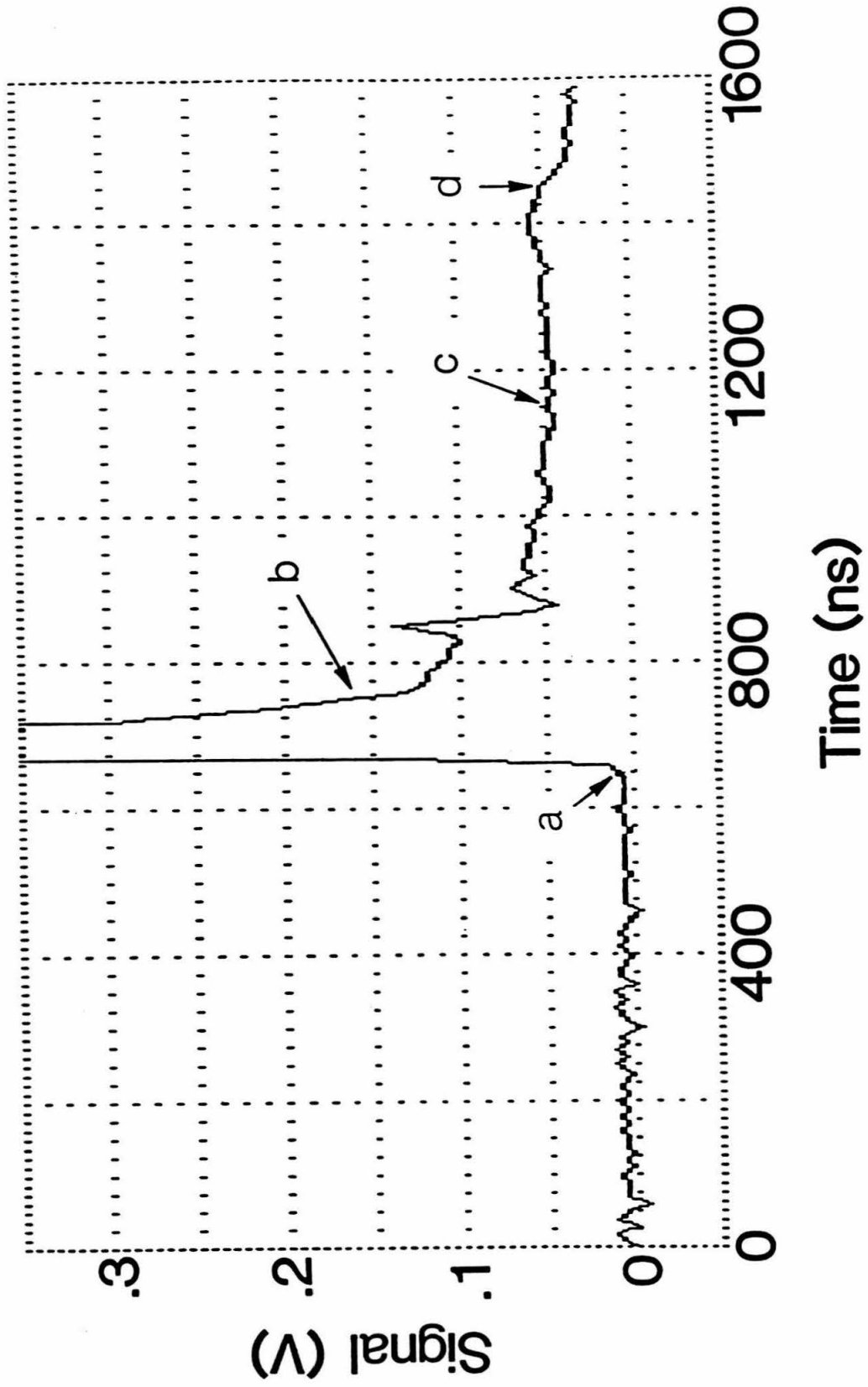
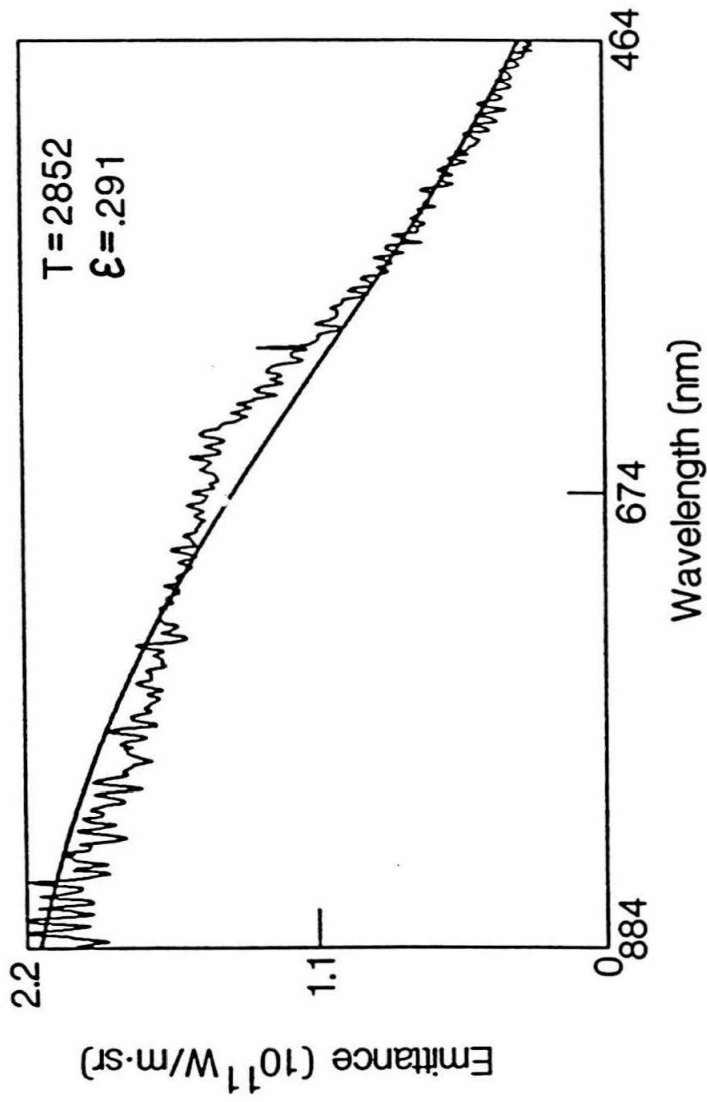




Figure 6. Typical spectrum and fit from a porous sample experiment (shot 723). Aside from the statistical noise in the spectrum, an excess of short wavelength radiation and a hump are evident, resulting from the change in sample temperature with time and processes occurring in the window.



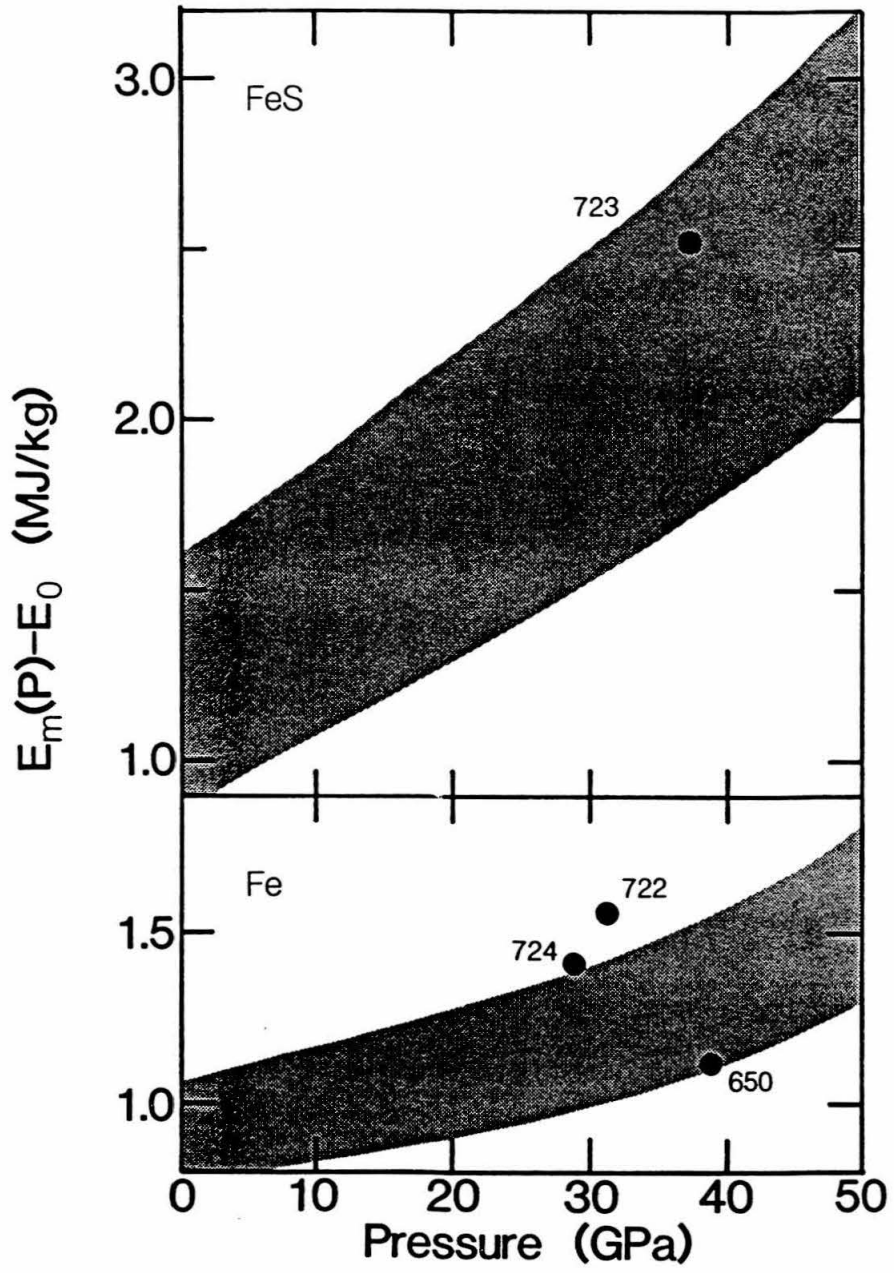
A further problem with the porous sample data is that the final thermodynamic state of the samples are only poorly known. Because of this, we chose only to obtain melting temperatures from these experiments. In order to determine which experiments can be used, we began by assuming that, even though the continuum mechanics approach to shock waves cannot accurately describe the propagation of a shock wave in a porous medium (Thouvenin, 1964), the thermodynamic conditions in the equilibrated shocked sample can be at least approximated by the normal equations used in shock mechanics. Using this assumption and assuming a suitable isentrope to connect the final state (for which the pressure is known) to the shocked state and taking the specific energy increase due to the shock process to be  $\frac{1}{2}u_p^2$ , we then compare the energy of the final (observed) state with the estimated energy required to completely melt the sample at that pressure. Samples that fall above the required energy for melting are assumed to give no information concerning the melting behavior of the sample and are thus ignored. Figure 7 shows the results of this analysis for the four experiments with porous samples. We find that, of the four, only experiments 650 and 723 represent final states that fall in the mixed phase regime. With these, we apply the results of Model III, equation (22) to obtain the melting temperatures. The resulting melting temperatures are given in table 5 and figure 4. Because of the problems already enumerated, these are best considered as upper limits to the melting temperatures.

Table 5.

Melting and Hugoniot temperatures determined from the interface temperatures of porous samples presented in table 2.

Experiment	Sample	Pressure (GPa)	Melting Temperature (K)
650	Fe	39±26	2993±35
723	Fe <sub>.88</sub> S	37.4±18.6	2925±35

Figure 7. Energy increases from ambient conditions required to melt Fe and FeS, with the estimated equilibrium internal energies of the initially porous samples after they reach the final state. The lower limits of the shaded regions indicate the estimated positions of incipient melting (i.e., the onset of melting), with the upper limits indicating the completion of melting. As can be seen, only experiments 650 and 723 fall within the limits of the mixed phase regions.



**PHASE RELATIONS IN THE IRON-SULFUR SYSTEM.**

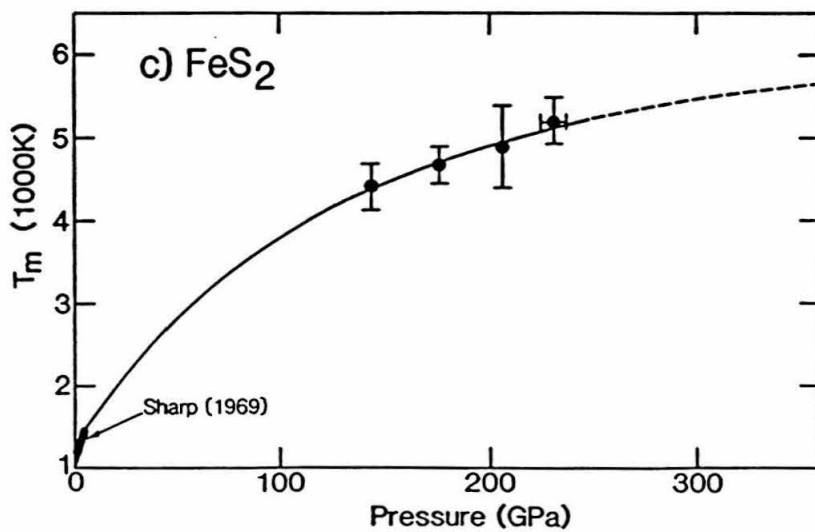
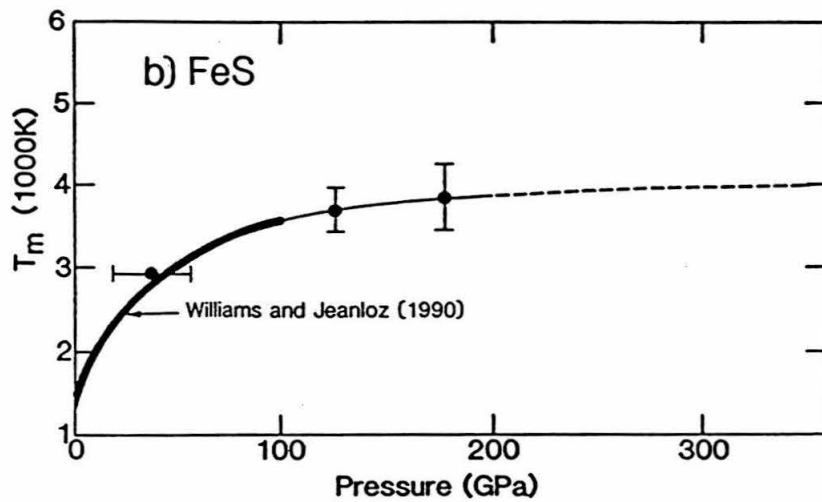
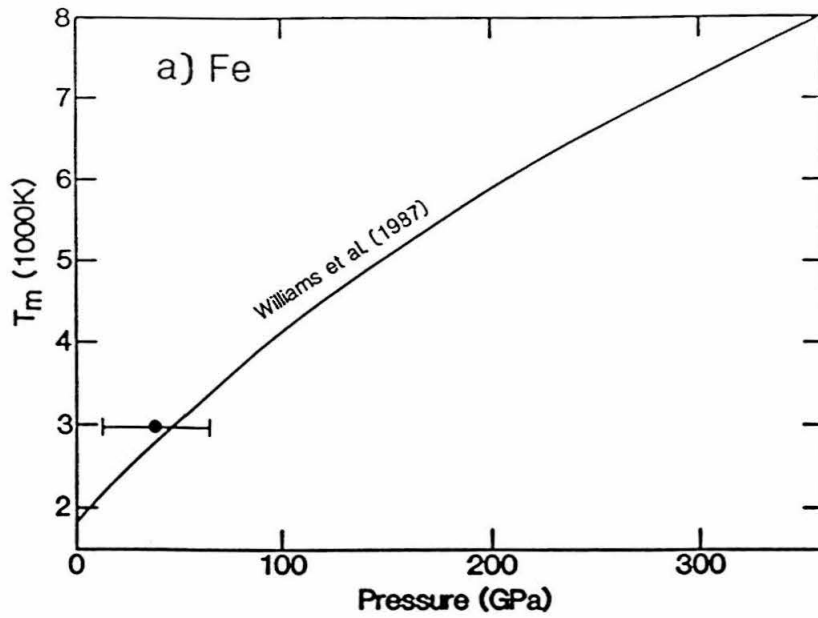
We now can turn to the application of these data to constraints on the Fe-S phase diagram. Let us begin by considering the melting data point for Fe. The primary purpose of the Fe experiments was to validate the techniques used for porous materials, but a secondary goal was to evaluate the static melting data using a completely different technique. Figure 8a shows the Fe melting curve of Williams et al. (1987), along with the single melting datum obtained from shot 650 in the present study. The uncertainties in the pressure of this particular shot are large, but this datum is consistent with the melting curve of Fe from Williams et al. (1987), if we keep in mind our earlier statement that experiments with porous samples provide what are best viewed as upper limits on the melting temperatures. It must be remembered that the present experiments with porous samples are best interpreted as upper bounds on the melting temperatures.

We now turn to the melting data for FeS. Figure 8b presents the data for the melting along with the melting curve of Williams and Jeanloz (1990) and the best fit melting curve determined from the combination of the present data with the results of Williams and Jeanloz (1990). As can be seen, the present data are completely consistent with the Williams and Jeanloz (1990) data.

In order to estimate a best fit melting curve, we wished to use a physically valid expression that could then be used for extrapolation of the curve to higher pressures. The Lindemann law (Lindemann, 1910) relates the temperature of melting,  $T_m$ , to the density of the solid at the melting point,  $\rho_m$ , via the relation (Gilvarry, 1956)

Figure 8. (a) The Fe melting curve of Williams et al. (1987), along with the melting datum from shot 650. (b) Our experimental melting temperatures for FeS, along with the melting curve of Williams and Jeanloz (1990) and our best fit melting curve to the combined data set. (c) Our experimental melting temperatures for FeS<sub>2</sub>, along with the best fit Lindemann melting curve.





$$\frac{d \ln T_m}{d \ln \rho_m} = 2(\gamma_L - 1/3) \quad (31)$$

and is based on the notion that the structure of a single solid phase is invariant along the melting curve. The lattice Grüneisen parameter,  $\gamma_L$ , is often parameterized as a function of density alone:

$$\gamma_L = \gamma_{L0}(\rho/\rho_0)^n \quad (32)$$

The  $\rho$ - $P$ - $T$  relationship from Brown et al. (1984) was used to obtain the  $\rho$ - $T$  curve from the  $P$ - $T$  curve. The specific heat is given by

$$C_V = 3R + C_e \quad (33)$$

The first term is simply the Dulong-Petit high temperature limit of the Debye lattice specific heat and  $C_e$  is the electronic specific heat. We get  $C_e$  by generalizing the form presented by Anderson and Ahrens (1990):

$$C_e = a \tanh^{3/2}(T/\theta) + AT(1+T)^{-1} + XT + YT^2 \quad (34)$$

where  $a = 22.765 \text{ J/mol} \cdot \text{K}$  and

$$\theta(\text{K}) = 2.2105(\rho n_e/\mu)^{1.434} \quad (35)$$

$$A(\text{J/mol} \cdot \text{K}) = 6.044 \times 10^{-6} \rho n_e/\mu - 1.385 \quad (36)$$

$$X(\text{J/mol} \cdot \text{K}^2) = 1.042 \times 10^{-9} \rho n_e/\mu - 4.657 \times 10^{-4} \quad (37)$$

$$Y(\text{J/mol} \cdot \text{K}^3) = 1.675 \times 10^{-13} \rho n_e / \mu - 5.109 \times 10^{-19} (\rho n_e / \mu)^2 \quad (38)$$

for  $\rho$  in  $\text{kg/m}^3$  and the molecular weight  $\mu$  in  $\text{kg/mol}$ . Here,  $n_e$  is the number of free electrons per atom. For metallic solids,  $n_e$  is generally assumed to be 1, but  $n_e$  for liquid metals is about 1.5. The equation of state parameters are listed in table 6. We fit equations (31) and (32) to the curve of Williams and Jeanloz (1990), combined with the present data, and obtain for the high pressure phase (hpp) of FeS  $\gamma_{L0} = 2.00 \pm .26$  and  $n = -2.93 \pm .98$  for  $\rho_0 = 5340 \text{ kg/m}^3$ . This value of  $\gamma_{L0}$  is quite a bit larger than the estimated thermodynamic Grüneisen parameter  $\gamma_0 = 1.54$ , obtained from shock wave data by Brown et al. (1984) under the assumption that  $n = -1$ . It should also be noted that, since the material being studied is metallic under the conditions of interest, the thermodynamic value will also have a term associated with the electronic energy. Part of the apparent disagreement may be due to the assumption that  $n = -1$  for the thermodynamic value. Inaccuracies in the estimated thermodynamic properties for FeS can also introduce inaccuracies into both  $\gamma_0$  and  $\gamma_L$ . These effects should not significantly influence the  $P$ - $T$  fit of the melting curve, since that is the projection in which the experimental data lie.

Although the fit falls well within the uncertainties of the data, the deviations are nonrandom which, along with the large magnitude of  $n$  for  $\gamma_L$ , may indicate that we are dealing with melting behavior more complicated than can be accurately described by the simple Lindemann criterion.

Table 6.

Equation of state parameters used to obtain  $P$ - $\rho$ - $T$  relations in this study.

Material	$\rho_0$ (kg/m <sup>3</sup> )	$K_{S0}$ (GPa)	$K'$	$K''$ (GPa <sup>-1</sup> )	$E_{TR}^a$ (MJ/kg)	$\gamma_0$	$n$
FeS <sup>b</sup>	5340	117.8	4.1	-.0339	.26	1.54	-1
FeS <sub>2</sub> <sup>c</sup>	5011	162	4.7	-.03135	0	1.56	-1

---

(a) Energy of transition to the high pressure solid phase from the low pressure phase at 1 bar and 298 K.

(b) Brown et al. (1984)

(c) Ahrens and Jeanloz (1987)

In an attempt to improve extrapolations to higher pressures, which involve a factor of 2 increase in pressure in order to reach the pressure at the center of the earth (360 GPa, Dziewonski and Anderson, 1981), we obtain the empirical correction to bring the Lindemann law fit into slightly better agreement with the high pressure data:

$$T_m = T_{mL} + \Delta T_m \quad (39)$$

$$\Delta T_m = 377 - .1205\rho + 9.259 \times 10^{-6} \rho^2 \quad (40)$$

for  $\rho$  in  $\text{kg}/\text{m}^3$ , where  $T_{mL}$  is the melting temperature predicted by the Lindemann law. This correction is very small, having a magnitude of only about 150 K at 360 GPa. The present curve gives melting temperatures of  $3750 \pm 200$  K at 136 GPa,  $3990 \pm 700$  K at the inner core boundary (ICB) pressure of 330 GPa, and  $4000 \pm 750$  K at 360 GPa. One interesting note is that, regardless of the extrapolation, the slope of the melting curve vanishes to within the uncertainty of the present results. This behavior becomes apparent in the highest pressure data. This fact, combined with the relatively small amount of scatter in the data and the good agreement between data obtained from two very dissimilar types of experiments, leads us to conclude that it is a real effect. If we assume congruent melting, this behavior would indicate that the liquid and the solid have the same density. An alternative view would be that FeS does not melt congruently at very high pressures. A third alternative is the possibility that an as yet unobserved solid state phase transformation at higher pressures, eventually causes an

increase in the slope of the melting curve. Use of this melting curve alone cannot address these issues and there are currently no data with which to evaluate the possibility of a solid state phase change.

Let us now turn to the melting data for  $\text{FeS}_2$ . Figure 8c presents the data for the melting curve of  $\text{FeS}_2$ , along with the best fit Lindemann melting curve. For the  $P$ - $T$ - $\rho$  relations, we use the equation of state parameters (table 6) obtained for pyrite by Ahrens and Jeanloz (1987), although the present results allow us to see that those parameters are derived from data involving at least two different phases, in conjunction with the specific heat discussed above. Again, the curve presented here should not be affected by inaccuracies in the parameters for  $\text{FeS}_2$  because the curve is anchored to data that occur in  $P$ - $T$  space, not  $\rho$ - $T$  space. Thus, the  $P$ - $T$  projection of the melting curve should be reasonably accurate, regardless of questions about the  $\rho$ - $T$  projection. Using equations (31) and (32), we find values of  $\gamma_{L0} = 2.79 \pm 0.81$  and  $n = -2.51 \pm 1.89$ , for  $\rho_0 = 5011 \text{ kg/m}^3$ . This compares with an estimated thermodynamic value of  $\gamma_0 = 1.54$  for the assumption that  $n = -1$  (Ahrens and Jeanloz, 1987). The resulting melting curve is significantly steeper than the FeS curve, with  $T_m = 4280 \pm 200 \text{ K}$  at 136 GPa,  $5570 \pm 500 \text{ K}$  at 330 GPa, and  $5670 \pm 550 \text{ K}$  at 360 GPa. Since there may be some question about the accuracy of the current pyrite equation of state, which we can now see includes data for both the solid and liquid phases, both the lattice and thermodynamic Grüneisen parameters may need revision in the future. It should also be noted that, at pressures below 6.4-8 GPa, the curve is a decomposition curve, rather than a melting curve (Sharp, 1969).

The success of the Lindemann criterion in providing suitable fits to the data indicates that this functional form is quite satisfactory in describing the melting curves of metals and ionic compounds. Some of the disagreement between the resulting lattice Grüneisen parameters and their thermodynamic counterparts may be due to uncertainties in the data used to obtain the lattice and thermodynamic values and, consequently, in the fit parameters themselves. The thermodynamic Grüneisen parameter is a notoriously difficult quantity to determine accurately and any variation in the thermodynamic value will affect the lattice value we obtain, since the thermodynamic value is required for the transformation to  $\rho$ - $T$  coordinates. However, the magnitude of this disagreement suggests that the assumptions underlying the Lindemann law need reexamination.

At low pressures,  $\text{FeS}_2$  undergoes peritectic decomposition (i.e., incongruent melting) to pyrrhotite ( $\text{Fe}_{1-x}\text{S}$ ) and sulfur. However, the present results indicate that the pyrite melting/decomposition curve crosses the melting curve of  $\text{FeS}$  in the pressure range 40-50 GPa, suggesting that the  $\text{FeS}$ - $\text{FeS}_2$  subsystem phase diagram has undergone a fundamental change below this pressure. This change almost certainly involves the transition to congruent melting by  $\text{FeS}_2$ . This was suggested by Sharp (1969), but for lower pressures than the present results would indicate. The change in the phase diagram may also be affected by the transition of elemental sulfur to a semiconductor at about 16.5 GPa and to the metallic state at about 50 GPa (Chhabildas and Ruoff, 1977; Dunn and Bundy, 1977; Postnov et al., 1987), although  $\text{FeS}$  appears to become metallic at lower pressures (about 3.4 GPa, King and Prewitt, 1982). One could also argue that we are simply observing the

melting of metastable  $\text{FeS}_2$ , which might be kinetically prohibited from decomposing on the short timescale involved in the experiments. We find this argument untenable because of the results of experiment LGG217, in which we observe an initially very high temperature state (i.e., liquid), but freezing at a later time, after conduction has transferred enough heat to the window. The melting temperature obtained from this experiment is consistent with the trend established by the experiments using  $\text{FeS}_2$  thin films.

A consequence of the behavior of the FeS- $\text{FeS}_2$  subsystem is that we now see that the  $\epsilon$ -Fe-S phase diagram proposed by Anderson et al. (1989) is no longer tenable. This is because, even in the  $\gamma$ -Fe  $P$ - $T$  stability field, the Anderson et al. (1989) model would lead us to expect that  $\text{FeS}_2$  continues to melt at temperatures lower than the FeS melting temperatures at high pressure. Since the present data indicate that this is not the case, we conclude that a model calling for complete solid solution between S and  $\epsilon$ -Fe is inconsistent with the data. Instead, we must assume eutectic behavior throughout the pressure range of the core.

In the development of the phase diagram for the Fe-S system in the regime where sulfur is metallic, the present data allow considerable leeway in the calculation of the phase boundaries. This is due partly to the uncertainties in the experimentally determined melting curves, but also on the paucity of data concerning the phase relationships of intermediate compositions at the relevant pressures. In particular, the only applicable data are provided by the melting experiments performed by Williams and Jeanloz (1990) at pressures up to 90 GPa for Fe with 10% S by weight (mole fraction  $x_S = .162$ ). Their data place an upper bound



on the Fe-FeS eutectic temperature and a lower bound on the liquidus temperature for  $x_S = .162$ . While the temperatures of the eutectic and liquidus are only bounded by these data, they do seem to require that the system continues to demonstrate eutectic behavior at pressures up to 90 GPa, consistent with the present results.

To obtain a better idea of the behavior to be expected from the Fe-S system at very high pressures, we turn to suitable low pressure analogs, namely bimetallic systems containing a transition metal and an s,p metal. This presents a large set of systems for consideration, but we are most interested in cases where the transition metal remains in a closest-packed structure up to the melting point, as iron does at high pressures. In the case of compound-forming systems, we further require that at least one of the stoichiometries of the Fe-S system (namely 1:1 and 1:2 transition metal:s,p metal ratio) be represented by the stable solid phases in the system.

Let us first note that the thermodynamic potentials and physical behavior of transition metal-semimetal and many intermetallic binary systems can be accurately modelled by postulating that the liquid contains three species—that in addition to individual atoms of the transition metal A and semimetal B, there exists a finite and nonnegligible concentration of molecules  $A_xB_y$  (Jordan, 1970; Prigogine and Defay, 1954; Ramachandrarao and Lele, 1985). This is known as an associated solution, because of the presence of the associated species  $A_xB_y$ . The relative abundances of free atoms of A and B and molecules of  $A_xB_y$  are assumed to be described by the dissociative equilibrium



which has an equilibrium constant  $K_{eq}$ :

$$K_{eq} = x'_A x'_B / x'_{AB} \quad (42)$$

where the primed quantities refer to the "effective" mole fractions of the species. Although some intermetallic systems show evidence of larger complexes (Ramachandrarao and Lele, 1985), we will assume here that the associated species is AB, with both  $x$  and  $y$  equal to 1. We do this for two reasons. First, this is the most common case cited in the literature. Second, the forces binding an intermetallic complex together are weak (since there will be little covalent character to the bonds involved) and a larger complex is probably less stable under most circumstances. Now, since the total number of atoms of A in the system (both free and combined with B in molecular AB) is given by

$$n_A = n'_A + n'_{AB} \quad (43)$$

and similarly with B, the total true mole fraction of A is given by

$$x_A = (x'_A + x'_{AB}) / (1 + x'_{AB}) \quad (44)$$

From these relations, we can obtain the species fractions from the actual liquid elemental composition via

$$x'_{AB} = -[b + (b^2 - 4)^{1/2}]/2 \quad (45)$$

$$x'_A = x_A(1 + x'_{AB}) - x'_{AB} \quad (46)$$

$$x'_B = 1 - x'_A - x'_{AB} \quad (47)$$

$$b = (1 + K_{eq})(x_A^2 - x_A)^{-1} + 2 \quad (48)$$

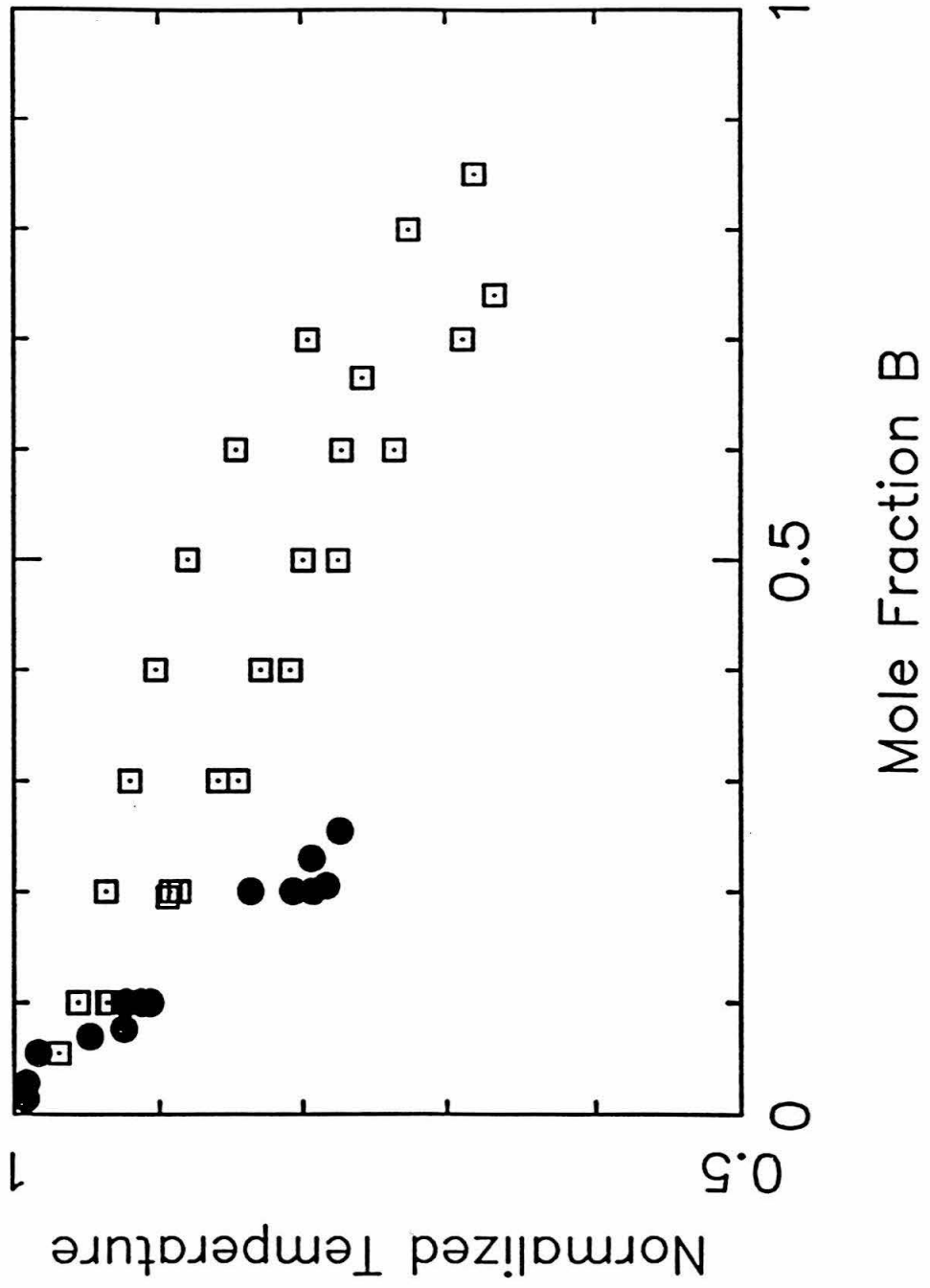
In order to determine whether this description also applies to systems containing s,p metals, in addition to semimetals, we examine the liquidi in equilibrium with pure, closest-packed transition metals melting (dissolving) into liquid solutions with s,p metals. Here, we have defined transition metals to include metals with d-electrons, no f-electrons, and no partially-filled s or p orbitals. We include alkali, alkaline earth, and post-transition metals in the category of s,p metals. As a test, let us compare such liquidi from compound-forming systems with those from systems that have no stable intermediate solid phases. Since liquidi describing the melting of the pure transition metal endmembers should be similar if the liquids have similar speciations, a gross dissimilarity in the liquidi would be indicative of association in the liquids of the compound-forming systems. The absence of any significant dissimilarity would probably indicate that such speciation effects, if present, could be safely ignored. The data for this comparison are for the systems listed in table 8 and are taken from

Table 7.

The systems for which liquidi are presented in figure 9.

System	Compound-forming?
Cd-Ca	Yes
Cd-Ga	No
Cd-In	No
Cd-Na	Yes
Cd-Sb	Yes
Cd-Sn	No
Co-Sb	Yes
Co-Sn	Yes
Ni-Mg	Yes
Zn-Ge	No
Zn-Mg	Yes
Zn-Sb	Yes
Zn-Sn	No

Figure 9. Liquidi for pure closest-packed transition metals melting into solutions with an s,p metal, shown as the liquidus temperature, normalized to the melting point of the transition metal, plotted against the mole fraction of the s,p metal in the liquid. The filled circles represent compound-forming systems and the open squares represent systems that do not form intermediate solid phases.



the phase diagrams presented by Hansen and Anderko (1958). Figure 9 contains the data for the two cases, presented as the normalized liquidus temperature (temperature divided by the melting point of the pure transition metal) plotted against the mole fraction of the s,p metal in the liquid. Although the data for the cases with no intermediate compounds show a spread of slopes liquidus slopes, there is an obvious and statistically significant difference in slope between the cases in which compounds are formed and the cases in which they are not. This difference would require that the average entropies of melting of the pure transition metals varies by a factor of two between the two cases. It should be noted that this effect remains if other models for the entropy or enthalpy of melting are used. Since this variation is not due to intrinsic differences between the transition metals involved in the two cases (in fact, the same transition metals occur in both cases), we conclude that the associated solution model is applicable to transition metal - s,p metal binary systems.

In the present model, we have chosen to assume that the ternary solution containing A, B, and AB is ideal. This is in contrast to the work of Jordan (1970), who assumed regular solution behavior in the metal-semimetal systems. Since thermochemical data are lacking for the Fe-S system at high pressures, we have made the simple, if somewhat unrealistic, assumption that the equilibrium constant  $K_{eq}$  is independent of temperature and pressure. Dependence on composition is precluded by the assumption of ideality in the liquid solution. At a given pressure, the liquidus temperature required for equilibrium with a given solid compound is found by requiring that the change in the chemical potentials of the species be zero during passage from one phase to the

other. Thus, for an ideal liquid solution, the melting of the pure transition metal is described by

$$\int_{T_{mA}}^{T_1} \frac{\Delta H_{mA}}{RT^2} dT = \int_1^{x'_{1A}} \frac{dx'_A}{x'_A} \quad (49)$$

where  $\Delta H_{mA}$  is the enthalpy change on melting or dissolution into the liquid,  $T_{mA}$  is the melting point of the pure transition metal, and  $T_1$  and  $x'_{1A}$  are the temperature and species mole fraction of the pure transition metal. The value of  $x'_{1A}$  is found from the elemental composition of the liquid via equations (45), (46), and (48). The melting of solid compound AB is presumed to involve a direct transition from solid AB to liquid AB, with dissociation being a subsequent process. The liquidus is then described by an equation analogous to equation (49):

$$\int_{T_{mAB}}^T \frac{\Delta H_{mAB}}{RT^2} dT = \int_{x'_{0AB}}^{x'_{1AB}} \frac{dx'_{AB}}{x'_{AB}} \quad (50)$$

The melting of  $AB_2$  proceeds by decomposition into AB and B, and is described by:

$$\int_{T_{mAB}}^T \frac{\Delta H_{mAB_2}}{RT^2} dT = \int_{x'_{0AB}}^{x'_{1AB}} \frac{dx'_{AB}}{x'_{AB}} + \int_{x'_{0B}}^{x'_{1B}} \frac{dx'_B}{x'_B} \quad (51)$$



For a given solid phase  $i$ , the enthalpy of equilibrium melting is given by

$$\Delta H_{mi} = T\Delta S_{mi} \quad (52)$$

where  $\Delta S_{mi}$  is the entropy change on melting. Let us assume that  $\Delta S_{mi}$  is independent of the temperature and of the composition of the coexisting equilibrium liquid. Then, equations (49) through (51) reduce to

$$T_1 = T_{mA} X'_{1A} R/\Delta S_{mA} \quad (53)$$

$$T_1 = T_{mAB} (X'_{1AB}/X'_{0AB}) R/\Delta S_{mAB} \quad (54)$$

and

$$T_1 = T_{mAB_2} \left( \frac{X'_{1AB} X'_{1B}}{X'_{0AB} X'_{0B}} \right) R/\Delta S_{mAB_2} \quad (55)$$

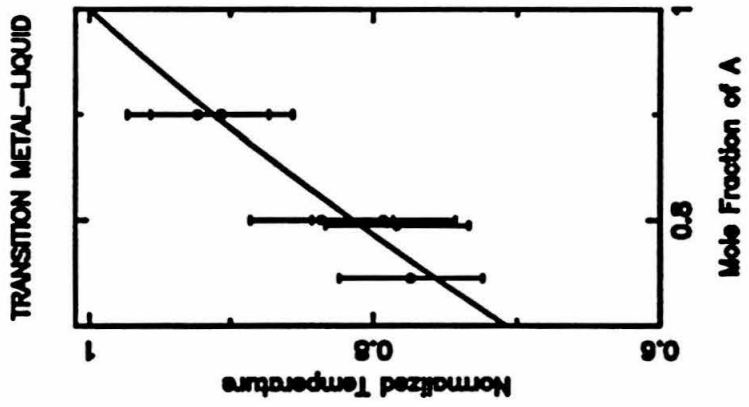
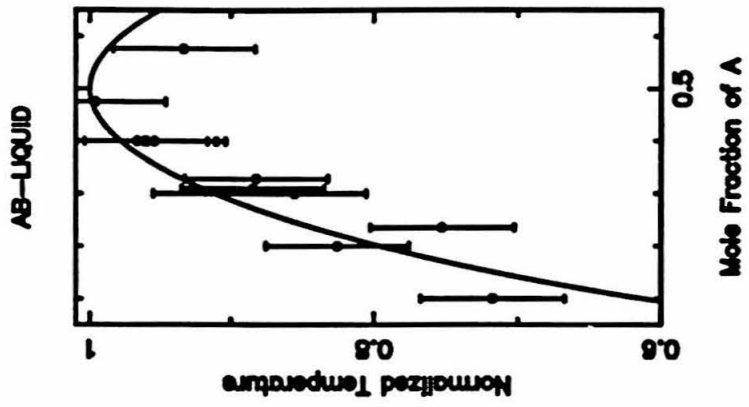
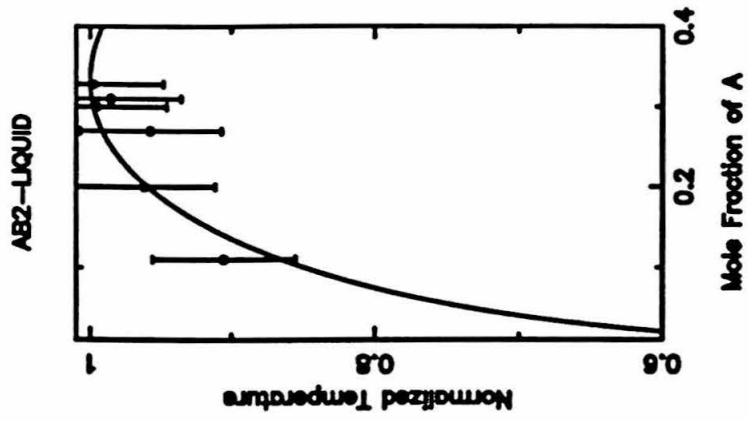
In order to calculate the Fe-S phase diagram, we chose to use the average best fit properties for transition metal - s,p metal systems. We performed a least squares fit of the liquidus of the pure transition metal A and the two compounds AB and AB<sub>2</sub>, with the fit parameter being  $K_{eq}$ . The data used (Hansen and Anderko, 1958) are given in table 8 and presented with the resulting fit in figure 10 in the form of liquidus temperatures normalized to the melting point of the equilibrium solid. We selected the data to meet the following requirements: (1) the system should have solid compounds with stoichiometries close to both 1:1 and

Table 8.

Data used to obtain the value of  $K_{eq}$  for this study.

System	Equilibrium solid	Mole fraction of s,p metal	Normalized Temperature
Co-Al	CoAl	.6	.9607
		.7	.8554
		.765	.7524
Co-Ge	CoGe	.525	.9958
		.6	.9594
		.69	.8847
	CoGe <sub>2</sub>	.69	.9851
		.73	.9569
Co-Sb	Co	.1	.9229
		.2	.8360
		.255	.7738
Co-Sn	Co	.1	.9063
		.2	.7928
		.205	.7834
Ni-Sb	NiSb	.6	.9661
		.7	.9046
		.8	.8255
		.9	.7173
Pd-Sb	PdSb	.423	.9330
		.6	.9537
		.672	.8822
	PdSb <sub>2</sub>	.672	.9976
		.7	.9953
		.8	.9612
		.89	.9053

Figure 10. Best fit liquidus for melting in compound-forming transition metal - s,p metal systems. (a) Pure transition metal; (b) 1:1 stoichiometry; (c)  $AB_2$  compounds, where A represents the transition metal.



1:2; (2) the solid in equilibrium with the liquidus being considered should not vary by more than 7% from the ideal composition (i.e., solid solution on the side of the liquidus should be limited to no more than 7%). Because no uncertainties were presented for the data, we have assumed that all the data have an uncertainty of .05 in the normalized temperature. The resulting value of  $K_{eq}$  is  $.99 \pm .67$ . The fit could be improved if we allowed the entropies of fusion to vary. This was tried, but resulted in values for  $\Delta S/R$  of the order of 2-3 per gram-atom, about twice what is expected. Although such high values cannot be ruled out by the shock temperature data, they are highly suspect and we therefore chose to use the values of  $\Delta S/R$  of 1.2 for Fe (Hultgren et al., 1963; Chase et al., 1985), 2.52 for FeS, and 4.32 for FeS<sub>2</sub>. Some improvement might also be obtained by assuming nonideality in the liquid solution, such as regular solution behavior, but uncertainties in the known parameters of the Fe-S system do not justify the resulting increase in model complexity.

Let us now consider the phase diagram of the Fe-S system. In particular, we will only deal with the region defined by  $x_{Fe} \geq .3$ , thus avoiding the obvious problems presented by our lack of knowledge concerning the behavior of metallic sulfur. We apply equations (53) - (55), where A is Fe and B is S, and use the values of  $\Delta S$  from the shock temperature results and the  $K_{eq}$  determined for the "average" transition metal - s,p metal system.

Figure 11 contains a series of isobaric phase diagrams at 50 GPa intervals from 50 GPa to 300 GPa. Figure 12 presents the  $x_S$ - $P$  projection of the liquidus surface. Two striking features are readily apparent. First, the present model indicates that FeS<sub>2</sub> may still undergo

Figure 11. Isobaric phase diagrams for the Fe-S system.

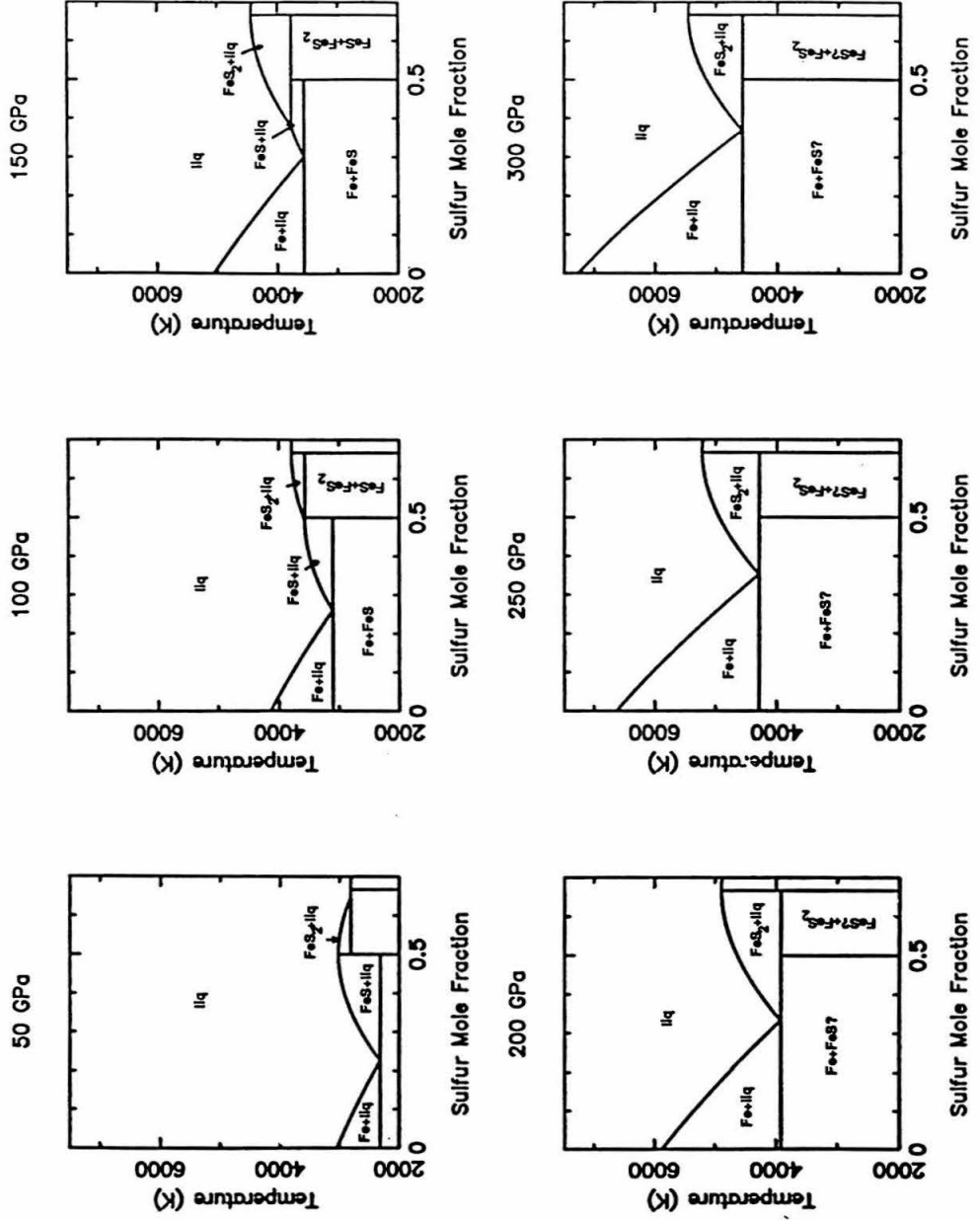
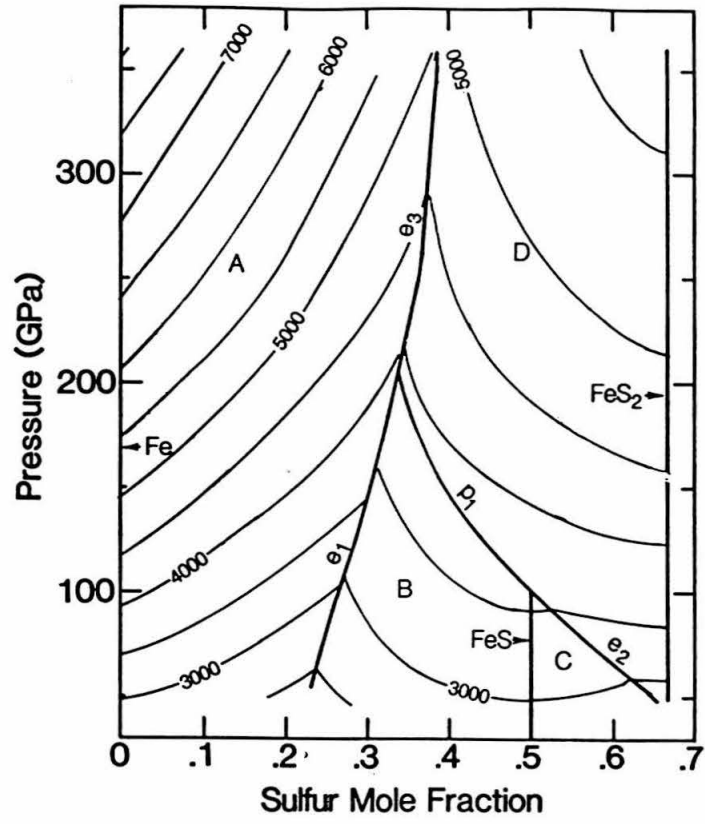


Figure 12. Liquidus surface for the Fe-S system. The temperature contour interval is 500 K. Region A denotes the portion of the liquidus in equilibrium with pure Fe. Regions B and C are the regions where the liquidus is in equilibrium with solid FeS. Region D is in equilibrium with FeS<sub>2</sub>. The lines labelled e<sub>1</sub>, e<sub>2</sub>, and e<sub>3</sub>, are, respectively, the Fe-FeS, FeS-FeS<sub>2</sub>, and Fe-FeS<sub>2</sub> eutectics. Line p<sub>1</sub> is the FeS peritectic.





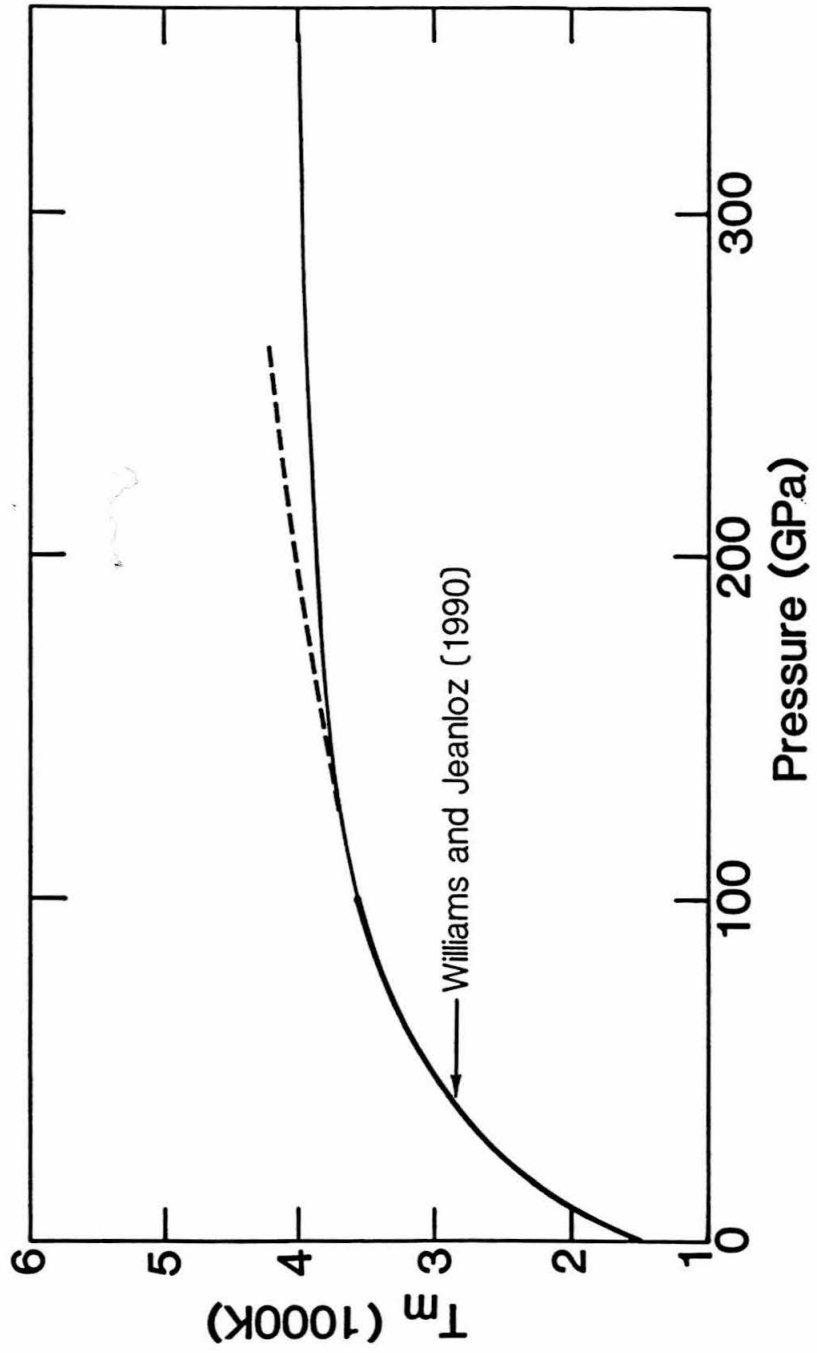
peritectic decomposition at pressures up to 40-50 GPa. The lack of FeS<sub>2</sub> melting data for pressures between 6.5 GPa and 120 GPa make the onset pressure for congruent melting somewhat uncertain, but it is almost certainly higher than the pressure range of 6.5-8 GPa suggested by Sharp (1969). The second feature is the onset of peritectic decomposition of FeS to FeS<sub>2</sub> and liquid at a pressure in the region of 100 GPa. Although this seems unusual, given the possible importance of FeS as an associated species in the melt, such behavior is observed in some other intermetallic systems (Au-Al, for example), and the instability of the solid may simply be due to the absence of an energetically favorable crystal structure containing FeS as the only species.

If we assume that the "melting" temperatures we observe for FeS at pressures greater than 100 GPa are actually the decomposition temperatures, then we can use equations (54) and (55) to estimate the metastable melting curve for FeS. This is presented in figure 13. This curve exhibits a more positive  $dT/dP$  slope than the fit to the experimental data. In fact, the flattening of the experimental curve may be a direct result of the onset of peritectic decomposition.

The eutectic with Fe remains in equilibrium with solid FeS up to a pressure of about 170 GPa, where extrapolation of the curves suggests that the peritectic curve intersects the eutectic curve, and the eutectic enters a region of equilibrium with Fe and FeS<sub>2</sub>.

Figure 13. Metastable FeS melting curve compared to the best fit experimental curve from figure 3.

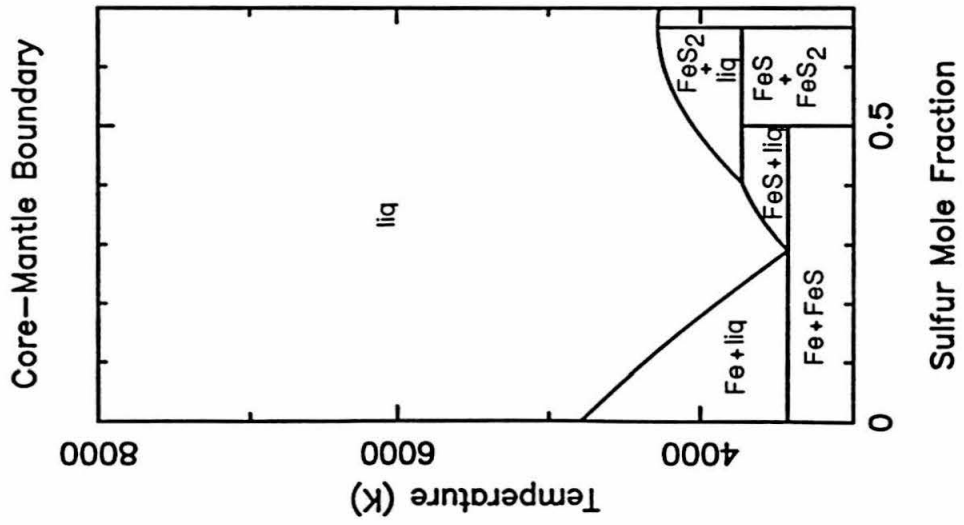
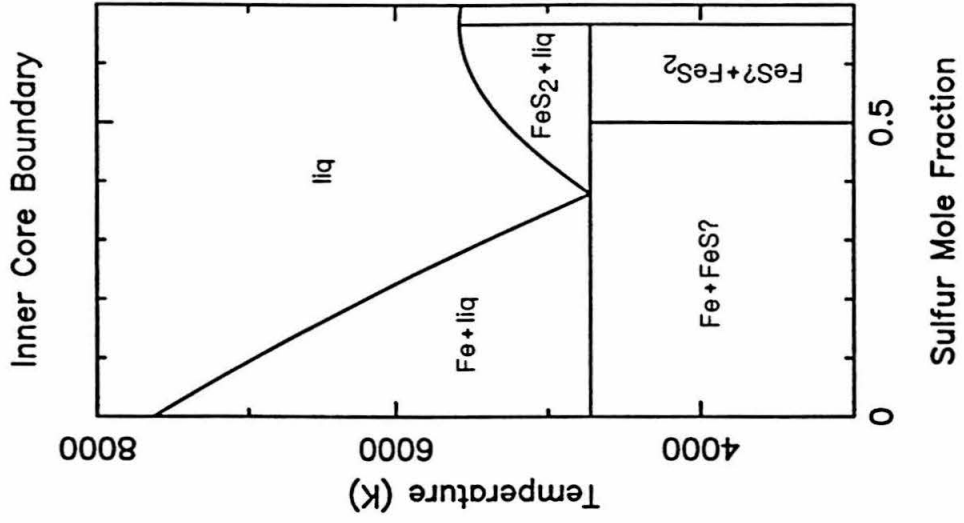




## TEMPERATURE AND STATE OF THE OUTER CORE.

We now turn to the question of the state and temperature of a hypothetical Fe-S core for the earth. We begin by recognizing the two extreme cases for the physical state of the outer core. In the first, more traditional case, the outer core is completely liquid throughout and the ICB represents the onset of crystallization. In other words, the  $P$ - $T$  conditions of the ICB fall on the liquidus of the outer core composition. From figure 14, we find that this corresponds to a temperature of 6300-6600 K at the ICB of a 10% sulfur (by weight) core. The temperature of the CMB is then obtained by simply migrating along an adiabat for the outer core liquid. If we assume that the  $dT/dP$  slope of the outer core adiabat is similar to that for the adiabat of pure liquid Fe under similar conditions, then, using the adiabats for Fe of Anderson and Ahrens (1990), we find that the corresponding CMB temperature is on the order of 4900 K. This is slightly higher than the findings of Williams and Jeanloz (1990). They also note that this temperature is more than 1000 K higher than estimates for the temperature at the base of the mantle, based on estimated mantle geotherms. Such a discrepancy is usually explained by invoking chemical layering at one or more levels, which results in the presence of nonconvecting boundary layers. The location most often cited as a possible location of such layering is the D" layer at the CMB. Such an extreme temperature drop, however, might require the presence of boundary layers at other levels in the mantle, which is disputed by some authors (Davies, 1984; Olsen et al., 1990). We find this core model unattractive from another standpoint. Fearn et al. (1981) has pointed out that the growth of the inner core from a multicomponent liquid (i.e., the outer core) should result in

Figure 14. Isobaric phase diagrams for the Fe-S system at the pressures of the core-mantle boundary and inner core boundary of the earth.



dendritic morphology for the solid-liquid interface and that the inner core should thus be partially molten. If the ICB falls on the outer core liquidus, the outer levels of the inner core would probably be mostly liquid. This presents problems for the interpretation of seismic data since the ICB is a seismologically-constrained boundary. It also is inconsistent with the upper bound of 50% liquid in the inner core found by Anderson and Ahrens (1990).

In an alternative case, first recognized by Busse (1972) and Malkus (1973), the outer core contains suspended solid particles (i.e., a slurry). The ICB in this case has no special thermodynamic significance. Rather, it is simply the depth at which the volume fraction of solid causes sufficient connectivity in the solid to create a seismologically observable rigidity. The volume fraction at which this occurs is uncertain and depends on both the and size distribution of shapes the solid particles. An upper limit is the rheologically critical melt fraction (RCMF: Arzi, 1978). For rocks, the RCMF generally falls in the vicinity of  $.8 \pm .1$ . This corresponds to the point at which a slurry becomes rigid from a rheological standpoint. The critical solid volume fraction that corresponds to a seismologically-observable rigidity may be considerably lower, however.

The lower limit on the temperature of the ICB is provided by the Fe-FeS<sub>2</sub> eutectic. This falls at about 4700 K in the present model. This is ~200 K higher than the value found by Williams and Jeanloz (1990), which is within the resolution of the present data, even though the eutectic S-bearing solid in their model (FeS) is different from that indicated by the present model (FeS<sub>2</sub>). If the mole fraction of sulfur in the outer core is on the order of .16, then the minimum volume



fraction of solid at the 330 GPa eutectic temperature falls in the range of .55-.60. To extrapolate this to the top of the core, we again follow an adiabat. This time, however, we note that, since the  $dT/dP$  slope of the adiabat is steeper than for the liquidus of a constant-composition liquid, the solid particles will be resorbed as a fluid parcel rises to shallower levels. This phenomenon will be accompanied by a conversion of sensible heat to latent heat, resulting in a temperature gradient that is superadiabatic for an entirely liquid system. Upon extrapolation back along a liquid adiabat, we find that the CMB temperature corresponding to  $T_{ICB} = 4700$  K is only negligibly higher than the 136 GPa eutectic temperature of 3450 K (figure 10). Since the eutectic migrates to more iron-rich compositions with decreasing pressure, the minimum solid volume fraction at the eutectic decreases to  $\sim .45$  at the CMB. We can estimate a lower bound on the temperature decrease due to the latent heat effect, since  $\Delta H_{mFe} = T\Delta S_{mFe}$ . For a fraction  $f$  of the total system volume being resorbed,

$$\delta T \geq T_{ICB} f \Delta S_{mFe} / C_{vFe} \quad (56)$$

If  $\Delta S_{mFe} = 1.0799R$  and  $C_{vFe} \approx 4.5R$  (Anderson and Ahrens, 1990), for  $f \sim .1$ ,  $\delta T \geq 72$  K. Our present results indicate that this temperature drop is more than sufficient to keep the outer core at the eutectic temperature throughout its depth.

The idea of a slurry in the bulk of the outer core has been discounted on two basic points. First, Loper and Fearn (1983) assert that nucleation is difficult to initiate in the absence of a solid interface. This assertion, which derives from experimental observations

of the freezing of multicomponent systems, contains one major flaw. Since the core is not a spatially isobaric system, as are laboratory experiments, the convective downwelling of the outer core fluid results in strong supercooling of that fluid. Barring a glassy transition, this supercooling could be quite sufficient to initiate essentially spontaneous nucleation of particles to form a slurry, as can be easily observed in strongly supercooled solutions in the laboratory.

The second objection to an outer core slurry, due to Loper (1978), is that the latent heat effect discussed earlier will stabilize the outer core against convection, since the temperature gradient is superadiabatic for a completely liquid system. This effect would be compounded by the fact that the resorption of crystals would drive the liquid to a more Fe-rich, and thus more dense, composition. This is true if the particle settling rates exceed the convective velocities within the outer core or if the "particles are actually dendrites extending from, and attached to, the inner core. If, however, the particles are entrained, as suggested by Williams and Jeanloz (1990), then we must consider the solid particles to be a part of the fluid. In this case, the question of changes in the liquid composition becomes moot since the bulk fluid composition is constant. The cooling latent heat effect will still occur, which will drive the bulk fluid to a greater density due to thermal expansion, but this must compete with the volume effect of conversion of the solid crystals to the liquid state. This competition can be easily quantified. For the system to be convectively unstable, the condition must be met that

$$\Gamma = (c_p \rho / \alpha T) (dT_m / dP) > 1 \quad (57)$$

If we choose reasonable limiting values to minimize this value for the outer core, namely  $c_p = 4R$ ,  $\rho = 11000 \text{ kg/m}^3$ ,  $T = 7000 \text{ K}$ ,  $\alpha = 1.1 \times 10^{-5}$  (estimated from Anderson and Ahrens, 1990), and  $(dT_m/dP) = 1.29 \times 10^{-8} \text{ K/Pa}$  (estimated from Williams et al., 1987), then we get  $\Gamma \sim 1.18$ . Since this is probably a lower limit, we find that the presence of a slurry with entrained solid particles in the outer core will not interfere with convection.

In reality, the core probably falls somewhere between the eutectic case and the completely liquid case, meaning that the outer core probably contains some solid material, but is not at the eutectic temperature. If this is true, the latent heat effects discussed here will still apply, and can be considerably larger, thus making the core even more superadiabatic. If we now set an upper limit on the liquid fraction at the ICB of 70% (assuming that the bulk inner core is 50% liquid, but is more liquid-rich at the ICB than at the center) and an upper limit on the solid content of 80%, based on the rheological criterion, then we get, by applying the lever rule to the phase diagram,  $4700 \text{ K} \leq T_{\text{ICB}} \leq 5800 \text{ K}$  for an iron-sulfur core. Extrapolation to the CMB along a liquid adiabat and correcting for the latent heat effect to keep the total heat content of a parcel constant, we find  $3400 \text{ K} \leq T_{\text{CMB}} \leq 4000 \text{ K}$ . In the low solid (i.e., high  $T$ ) case, the solid particles may be completely resorbed prior to reaching the top of the core. In this case, the temperature-buffering effect of the latent heat results in a temperature reduction of more than 300 K.

As a final note, we must realize that the details of the composition of the core are essentially unconstrained, except that the

dominant element is Fe and that there is a substantial low atomic weight component. Certainly, both sulfur and oxygen are likely to be present at some concentration, but the relative abundances of these and other elements are still largely a matter of speculation. There are some reasons to expect that the oxygen abundance of the core is relatively low. Some very loose limits may be placed on the oxygen content of the outer core by requiring that the solid phase in the core be more dense than the liquid, but the addition of a third component, such as sulfur, makes this a very uncertain exercise. We can also require that all the oxygen in the core must have been incorporated during core formation by reaction of downward migrating Fe-rich materials with silicates in the protomantle (Stevenson, 1981) at relatively low pressures. Since oxygen becomes significantly soluble in liquid Fe only at relatively high pressures and temperatures (Knittle and Jeanloz, 1987; Ohtani and Ringwood, 1984), much of the Fe now in the core may not have been exposed to silicates under suitable conditions for the dissolution of O. This would be especially true if the presence of sulfur caused the formation of the protocore to proceed at lower temperatures. The dissolution of O into the outer core at the core-mantle boundary is unlikely because of dynamical considerations that come into play in attempting to mix a light element-enriched (i.e., less dense) alloy downward into the bulk of the core. The problem also involves heavy elements other than Fe, such as Ni, which might be responsible for as large a weight fraction of the core as the light elements. Based on these considerations, we may expect that the effects of oxygen in the core can be largely offset by the presence of other elements in addition to oxygen and sulfur, if these elements have the general effect of

depressing the liquid of Fe-rich alloys. If this is the case and if we further presume that the core has a substantial sulfur content, most of which would have been incorporated into the core early during accretion (Anderson and Ahrens, 1986; Ahrens and Jeanloz, 1987), then our present model of the physical state and temperature of the core is probably applicable over a wide range of compositions. Thus we expect that the outer core may have a substantial quantity of suspended solid particulate matter and a temperature gradient that is steeper than a pure liquid adiabat, with temperatures at the inner core boundary ranging from 4700 K to 6000 K and temperatures at the top of the core ranging from 3400 K to 4200 K.

#### CONCLUSION.

Based on our new experimental data for the temperatures of FeS and FeS<sub>2</sub> under shock compression, we have been able to constrain the melting behavior of these materials to core pressures. The incorporation of these results into phase diagram calculations, along with constraints provided by analog systems and previously measured melting curves for Fe and compositions in the Fe-S system has allowed us to obtain a clearer picture of the behavior of the Fe-S system at the pressures present in the earth's core. A new and unexpected result is that FeS undergoes peritectic decomposition at pressures above 100 GPa, with the result that FeS<sub>2</sub> becomes the stable S-bearing solid phase in equilibrium with the liquid over a wide range of conditions.

We have used the Fe-S phase diagram to constrain temperatures in a hypothetical S-rich core. We find that the minimum temperature for the top of an all liquid outer core falls in the vicinity of 4700 K, in

agreement with earlier studies. However, the probable geometry of the inner core boundary, combined with the definition of the inner core (i.e., based on seismological observations), point toward an outer core that has some quantity of solid material suspended in it. A better model for the temperature of the outer core is thus one with an ICB temperature in the range from 4300 K to 6000 K and a temperature at the top of the outer core in the range from 3200 K to 4200 K.

**REFERENCES.**

Ahrens, T. J. (1979). Equations of state of iron sulfide and constraints on the sulfur content of the earth, *J. Geophys. Res.*, 84, 985-998.

Ahrens, T. J. (1987). Shock wave techniques for geophysics and planetary physics, in *Methods of Experimental Physics 24A*, edited by C. G. Sammis and T. L. Henyey, Academic Press, New York, 185-235.

Ahrens, T. J., and Jeanloz, R. (1987). Pyrite: shock compression, isentropic release, and composition of the earth's core, *J. Geophys. Res.*, 92, 10363-10375.

Ahrens, T. J., Tan, H., and Bass, J. D. (1990). Analysis of shock temperature data for iron, *High Press. Res.*, in press.

Anderson, W. W., and Ahrens, T. J. (1986). Shock wave experiments on iron sulfide and sulfur in planetary cores (abstract), *Lunar Planet. Sci.*, XVII, 11-12.

Anderson, W. W., Ahrens, T. J., and Svendsen, B. (1987). Melting in the Fe-FeS system and its relation to the compositions of the core of earth and Mars (abstract), *Lunar Planet. Sci.* XVIII, 21-22.

- Anderson, W. W., Svendsen, B., and Ahrens, T. J. (1989). Phase relations in iron-rich systems and implications for the earth's core, *Phys. Earth Planet. Inter.*, 55, 208-220.
- Anderson, W. W., and Ahrens, T. J. (1990). A liquid iron equation of state for geophysical applications, *Geophys. J. Int.*, submitted.
- Arzi, A. A. (1978). Critical phenomena in the rheology of partially melted rocks, *Tectonophysics*, 44, 173-184.
- Bass, J. D., Svendsen, B., and Ahrens, T. J. (1987). The temperatures of shock-compressed iron, in *High Pressure Research in Mineral Physics*, edited by M. Manghnani and Y. Syono, Terra, Tokyo, 393-402.
- Born, M., and Wolf, E. (1980). *Principles of Optics*, 6th ed. New York, Pergamon, 808pp.
- Boslough, M. B. (1984). *Shock-Wave Properties and High-Pressure Equations of State of Geophysically Important Materials*, Ph.D. Thesis, California Institute of Technology, Pasadena, California.
- Brett, R., and Bell, P. M. (1969). Melting relations in the Fe-rich portion of the system Fe-FeS at 30 kb pressure, *Earth. Planet. Sci. Lett.*, 6, 479-482.
- Brown, J. M., Ahrens, T. J., and Shampine, D. L. (1984). Hugoniot data for pyrrhotite and the earth's core, *J. Geophys. Res.*, 89, 6041-6048.



Brown, J. M., and McQueen, R. G. (1986). Phase transitions, Grüneisen parameter, and elasticity for shocked iron between 77 GPa and 400 GPa, *J. Geophys. Res.*, 91, 7485-7494.

Busse, F. H. (1972). Comment on paper by G. Higgins and G. C. Kennedy, The adiabatic gradient and the melting point gradient in the core of the earth, *J. Geophys. Res.*, 77, 1589-1590.

Carslaw, H. S., and Jaeger, H. (1959). *Conduction of Heat in Solids*, 2nd edition, Oxford University Press, Oxford, U. K.

Carter, W. J. (1973). Equation of state of some alkali halides, *High Temp. High Press.*, 5, 313-318.

Chase, M. W., Davies, C. A., Downey, J. R., Frurip, D. J., McDonald, R. A., and Syverud, A. N. (1985). *JANAF Thermochemical Tables*, 3rd. ed., *J. Phys. Chem. Ref. Data*, 14, Supplement 1.

Chhabildas, L. C., and Ruoff, A. L. (1977). The transition of sulfur to a conducting phase, *J. Chem. Phys.*, 66, 983-985.

Davies, G. F., (1984). Geophysical and isotopic constraints on mantle convection: an interim synthesis, *J. Geophys. Res.*, 89, 6017-6040.

Dziewonski, A. M., and Anderson, D. L. (1981). Preliminary reference earth model, *Phys. Earth Planet. Inter.*, 25, 297-356.

Dunn, K. J., and Bundy, F. P. (1977). Electrical behavior of sulfur up to 600 kbar—metallic state. *J. Chem. Phys.*, 67, 5048-5053.

Fearn, D. R., Loper, D. E., and Roberts, P. H. (1981). Structure of the earth's inner core, *Nature*, 292, 232-233.

Fink, D. G., and Christiansen, D. (editors) (1982). *Electronic Engineers' Handbook*, 2nd edition, McGraw-Hill.

Gilvarry, J. J., (1956). Grüneisen's law and the fusion curve at high pressures, *Phys. Rev.*, 102, 317-325.

Grover, R., and Urtiew, P. A. (1974). Thermal relaxation at interfaces following shock compression, *J. Appl. Phys.*, 45, 146-152.

Hansen, M., and Anderko, K. (1959). *Constitution of Binary Alloys*, 2nd ed., McGraw-Hill Book Company, New York, 1305 pp.

Hultgren, R., Orr, R. L., Anderson, P. D., and Kelley, K. K. (1963). *Selected Values of Thermodynamic Properties of Metals and Alloys*, J. Wiley and Sons, New York, 963 pp..

Jordan, A. S. (1970). A theory of regular associated solutions applied to the liquidus curves of the Zn-Te and Cd-Te systems, *Met. Trans.*, 1, 239-249.

- King, H. E., and Prewitt, C. T. (1982). High-pressure and high-temperature polymorphism of iron sulfide (FeS), *Acta Cryst.*, B38, 1877-1887.
- Kittel, C. (1966). *Introduction to Solid State Physics*, John Wiley and Sons, New York.
- Knittle, E., Williams, Q., and Jeanloz, R. (1987). Reaction of core constituents with silicates and oxides: implications for the composition of the core-mantle boundary (abstract), *EOS*, 68, 1210.
- Kondo, K., and Ahrens, T. J. (1983). Heterogeneous shock-induced thermal radiation in minerals, *Phys. Chem. Minerals*, 9, 173-181.
- Lindemann, F. A. (1910). Über die Berechnung molekularer Eigenfrequenzen, *Phys. Z.*, 11, 609-612.
- Loper, D. E. (1978). Some thermal consequences of a gravitationally powered dynamo, *J. Geophys. Res.*, 83, 5961-5970.
- Loper, D. E., and Fearn, D. R. (1983). A seismic model of a partially molten inner core, *J. Geophys. Res.*, 88, 1235-1242.
- Lyzenga, G. A. (1980). *Shock Temperatures of Materials: Experiments and Applications to the High-Pressure Equation of State*, Ph.D. Thesis, California Institute of Technology, Pasadena, California, 208 pp.

Malkus, W. V. R. (1973). Convection at the melting point, a thermal history of the earth's core, *Geophys. Fluid Dyn.*, 4, 267-278.

Marsh, S. P. (1980). *LASL Shock Hugoniot Data*. University of California Press., Los Angeles, 658pp..

Mason, G. (1966). Composition of the earth, *Nature*, 211, 616.

Morgan, J. W., and Anders, E. (1980). Chemical composition of earth Venus, and Mercury, *Proc. Natl. Acad. Sci. U. S. A.*, 77, 6973-6977.

Mott, N. F., and Jones, H. (1959). *The Theory of the Properties of Metals and Alloys*, Dover, New York.

Ohtani, E., and Ringwood, A. E. (1984). Composition of the core. I. Solubility of oxygen in molten iron at high temperature, *Earth Planet. Sci. Lett.*, 71, 85-93.

Olsen, P., Silver, P. G., and Carlson, R. W. (1990). The large-scale structure of convection in the earth's mantle, *Nature*, 344, 209-215.

Postnov, V. I., Anan'eva, L. A., Dremin, A. N., Nabatov, S. S., and Yakushev, V. V. (1987). Electrical conductivity and compressibility of sulfur under shock loading, *Combustion, Explosion, and Shock Waves*, 22, 486-488.

Prigogine, I., and R. Defay (1954). *Chemical Thermodynamics*, Wiley, New York.

Ramachandrarao, P., and Lele, S. (1985). Calculation of liquidus lines in compound forming systems, *Mater. Sci. Forum*, 3, 449-454.

Rice, M. H., McQueen, R. G., and Walsh, J. M. (1958). Compression of solids by strong shock waves, in *Solid State Phys.*, 6 (F. Seitz and D. Turnbull, eds.), Academic Press, New York, 1-63.

Rigden, S. M., Ahrens, T. J., and Stolper, E. M. (1984). Densities of liquid silicates at high pressures, *Science*, 226, 1071-1074.

Ringwood, A. E. (1977). Composition of the core and implications for origin of the earth, *Geochem. J.*, 11, 111-136.

Ringwood, A. E., and Kesson, S. E. (1977). Composition and origin of the moon, *Proc. Lunar Sci. Conf.* 8th, 371-398.

Schmitt, D. R., and Ahrens, T. J. (1983). Temperatures of shock-induced shear instabilities and their relationship to fusion curves, *Geophys. Res. Lett.*, 10, 1077-1080.

Schmitt, D. R., Svendsen, B., and Ahrens, T. J. (1986). Shock-induced radiation from minerals, in *Shock Waves in Condensed Matter*, Y. M. Gupta, ed., Plenum Publishing Company, 261-265.

- Sharp, W. E. (1969). Melting curves of sphalerite, galena, and pyrrhotite and the decomposition curve of pyrite between 30 and 65 kilobars, *J. Geophys. Res.*, 74, 1645-1652.
- Stevenson, D. J. (1981). Models of the earth's core, *Science*, 214, 611-619.
- Tan, H., and Ahrens, T. J. (1990). Shock temperature measurement for metals, *High press. Res.*, in press.
- Thouvenin, J., (1964). Action d'une onde de choc sur un solide poreux, *Compt. Rend.*, 258, 3461-3464.
- Urtiew, P. A., and Grover, R. (1974). Temperature disposition caused by shock interactions with material interfaces, *J. Appl. Phys.*, 45, 140.
- Usselman, T. J. (1975a). Experimental approach to the state of the core: Part I. The liquidus relations of the Fe-rich portion of the Fe-Ni-S system from 30 to 100 kb, *Am. J. Sci.*, 275, 278-290.
- Usselman, T. J. (1975b). Experimental approach to the state of the core: Part II. Composition and thermal regime, *Am. J. Sci.*, 275, 291-303.
- Williams, Q., Jeanloz, R., Bass, J., Svendsen, B., and Ahrens, T. J. (1987). The melting curve of iron to 250 gigapascals: a constraint on the temperature at earth's center, *Science*, 236, 181-182.

Williams, Q., and Jeanloz, R. (1990). Melting relations in the iron-sulfur system at ultrahigh pressures: implications for the thermal state of the earth, *J. Geophys. Res.*, in press.

Part II

EMPIRICAL EQUATION OF STATE FOR ORGANIC COMPOUNDS AT HIGH PRESSURES

William W. Anderson and Thomas J. Ahrens

Division of Geological and Planetary Sciences, California Institute of  
Technology, Pasadena, California, 91125.

For submission to High Pressure Research.



**ABSTRACT**

Organic compounds find many applications that subject them to high pressures. This leads to the need to be able to calculate equation of state parameters for organic compounds, but the wide variety of different compositions and molecular structures involved limit the utility of strictly theoretical formulations. We suggest that the use of properties that can be obtained by the summation of empirically-determined contributions from structural functional groups allows the prediction of high pressure states for many substances for which high pressure measurements do not exist and for which measured equation of state parameters are incomplete. This approach has been used in the past to calculate low pressure properties, however, we find that previous tabulations of material properties for organic liquids are too simplistic and not sufficiently accurate for our purposes. We have redetermined the group contributions for molar volume, thermal expansivity, specific heat, and the Rao function for liquid hydrocarbons and oxygen-bearing hydrocarbons. We also develop a highly successful scheme for the calculation of pressure derivatives of the bulk modulus from the temperature dependence of the sound speed and present a partial tabulation of contributions to the temperature derivative of the sound speed. Our results are tested by comparison with shock wave compression data for organic liquids and found to be very successful in predicting the Hugoniot curves, except in the case where breakdown of aromatic rings occurs. A similar test of previous tabulations for polymers shows systematic differences, suggesting that the Rao function contributions for polymers differ from those for low molecular liquids. This

technique, with better determinations for polymers, may aid in the development of tailored materials for applications such as spacecraft exteriors and composite armors.

## INTRODUCTION

Organic compounds encompass a wide variety of materials that have found use in virtually every area of modern human endeavor. Numerous applications, including the use of liquid hydrocarbons for pressure transmitting media and incorporation of polymers into many different products, may subject these materials to high static or dynamic pressures. In addition, organic materials in extraterrestrial materials (i.e., meteorites and comets) are commonly shocked to high pressures during impact events with other bodies. This method of producing high pressures, i.e., shock waves, can involve extreme pressures, in the megabar range. With so many such opportunities for exposure of organic compounds to high pressures, a method for predicting the behavior of these compounds under such conditions would be very useful.

Organic compounds include a seeming endless variety of substances, with a large variety of molecular structures. This complexity has been a source of frustration in attempts to use first principles developments to produce quantitatively accurate descriptions of the properties of such materials. The obvious alternative is to develop a series of empirical relations between molecular structure and physical properties. One method that has gained wide acceptance (van Krevelen, 1972) is to find a series of properties, or appropriate surrogates, which can be obtained by the summation of contributions from the different structural units that make up molecules of the compound in question. Such an approach is by nature approximate, but is perhaps the best available when data for a given compound are lacking.

One of the shortcomings of previous tabulations of group contributions is the assumption that such contributions are absolutely

constant, unaffected by the environment in which the functional groups are placed. This problem is most severe for low molecular liquids. In the present study, we have attempted to improve on the existing tabulations for liquid hydrocarbons and oxygen-bearing organic compounds. Lists of group contributions are presented for the molar volume, volume thermal expansivity, molar heat capacity, and the Rao function. We also develop a method for estimating the pressure derivatives of the bulk modulus, based on a series of assumptions, and find that suitable additive quantities exist to allow those derivatives to be obtained. We can use the techniques presented here to obtain sets of properties sufficiently accurate to allow the calculation of behavior under shock compression.

#### **THE MODEL .**

In the following development, we use functional group systematics to calculate the properties of compounds at 1 bar and normal temperature (293 K). These properties can then be used with well-established equations of state to predict the behavior of these materials at higher pressures and temperatures. Measured values of some properties, such as density and heat capacity, have been tabulated for many materials. It is, of course, always preferable to use the measured values when they are available. Many properties, such as the bulk modulus, however, are known only for a few organic compounds. Another problem may arise when the compound of interest is in the gas phase at NTP. In such cases, it is useful to turn to a development such as the one presented here to fill out the list of properties needed for calculations involving the condensed phases at high pressures and temperatures.

### Additive functional group contributions.

#### *Molecular Weight.*

The ultimate additive property, for all chemical compounds, is the molecular weight, or, more correctly, the molecular mass. This is because mass is an intrinsic property of matter. Regardless of its environment (excepting cases not important to the present discussion), the mass of an atom is constant. This is the reason we can calculate molecular weights simply from the elemental formula of a compound. We do this in Table 1, simply as a convenience to the reader, for the functional groups used in this study. We have assumed the normal terrestrial isotopic abundances for the elements, giving rise to the fractional values in the table.

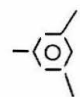
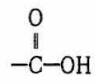
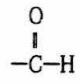
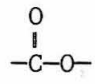
#### *Molar Volume.*

Density is one of the most basic properties to any equation of state. It is also one of the most easily measured properties of a material and thus has been measured for most phases that are stable at NTP. Extensive tabulations of the densities of organic compounds are provided by Weast (1977), Dean (1985), and Egloff (1939). The last of these is limited to hydrocarbons, but contains probably the most exhaustive tabulation of densities extant for that class of compounds. A tabulation of the densities of a number of polymers is given by van Krevelen (1972). Although these lists are extensive, they do not provide information on the condensed phases of compounds that are

Table 1.

Group contributions to the molecular weight,  $\mu$ .

Group	$\mu$ (Mg/Mmol)
$-\text{CH}_3$	15.035
$-\text{CH}_2-$	14.027
$\begin{array}{c}   \\ -\text{CH}- \end{array}$	13.019
$\begin{array}{c}   \\ -\text{C}- \\   \end{array}$	12.011
$=\text{CH}_2$	14.027
$-\text{CH}=\text{}$	13.019
$=\text{C} \begin{array}{l} / \\ \backslash \end{array}$	12.011
$=\text{C}=\text{}$	12.011
$\equiv\text{CH}$	13.019
$-\text{C}\equiv$	12.011
$-\langle \text{O} \rangle$	77.107
$\begin{array}{c}   \\ -\langle \text{O} \rangle \end{array}$	76.099
$\begin{array}{c} / \\ -\langle \text{O} \rangle \end{array}$	76.099
$-\langle \text{O} \rangle -$	76.099
$\begin{array}{c} / \backslash \\ -\langle \text{O} \rangle \end{array}$	75.091
$\begin{array}{c}   \\ -\langle \text{O} \rangle - \end{array}$	75.091

	75.091
-H	1.008
-OH	17.007
-O-	15.999
=O	15.999
	45.018
	29.019
	44.010

gaseous at NTP. Hence, we still require a system for predicting the densities of such compounds.

As we might expect, density is not an additive quantity. The usual quantity that is determined in this scheme is the molar volume,  $v$ , which is obtained from

$$v = \sum_i n_i v_i \quad (1)$$

Where  $v_i$  is the volume contribution of the  $i$ 'th functional group, and  $n_i$  is the number of that particular functional group in each molecule (or monomer in the case of a polymer). Mass density is then obtained by dividing the molar mass  $\mu$  (i.e., molecular weight) by  $v$ . A successful scheme for predicting  $v$  for solids must be able to account for the crystal structure. Currently there is no satisfactory way to predict crystal structure, so we cannot presently apply this analysis to low molecular organic solids.

The case for liquids is considerably simpler than for solids. Numerous authors have studied the contributions of organic functional groups to the molar volumes of liquids, and a series of different determinations of these contributions has been published (van Krevelen, 1972). We have performed a new study of the contributions of 24 different functional groups. For this study, data for the densities of liquid hydrocarbons were taken from the extensive tabulations of Egloff (1939), while the densities tabulated in section C of Weast (1977) were used for species containing oxygen in addition to H and C. The methods we used to obtain the contributions of the different functional groups



were fairly straightforward. When possible, we quantified the contribution of a group using linear regression analysis of the systematic variations of molar volume within a homologous series, as typified by the normal alkanes. Once we had obtained as many contributions as possible by this technique, we then determined the contributions by other groups by subtracting the (now known) contributions of these groups from the volumes of compounds not in a homologous series, but having only one undetermined group. We then averaged these residual values for each group. In cases where the spread in the residuals was unusually large, we searched for systematic variations indicative of influence by the surroundings. This led us to develop variable expressions for the contributions of some groups, taking into account the fact that the volume contributions of those groups do vary, depending on the environments in which they are found. These are the expressions presented in lieu of simple constants in table 2. Let us note here that this approach was taken with all the different properties discussed here and this is the reason we present some group contributions as more involved expressions than simple constants. Our results for the functional groups contributions to the molar volumes of low molecular liquids are given in table 2. Checks were performed by comparing molar volumes, calculated via equation (1) from the values listed in table 2, with molar volumes for complicated compounds that were not used in the fitting process. Most group contributions are well constrained, often giving molar volumes accurate to .1% (figure 1). A few groups, namely oxygen bearing ones, appear to present large nonsystematic variations in the volume contributions, leading to errors

Figure 1. Comparison of experimentally determined molar volumes (in units of  $\text{m}^3/\text{Mmol}$ ) for a number of organic liquids with volumes predicted by the present results. The circles represent hydrocarbons, while the squares represent oxygen-bearing compounds.

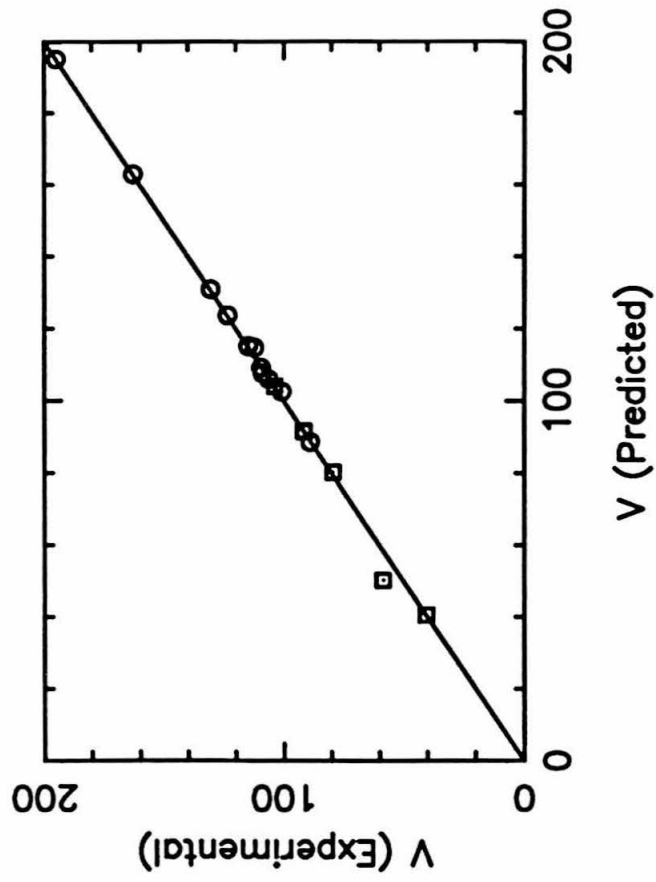
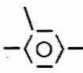
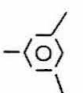
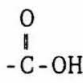
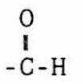
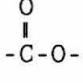


Table 2.

Group contributions to molar volumes for organic liquids and glassy and rubbery polymers, denoted by  $v_1$ ,  $v_g$ , and  $v_r$ , respectively. All contributions are given in units of  $\text{m}^3/\text{Mmol}$ .

Group	$v_1$	$v_g$	$v_r$
$-\text{CH}_3$	33.435	23.90	22.80
$-\text{CH}_2-$	16.030 <sup>(1)</sup> 15.466 <sup>(2)</sup>	15.85	16.45
$\begin{array}{c}   \\ -\text{CH}- \end{array}$	$1.897n_{\text{met}} - 4.589^{(1,3,4)}$ $1.072n_{\text{met}} - 1.940^{(2,3,4)}$	9.45	9.85
$\begin{array}{c}   \\ -\text{C}- \\   \end{array}$	$3.066n_{\text{met}} - 27.021^{(3,5)}$	4.60	4.75
$=\text{CH}_2$	31.293		
$-\text{CH}=\text{}$	12.646		13.87
$=\text{C} \begin{array}{l} / \\ \backslash \end{array}$	-7.442		6.13
$=\text{C}=\text{}$	8.179		
$\equiv\text{CH}$	25.366		
$-\text{C}\equiv$	$8.458 - 2.757n_{\text{met}} / (n_{\text{met}} + n_{\text{et}})^{(3)}$		
$-\langle \text{O} \rangle$	72.724	72.70	64.65
$\begin{array}{c}   \\ -\langle \text{O} \rangle \end{array}$	53.961		
$\begin{array}{c} / \\ -\langle \text{O} \rangle \end{array}$	56.961		
$-\langle \text{O} \rangle -$	57.039	65.50	61.40
$\begin{array}{c} / \backslash \\ -\langle \text{O} \rangle \end{array}$	34.037		

	36.874	59.50	
	38.859		
-H	17.405 <sup>(6)</sup> 18.647 <sup>(7)</sup> 20.088 <sup>(8)</sup> 15.932 <sup>(9)</sup>		
-OH	(See note 10)	9.70	
-O-	5.349	10.00	8.50
=O	10.849+.873n <sub>C</sub> <sup>(3)</sup>		
	21.742+1.069n <sub>C</sub> <sup>(3)</sup> 27.286+.919n <sub>C</sub> <sup>(3,11)</sup>		
	20.010+.856n <sub>C</sub> <sup>(3)</sup>		
	10.218+1.068n <sub>C</sub> <sup>(3,12)</sup> 11.384+1.275n <sub>C</sub> <sup>(3,13)</sup>	23.00 18.25 <sup>(14)</sup>	24.60 21.00 <sup>(14)</sup>

- 
- (1) Not adjacent to an aromatic ring.  
(2) Adjacent to an aromatic ring.  
(3) n<sub>met</sub> is the number of methyl groups attached to the group in question; n<sub>et</sub> is the total number of -CH<sub>2</sub>- groups in the compound; n<sub>C</sub> is the total number of carbon atoms in the molecule.  
(4) Subtract 4.344 for each adjacent group having a triple bond.  
(5) Subtract 8.688 if an adjacent group has a triple bond.  
(6) Attached to a saturated carbon.  
(7) Attached to a carbon having a double bond.  
(8) Attached to a carbon having a triple bond.  
(9) Attached to an aromatic ring.  
(10) If attached to a carbon at the terminus of a chain, the contribution is v<sub>1</sub> = 7.604 + .606n<sub>C</sub> + (n<sub>OH</sub>-1)(1.743+½n<sub>C</sub>), where n<sub>OH</sub> is the total number of -OH groups in the molecule; If the carbon is not a terminal carbon, then v<sub>1</sub> = 6.995 + 1.141n<sub>C</sub> + (n<sub>OH</sub>-1)(6.577-.99n<sub>C</sub>); in the case of methanol, v<sub>1</sub> = 7.053.  
(11) If attached directly to a ring (see note 10).  
(12) If the oxygen is attached to a terminal carbon (see note 10).  
(13) If the oxygen is not attached to a terminal carbon.  
(14) In acrylic -COO- group.

(15) Nonaromatic rings require the correction  $\delta v_1 = 25.961 - 2.388n_r + 4.764n_{sc}$ , where  $n_r$  is the number of atoms forming the spine of the ring and  $n_{sc}$  is the number of side chains attached to the ring.

of the order of 1-3% in the total molar volumes of compounds containing those groups.

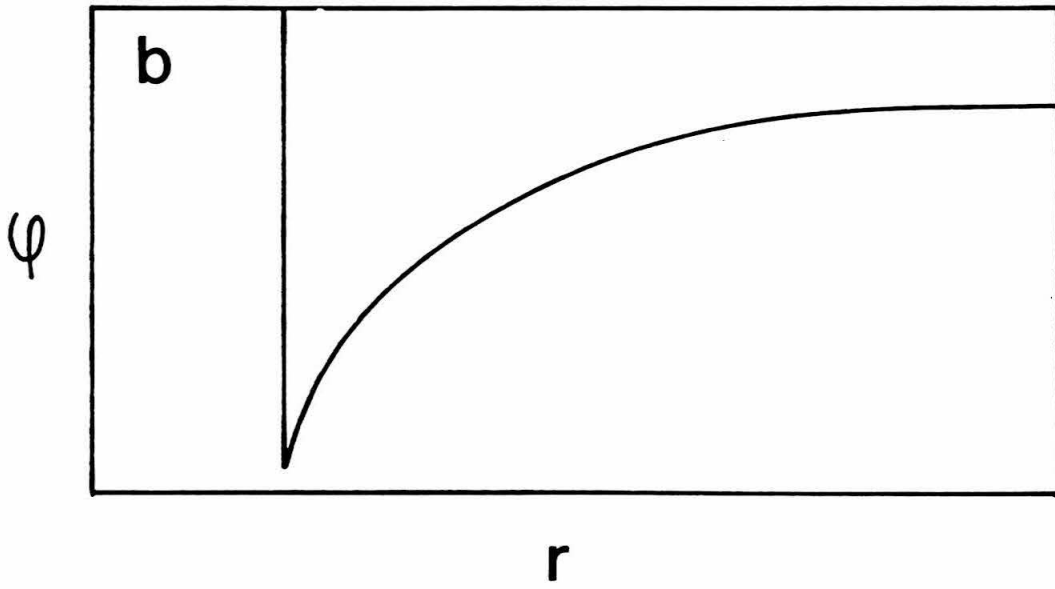
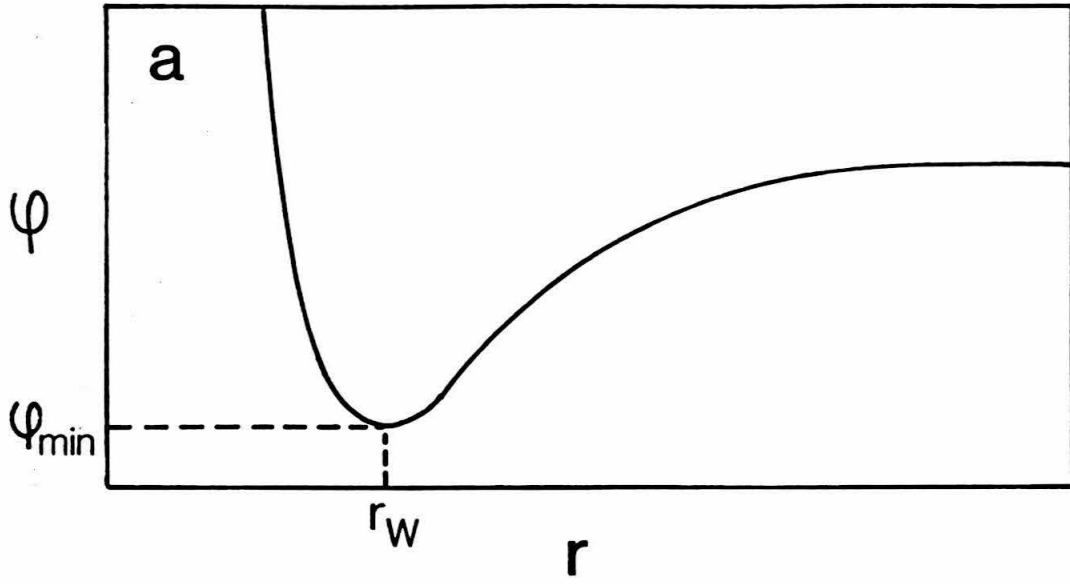
Polymers present a case that is, in many ways, intermediate between the low molecular liquids and solids. The NTP densities can be quite variable, depending on the polymer and the lengths of the polymer chains. Van Krevelen (1972) presents a tabulation of the group contributions applicable to glassy and rubbery polymers. Some of these are presented in table 2. If the limitations imposed on this technique for polymers are kept in mind, these contributions are quite satisfactory for most purposes.

#### *Thermal expansivity.*

The molar volume thermal expansivity,  $\epsilon$ , is also amenable to the determination of group contributions, since  $\epsilon$  is simply the temperature derivative of molar volume at constant pressure,  $(\partial v/\partial T)_p$ . In principle, we could take an approach completely analogous to that used for the molar volume. However, we can make use of a simple model for thermal expansion to develop a slightly different expression than a simple analog to equation (1). Let us begin by considering the phenomena involved. Thermal expansion is the result of asymmetry in the intermolecular potential (figure 2). A minimum in the potential energy,  $\phi_{\min}$ , exists when the centers of two molecules are separated by some distance, which is twice the effective radius of the molecule at the zero point. This effective radius is known as the van der Waals radius,  $r_w$ . Since the attractive term in the potential exhibits a weaker dependence on distance from the molecule than the repulsive term, the

Figure 2. (a) Schematic of a typical intermolecular potential.  
(b) Form assumed for the intermolecular potential in the discussion in the text of the phenomenon of thermal expansion. The potential consists of a hard sphere repulsion with an attractive term at larger  $r$ .





average intermolecular distance increases as the temperature, and hence the energy, is increased.

Let us now assume a simple basic potential for all organic compounds in which the molecules are thought of as hard spheres with London dispersion forces giving rise to the attractive term in the potential, resulting in an intermolecular potential of the form shown in figure 2b. Because of the phenomenon that gives rise to the London dispersion forces, namely polarization of "nonpolar" molecules by the instantaneous electron distribution, the strength of the attraction between two molecules at any particular distance increases roughly in proportion to the product of the volumes of the hard spheres, which in the present case is also roughly the van der Waals volumes. However, the attractive term varies with distance away from the center of a molecule according to

$$\varphi_a \propto r^{-6} \quad (2)$$

Hence, the potential well depth and the slope of  $\varphi_a$  in the vicinity of  $r_w$  are roughly constant. The primary consequence of this result is that the volume dependence on temperature (i.e., the thermal expansivity) is roughly the same for all compounds.

We take advantage of this result to describe the group contributions to the volume thermal expansivity  $\epsilon$  as a series of perturbations on an average value,  $\epsilon_0$ :

$$\epsilon = \epsilon_0 + \sum_i n_i \delta \epsilon_i \quad (3)$$

where  $n_i$  has the same usage as in equation (1) and  $\delta\epsilon_i$  is the perturbation by the  $i$ 'th functional group. We chose to obtain  $\epsilon_0$  from the average value for all the nonpolar liquids for which temperature derivatives of  $\rho$  are given by Egloff (1939). This yields  $\epsilon_0 = .13545 \text{ m}^3/\text{Mmol}\cdot\text{K}$ . Total values of  $\delta\epsilon$  for compounds were then obtained by subtracting this quantity from the thermal expansivities. From that point, the analysis of individual group contributions to  $\delta\epsilon$  proceeded by the same approach used to obtain contributions to the molar volumes in the previous section. The results are presented in table 3, with figure 3 giving a comparison of experimental results with our results. As might be expected, the largest perturbations are supplied by oxygen-bearing groups, since inclusion of those groups results in polar molecules and the introduction of hydrogen bonding in the case of OH-bearing groups. Also, we emphasize again that our purpose in developing more complicated expressions for some functional groups was to more accurately model the experimental data. In most cases, the form has no *a priori* theoretical basis, but was simply chosen for its ability to accurately represent the available data.

This approach to the determination of  $\epsilon$  should be applicable to low molecular solids as well as for liquids, but the effects of the crystal structure, primarily through the number of nearest neighbors, may be important. Polymers are a more complicated case, since the effects of intramolecular forces cannot be ignored. Van Krevelen (1972) notes that, for many polymers,

$$\epsilon \approx 10^{-3}v_w \quad (4)$$

where  $v_w$  is the van der Waals volume, as defined earlier. We have used this approximation, along with contributions to  $v_w$  suggested by van Krevelen (1972); to obtain a series of group contributions for polymers. This approach assumes that, for polymers,  $\epsilon_0 = 0$ . The resulting contributions for  $\delta\epsilon$  are presented in table 3.

#### *Heat capacity.*

The molar heat capacity is perhaps the single most successful application of additive functional group contributions to the estimation of the properties of organic compounds, with the obvious exception of the molecular weight. We have applied an analysis of the same type used for the molar volume to obtain the molar heat capacity at constant pressure for liquids:

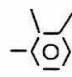
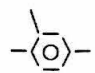
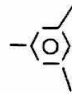
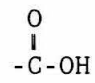
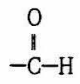
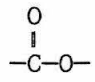
$$C_P = \sum_i n_i C_{Pi} \quad (5)$$

where  $C_{Pi}$  is the contribution of the  $i$ 'th group and  $n_i$  is the number of individuals of the  $i$ 'th group in a single molecule. This analysis was performed for heat capacities listed by Weast (1977). In table 4 we give the resulting values for contributions to the heat capacities of liquids,  $C_{Pi}$ . Figure 4 shows a comparison of calculated values with experimental values. It should be noted that the contributions for low molecular organic solids should be rather similar to those for the corresponding liquids. We suggest, therefore, that the values of

Table 3.

Group perturbations  $\delta\epsilon$  to the molar volume thermal expansivities of organic liquids,  $\epsilon_1$ , and organic polymers  $\epsilon_p$ . The thermal expansivities of the liquids are obtained by adding the perturbations to the average value of  $\epsilon_1$ , namely  $.13545 \text{ m}^3/\text{Mol}\cdot\text{K}$ . The expansivities of polymers are obtained simply by summing the values of  $\delta\epsilon_p$ .

Group	$\delta\epsilon_1^{(1)}$ ( $\text{m}^3/\text{Mmol}\cdot\text{K}$ )	$\delta\epsilon_p$ ( $\text{m}^3/\text{Mmol}\cdot\text{K}$ )
-CH <sub>3</sub>	.01933	.01367
-CH <sub>2</sub> -	.00538 <sup>(2)</sup> .01040 <sup>(3)</sup>	.01023
$\begin{array}{c}   \\ -\text{CH}- \end{array}$	-.02061- .00307 $n_{\text{met}}^{(2,4)}$ -.04222+ .00166 $n_{\text{met}}^{(3,4)}$	.00678
$\begin{array}{c}   \\ -\text{C}- \\   \end{array}$	-.04114 <sup>(2)</sup> -.04722 <sup>(3)</sup>	.00333
=CH <sub>2</sub>	.02093	.01194
-CH=	-.00352	.00847
$\begin{array}{c} / \\ =\text{C} \\ \backslash \end{array}$	-.03739	.00501
=C=	.00697	.00696
≡CH	-.02991	.01155
-C≡	.02507	.00805
$-\langle \overline{\text{O}} \rangle$	-.03966	.04584
$-\langle \overline{\text{O}} \rangle$	-.05115	.04332
$-\langle \overline{\text{O}} \rangle$	-.04919	.04332
$-\langle \overline{\text{O}} \rangle -$	-.04796	.04332

	- .07279	.04080
	- .06711	.04080
	- .06126	.04080
-H	.01292	.00252 <sup>(2)</sup> .00344 <sup>(3)</sup>
-OH	(See note 5)	.00804
-O-	- .03133 + .00319n <sub>et</sub> <sup>(4)</sup>	.00370
=O	- .04655 + .00517n <sub>C</sub> <sup>(4)</sup>	.00669
	- .12959 + .01708n <sub>C</sub> <sup>(4)</sup>	.01974
		.01514
	- .05208	

(1) Correction for nonaromatic ring:  $-.03798 + .02270n_{sc}$ , where  $n_{sc}$  is the number of side chains attached to the ring.

(2) Attached to aliphatic groups.

(3) Attached to aromatic groups.

(4)  $n_{met}$  is the number of methyl groups attached to the group in question;  $n_C$  is the total number of carbon atoms in the molecule;  $n_{et}$  is the total number of  $-CH_2-$  groups in the compound.

(5) If attached to a terminal carbon (see table 2, note (10)),  $\delta_{\epsilon_1} = -.14446 + .00107n_C + n_{OH}(.03328 + .00507n_C)$ ; if not attached to a terminal carbon,  $\delta_{\epsilon_1} = -.11758 + .02165n_C + n_{OH}(.01531 - .01009n_C)$ .

Figure 3. Comparison of experimental results for thermal expansivities of organic liquids with the predictions from our results. Circles represent hydrocarbons, while squares represent oxygen-bearing compounds.

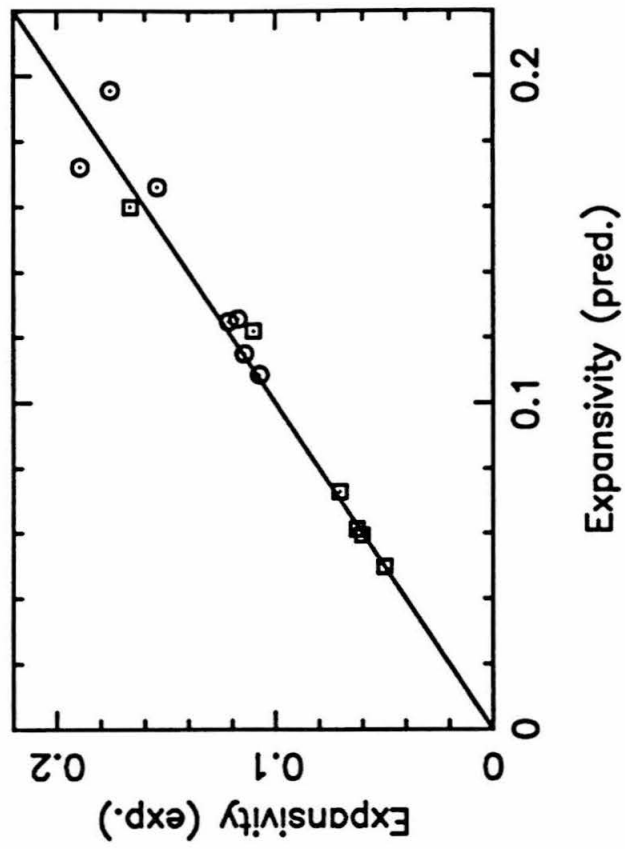
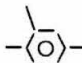
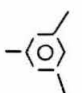
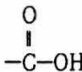
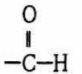
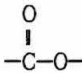




Table 4.

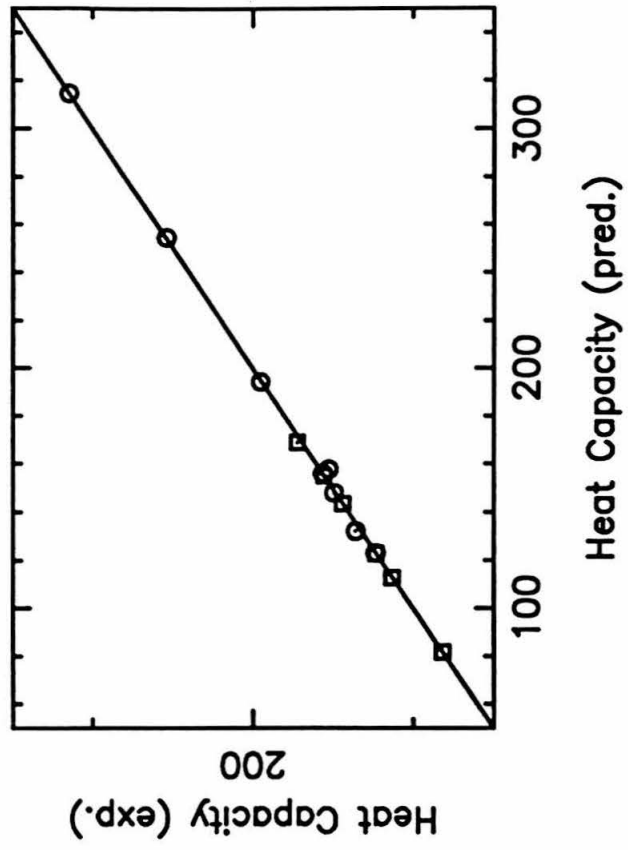
Group contributions to the molar heat capacities  $C_P$  of organic liquids, based on the present study, and organic polymers (from van Krevelen, 1977). The subscripts l and p refer to liquid and polymer, respectively. All quantities are given in values of J/mol·K.

Group	$C_{Pl}^{(1)}$	$C_{Pp}$
-CH <sub>3</sub>	37.03	36.82
-CH <sub>2</sub> -	30.08	30.38
$\begin{array}{c}   \\ -CH- \end{array}$	21.25	20.92
$\begin{array}{c}   \\ -C- \\   \end{array}$	$70.46 - 8.41n_C^{(2)}$	7.36
=CH <sub>2</sub>	$38.45 - 1.05n_C^{(2)}$	21.76
-CH=	25.23	21.34
$\begin{array}{c} / \\ =C \\ \backslash \end{array}$	20.59	15.90
=C=	24.48	
≡CH	36.94	
-C≡	24.48	
$-\langle \overline{\text{O}} \rangle$	119.08	123.01
$-\langle \overline{\text{O}} \rangle$	115.10	112.97
$-\langle \overline{\text{O}} \rangle$	109.08	112.97
$-\langle \overline{\text{O}} \rangle -$	108.37	112.97
$-\langle \overline{\text{O}} \rangle$	105.65	

	104.81	102.93
	98.53	
-H	13.10	
-OH	43.81+.88n <sub>C</sub> <sup>(2,3)</sup> 15.61+14.77n <sub>C</sub> <sup>(2,4)</sup> 62.68+.88n <sub>C</sub> <sup>(2,5)</sup>	44.77
-O-	34.85	35.56
=O	31.71	
	85.81	98.74
	50.96	
	65.73	64.85

- 
- (1) Nonaromatic rings require the addition of a term,  $\delta C_{P1} = -22.68$ .  
(2)  $n_C$  is the number of carbon atoms in the molecule.  
(3) If attached to a terminal carbon (see table 2, note (10)).  
(4) Not attached to a terminal carbon.  
(5) If attached to an aromatic ring.

Figure 4. Comparison of experimental heat capacities with predictions based on our results.



contributions to  $C_{P1}$  given in table 4 are also applicable to low molecular organic solids.

Van Krevelen (1972) presents a tabulation for contributions to  $C_P$  for polymers. We find these to be quite satisfactory and present some of his values for polymers in table 4.

*Bulk modulus and the Rao function.*

Next we come to the isentropic bulk modulus. Rao (1940, 1941) noted on the basis of empirical evidence that one could define an additive quantity,  $U$ , now known as the Rao function, which can be defined by the relation

$$K_S = \rho^7 (U/\mu)^6 \quad (6)$$

where  $K_S$  is the isentropic bulk modulus and  $\mu$  is the molecular weight and

$$U = \sum_i n_i U_i \quad (7)$$

where  $n_i$  is the same as in equations (1), (3), and (5) and  $U_i$  is the contribution of the  $i$ 'th group. One very useful property of  $U$  is that it is relatively insensitive to variations in density, temperature, and pressure. Another fortunate property of  $U$  is that the same values for contributions by functional groups should generally apply both to low molecular liquids and solids and to polymers. Although Van Krevelen

(1972) gives a series of group contributions to  $U$ , we found that bulk sound speeds calculated with these values displayed systematic variations from experimentally determined sound speeds. We have reevaluated the group contributions to  $U$ , making use of the experimental values of bulk sound speeds for low molecular liquids and some polymers tabulated by Forsythe (1954), Fay (1957), Sette (1961), Weast (1977), and Marsh (1980). The contributions for  $U$  were determined in a manner exactly analogous to that used for the molar volume and heat capacity. Some functional groups were not represented in the compounds for which we found data in the literature. In those cases, we used the values of van Krevelen (1972) or, lacking values there, made use of systematic trends established by the molar volume and heat capacities that also appeared to apply to  $U$  as well. The resulting values are presented in table 5.

Now we consider the pressure derivatives  $K' = (\partial K_S / \partial P)_S$  and  $K'' = (\partial^2 K_S / \partial P^2)_S$ . We postulate here that  $U$  can be written as a function solely of the density  $\rho$ . If this is the case, then we can obtain an expression for  $K'$  in the following manner. If  $U = U(\rho)$  then we can differentiate the expression in equation (6) with respect to the density:

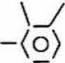
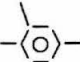
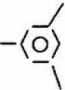
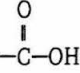
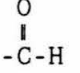
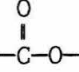
$$(\partial K_S / \partial \rho)_S = 7\rho^6(U/\mu)^6 + 6\rho^7(U^5/\mu^6)(dU/d\rho) \quad (8)$$

Then, noting that  $(\partial \rho / \partial P)_S = \rho / K_S$ , we can obtain  $K'$  by multiplying this by the expressions in equation (8), producing

Table 5.

Group contributions to the Rao function  $U$  and to  $\delta c'$ . The total value of  $c'$  is obtained by adding the appropriate values of  $\delta c'$  to the quantity  $c'_0 = -4.315 \text{ m/s}\cdot\text{K}$ . The units of  $U$  as presented in the table are  $\text{m}^{10/3}/\text{s}^{1/3}\cdot\text{Mmol}$  and the units of  $\delta c'$  are  $\text{m/s}\cdot\text{K}$ .

Group	$U^{(1)}$	$\delta c'$
$-\text{CH}_3$	291.8	.170
$-\text{CH}_2-$	191.1	-.045
$\begin{array}{c}   \\ -\text{CH}- \end{array}$	$125.4 - 33.8n_{\text{OH}}^{(2)}$ $170.2 - 33.8n_{\text{OH}}^{(3)}$	-.225
$\begin{array}{c}   \\ -\text{C}- \\   \end{array}$	8.6	-.405
$=\text{CH}_2$	265.9	-.045
$-\text{CH}=\text{}$	157.4	-.225
$\begin{array}{c} / \\ =\text{C} \\ \backslash \end{array}$	$54.9^{(2)}$ $36.5^{(3)}$	-.405
$=\text{C}=\text{}$	215.4	
$\equiv\text{CH}$	221.6	-.225
$-\text{C}\equiv$	117.1	-.405
$-\langle\bar{\text{O}}\rangle$	871.5	-.155
$\begin{array}{c}   \\ -\langle\bar{\text{O}}\rangle \end{array}$	788.2	
$\begin{array}{c} / \\ -\langle\bar{\text{O}}\rangle \end{array}$	772.7	
$-\langle\bar{\text{O}}\rangle-$	774.0	

	704.9	
	689.4	
	673.9	
-H	104.1 <sup>(3)</sup>	-.180
-OH	$125.5 - 1.17n_C + 7.44n_{OH}^{(4)}$	.870
-O-	70.3	-.805
=O	135.9	-.120
	308.3	.525
	302.9 <sup>(2)</sup> 284.5 <sup>(3)</sup>	-.525
	262.8	-1.15

(1) Nonaromatic rings require the addition of the correction  $\delta U = 24.8$  to the summed contributions of the subsidiary groups to the total value for the ring.

(2) When not attached to aromatic rings.

(3) When attached to aromatic rings.

(4)  $n_C$  is the total number of carbon atoms in the molecule;  $n_{OH}$  is the total number of -OH groups in the molecule.



$$K_S' = \frac{7\rho^7}{K_S} \left(\frac{U}{\mu}\right)^6 + \frac{6\rho^8 U^5}{K_S \mu^6} \frac{dU}{d\rho} \quad (9)$$

$$K_S' = 7 + 6 \frac{\rho}{U} \frac{dU}{d\rho} \quad (10)$$

In the same way, we get  $K''$  from

$$\left(\frac{\partial K_S'}{\partial \rho}\right)_S = 6 \left( \frac{1}{U} \frac{dU}{d\rho} - \frac{\rho}{U^2} \left(\frac{dU}{d\rho}\right)^2 + \frac{\rho}{U} \frac{d^2U}{d\rho^2} \right) \quad (11)$$

and again multiplying by  $\rho/K_S$ :

$$K_S'' = \frac{6}{K_{S0}} \left( \frac{\rho}{U} \frac{dU}{d\rho} - \frac{\rho^2}{U^2} \left(\frac{dU}{d\rho}\right)^2 + \frac{\rho^2}{U} \frac{d^2U}{d\rho^2} \right) \quad (12)$$

or

$$K_S'' = \frac{(K_S' - 7)(1 - K_S'/6)}{K_{S0}} + \frac{\rho^2}{K_{S0}U} \frac{d^2U}{d\rho^2} \quad (13)$$

We have already noted that  $U$  is relatively constant Rao (1941).

We will assume that  $d^2U/d\rho^2 = 0$ . If we were to further assume that  $dU/d\rho = 0$ , then we would find, upon substitution into equations (10) and (13),

that  $K' = 7$  and  $K'' = 0$ . Unfortunately, this approximation is insufficient for many purposes and is generally incorrect. We can, however, estimate  $dU/d\rho$  for a material if we have information about the variability of the bulk sound velocity  $c$ . Since

$$K_S = \rho c^2 \quad (14)$$

we have

$$(\partial K_S / \partial T)_P = \rho c (2(\partial c / \partial T)_P - c\alpha) \quad (15)$$

and

$$\left(\frac{\partial U}{\partial T}\right)_P = \frac{U}{6} \left[ \frac{1}{K_{S0}} \left[ \frac{\partial K_{S0}}{\partial T} \right]_P + 7\alpha \right] \quad (16)$$

and, using  $(\partial \rho / \partial T)_P = -\rho\alpha$ ,

$$dU/d\rho = (\partial U / \partial T)_P (\partial T / \partial \rho)_P \quad (17)$$

or

$$\frac{dU}{d\rho} = \frac{U}{6\rho} \left[ \frac{1}{K_{S0}\alpha} \left[ \frac{\partial K_S}{\partial T} \right]_P + 7 \right] \quad (18)$$

These equations may be rearranged to give

$$K_S' = 13 + \frac{2}{c\alpha} \left[ \frac{\partial c}{\partial T} \right]_P \quad (19)$$

During this analysis, we found from analysis of values for homologous series that the quantity  $c' = (\partial c / \partial T)_p$  is additive, with the group contributions being constants (within the resolution of the relatively sparse data) for most cases.

We determined group contributions to  $c'$  using values of  $c'$  (table 5) quoted by Weast (1977) and values calculated from data presented by Sette (1961) and Weast (1977). As in the case of the thermal expansivity, we found it easier to develop contributions to perturbations on a reference value  $c_0'$ :

$$c' = c_0' + \sum_i n_i \delta c'_i \quad (20)$$

where  $\delta c_i$  is the perturbation by the  $i$ 'th functional group. This allows the minimization of errors arising from inaccuracies in the determined contributions from groups that are poorly represented in the data. Instead of choosing an *a priori* value for  $c_0'$ , however, we determined its value during the process of solving for the group contributions. Because of the paucity of useful data, many group contributions could not be determined directly. In those cases, we have relied upon similarities of trends in group contributions among different properties, combined with those sound speed data that do exist, to estimate the values of these perturbations, which we call  $\delta c'$  (table 6). The value we obtain for  $c_0'$  is  $-4.315 \text{ m/s}\cdot\text{K}$ . It should be noted here that we have used only data for liquids. We suggest that values of  $c'$  calculated from the values in table 5 via equation (20) should be

generally applicable to low molecular solids and to polymers, but the validity of this suggestion has yet to be established.

### Calculation of high pressure states.

There are a number of equations of state that may be used to obtain a particular  $P$ - $V$ - $T$  state from the equation of state parameters that we can now obtain. We suggest the 4th order Eulerian finite strain formalism for compression along the isentrope defined by  $\rho$ ,  $K_{S0}$ ,  $K'$ , and  $K''$ :

$$P_S = \frac{3}{2}K_{S0}(x^7 - x^5)[1 + \xi_1 - \xi_1 x^2 + \xi_2(x^2 - 1)^2] \quad (21)$$

$$E_S = \frac{9}{2}V_0K_{S0} \left[ (\xi_1 + 1) \left( \frac{x^4}{4} - \frac{x^2}{2} + \frac{1}{4} \right) - \xi_1 \left( \frac{x^6}{6} - \frac{x^4}{4} + \frac{1}{12} \right) + \xi_2 \left( \frac{x^8}{8} - \frac{x^6}{2} + \frac{3x^4}{4} - \frac{x^2}{2} + \frac{1}{8} \right) \right] \quad (22)$$

where

$$x = (\rho/\rho_0)^{1/3} \quad (23)$$

and

$$\xi_1 = 3(4 - K_S')/4 \quad (24)$$

$$\xi_2 = \frac{3}{8}K_{S0}K_S'' + \frac{3}{8}K_S'(K_S' - 7) + \frac{143}{24} \quad (25)$$

Table 6.

Sound speeds and temperature derivatives for liquids. Also presented are predicted values of  $c$  and  $c'$ .

Compound	Experimental		Predicted		Reference (Exp.)
	$c$ (m/s)	$c'$ (m/s·K)	$c$ (m/s)	$c'$ (m/s·K)	
Benzene	1326	-4.75	1333	-4.65	1
	1295	-4.65			2
	1310				3
	1310				4
Toluene	1228	-4.30	1316	-4.30	1
	1320				5
	1310				3
o-Xylene	1360		1463		1
m-Xylene	1340		1314		1
p-Xylene	1330		1315		1
Cyclohexane	1284		1283		1
	1260				3
Cyclohexene	1305		1304		1
	1280				3
Methyl-cyclohexane	1247		1323		1
Pentane	1052		1019		1
Hexane	1113		1090		5
	1090				3
Heptane	1133	-4.16	1147	-4.20	2
	1165				4

Octane	1238		1195		4
Methyl acetate	1211		1171		5
Ethyl acetate	1187		1209		5
Propyl acetate	1182		1236		5
Butyl acetate	1179		1256		5
Amyl acetate	1347		1272		5
Methanol	1105	-3.27	1145	-3.275	1
	1103	-3.2			2
	1130				5
Acetone	1174	-4.5	1199	-4.095	2
	1203				5
Diethyl ketone	1314		1274		5
Methyl hexyl ketone	1324		1327		5
Ethanol	1207	-4.0	1166	-3.29	2
	1207				
Propanol	1234		1233		4
Butanol	1315		1277		4
Pentanol	1347		1308		4
Cyclohexanol	1622		1451		4
Diethyl ether	985	-4.87	981	-4.87	2
Ethylene glycol	1658	-2.1	1698	-2.665	2
	1600				3
Glycerol	1904	-2.2	1298	-2.02	2
	1900				3
1,3-Cyclohexa- diene	1280		1329		3

1,4-Cyclohexa- 1340  
diene

1329

3

- 
1. Sette (1961)
  2. Weast (1977)
  3. Marsh (1980)
  4. Fay (1957)
  5. Rao (1941)

States away from this isentrope may be calculated by performing a constant volume compression via the Mie-Grüneisen equation:

$$\int_{T_1}^{T_2} c_v dT = \int_{P_1}^{P_2} \frac{V}{\gamma} dP \quad (26)$$

where  $\gamma$  is the thermodynamic Grüneisen parameter:

$$\gamma = \alpha K_S / \rho c_P = \epsilon K_S / c_P \quad (27)$$

Now,  $c_P$  with the lower case letter represents the specific heat at constant pressure, rather than the molar heat capacity. We have made the common assumption here that  $v\theta\epsilon\gamma$  obeys

$$\gamma = \gamma_0 (\rho/\rho_0)^n \quad (28)$$

where the subscript 0 indicates the reference state (usually 1 bar and 298 K). Often,  $n = -1$  is assumed. It is a simple matter to solve numerically for the density if one begins with a  $P$ - $T$  condition, rather than a  $P$ - $\rho$  or  $\rho$ - $T$  condition. The temperature of the high pressure state is calculated by adding the difference in temperature obtained via equation (26) to the temperature along the isentrope, which is given by

$$T_S = T_0 \exp \left[ - \int_{V_0}^{V_1} \frac{\gamma}{V} dV \right] \quad (29)$$



### Calculation of shock Hugoniot curves.

A very important use for this technique is the prediction of shock Hugoniot curves for organic compounds, especially polymers. In general, this is accomplished by requiring the internal energy change from the initial state to the Hugoniot state to be equal to the energy change along the Rayleigh line connecting the initial state and the Hugoniot state:

$$\frac{1}{2}(P_H + P_0)(V_0 - V_H) = E_S + E_{tr} - \int_{P_S}^{P_H} \left(\frac{V}{\gamma}\right) dP \quad (30)$$

where the left-hand side is the internal energy increase due to the shock compression process, which follows a straight line (the Rayleigh line) in  $P$ - $V$  space, and the right hand-side is the sum of the energy for compression to the Hugoniot state volume along the reference isentrope ( $E_S$ ), the energy of transformation from the initial conditions to the reference conditions ( $E_{tr}$ , which includes any phase transformation energies), and the thermal energy required to raise the pressure to the Hugoniot pressure. The subscripts 0 and H refer to the initial and Hugoniot states, respectively, and  $V$  is the specific volume. The values for  $P_S$  and  $E_S$  are found from equations (21)-(25) for the Hugoniot state volume. If we make the usual assumption that  $\gamma$  is given by equation

(28), which implies that  $\gamma$  explicitly depends only on  $\rho$ , then, if  $P_0$  is negligible (the usual case), we can rearrange equation (30) to give

$$P_H = (E_S - P_S V_H / \gamma + E_{tr}) [\frac{1}{2}(V_0 - V_H) - (V/\gamma)_H]^{-1} \quad (31)$$

allowing the direct calculation of the Hugoniot pressure if the Hugoniot volume is known. It should be noted that the assumption that  $\gamma$  depends only on  $\rho$  may not be valid. In fact there are reasons to believe this is the case. However, using equation (28) generally provides quite satisfactory agreement with shock compression data for most materials and, in the case of liquid Fe (Anderson and Ahrens, 1990), also provides a satisfactory description of the temperatures along the shock Hugoniot curve.

In the present study, we will limit ourselves to the case where a negligible amount of chemical reaction occurs. In such cases, a different approach, such as that of Ree (1974), may be warranted. Since the problem may be compounded by the presence of free radicals, which we have not treated here, we cannot presently address the calculation of shock states with significant chemical reaction. This being the case, we will assume that the energy of transition  $E_{tr}$  is negligible.

#### **Comparison with experimental data.**

As a test and demonstration of this model, we have calculated the shock Hugoniot curves of several organic liquids and polymers for comparison with the experimental shock compression data presented by Marsh (1980). The values of the properties used in the calculation of

the Hugoniot curves are presented in table 7, along with the values determined from measured quantities.

Let us begin by comparing the predicted quantities in table 7 with the corresponding measured quantities. Generally, our technique provides a good description of the low molecular liquids. In the case of polymers, however, we find that the predicted values of  $K_{S0}$  and  $\gamma$  are generally low. Although not listed in table 7, the predicted values of the thermal expansion coefficient,  $\alpha$ , are somewhat low. These results suggest that the quantities presented by van Krevelen (1972) for polymers may need revision. We also note that the errors in  $K_{S0}$  imply that, contrary to the assumption made earlier, there are slight differences in  $U$  between polymers and low molecular compounds. Because of the extreme dependence of  $K_{S0}$  on  $U$ , small errors in  $U$  can lead to large errors in  $K_{S0}$ .

Next let us examine the shock compression results. Figures 5 and 6 present the calculated curves with the experimental data for the liquids from Marsh (1980). The plots are projected onto the  $P$ - $V$  and  $U_s$ - $u_p$  planes, where  $U_s$  and  $u_p$  are the shock wave velocity and the shocked material particle velocity, in the reference frame of the unshocked material. As can be seen, the parameters calculated in the manner discussed in the previous sections produce very good agreement with the data. This is somewhat surprising, since the higher pressure data almost certainly represent shocked states in which significant chemical reaction is occurring. Such good agreement suggests that there may be a trade-off between the energies of reaction and the differences in properties or that the reactions are kinetically inhibited from occurring on the timescales characteristic of the shock process. One

Table 7.

Predicted and measured properties of compounds for which the Hugoniot curves in figures 2-6 are calculated. The predicted properties were obtained by the methods described in the text. The Hugoniot calculations were performed using the predicted properties. The measured densities are taken from Egloff (1939) for the low molecular compounds and from Marsh (1980) for the polymers. The measured bulk moduli are obtained from the densities and sound speeds given by Marsh (1980). The measured values of  $\gamma_0$  for the low molecular compounds come from the combination of the measured bulk moduli listed in this table with the heat capacities given by Weast (1977) and thermal expansivities given by Egloff (1939). For the polymers, we used the measured heat capacities and thermal expansivities presented by van Krevelen (1972). For each compound, the predicted property is on the first line and the measured property is on the second.

Material	$\rho_0$ (kg/m <sup>3</sup> )	$K_{S0}$ (GPa)	$K'$	$K''$ (GPa <sup>-1</sup> )	$\gamma_0$
n-Hexane	657.90	.781	7.893	-.3607	.786
C <sub>6</sub> H <sub>12</sub>	659.42	.781			.698
1,3-Cyclohexadiene	849.94	1.387	6.167	+.0167	1.048
C <sub>6</sub> H <sub>8</sub>	840	1.376			
Benzene	881.10	1.565	7.309	-.0431	1.287
C <sub>6</sub> H <sub>6</sub>	878.66	1.502			1.204
Ethylene Glycol (1,2-Ethandiol)	1124.9	3.244	8.087	-.1166	.756
C <sub>2</sub> H <sub>6</sub> O <sub>2</sub>	1108.8	2.847			
Glycerol (1,2,3-Propanetriol)	1197.8	3.222	7.816	-.0767	.545
C <sub>3</sub> H <sub>8</sub> O <sub>3</sub>	1261.3	4.513			
Polypropylene (Polypropene)	857.0	3.098	5.567	-.0334	1.079
(-CH(CH <sub>3</sub> )CH <sub>2</sub> -) <sub>n</sub>	850	4.105			1.06-1.81
Poly-4-methyl- 1-pentene	857.0	3.098	5.399	-.0518	1.079
(-CH(CH <sub>2</sub> CH <sub>2</sub> (CH <sub>3</sub> ) <sub>2</sub> )CH <sub>2</sub> -) <sub>n</sub>	838	2.686			.615
Polystyrene (-CH(C <sub>6</sub> H <sub>5</sub> )CH <sub>2</sub> -) <sub>n</sub>	1062.8	4.212	5.457	-.0332	1.519
	1050				
Polyethylene (Polyethene)	885.0	2.719	5.292	-.0741	.916
(-CH <sub>2</sub> -) <sub>n</sub>	850	3.279			1.09-1.39

Figure 5. Pressure-volume projections of the shock Hugoniot curves of four organic liquids. The lines are calculated on the basis of properties (table 7) determined from tables 1 through 4 and 6 as discussed in the text. The data presented are from the tabulations by Marsh (1980).

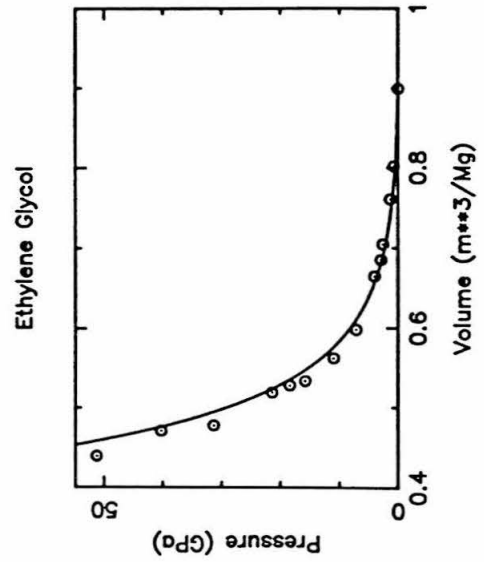
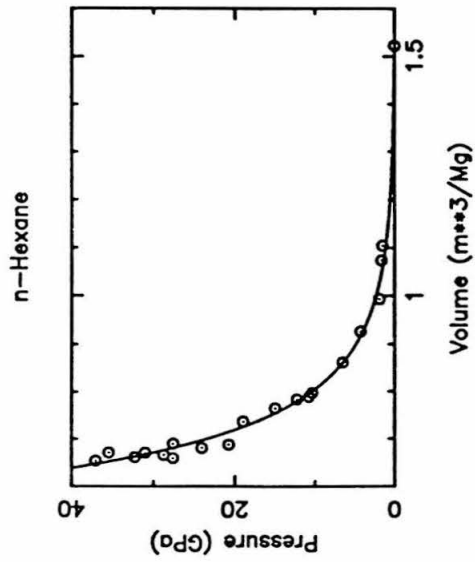
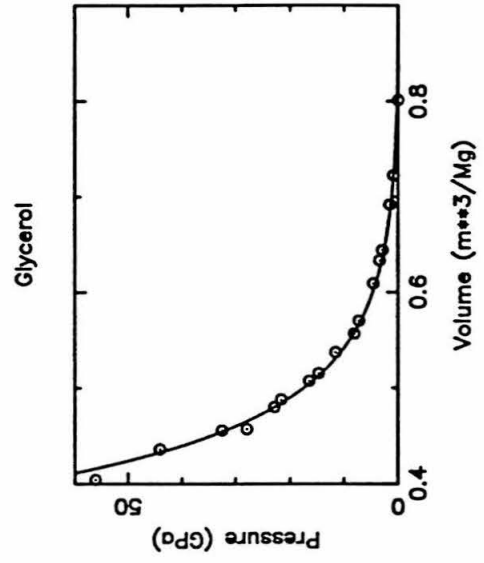
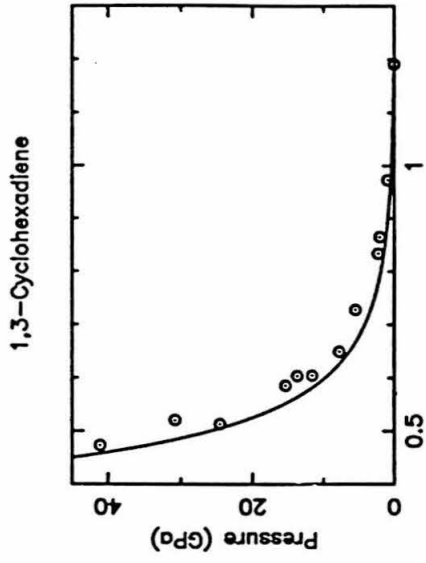
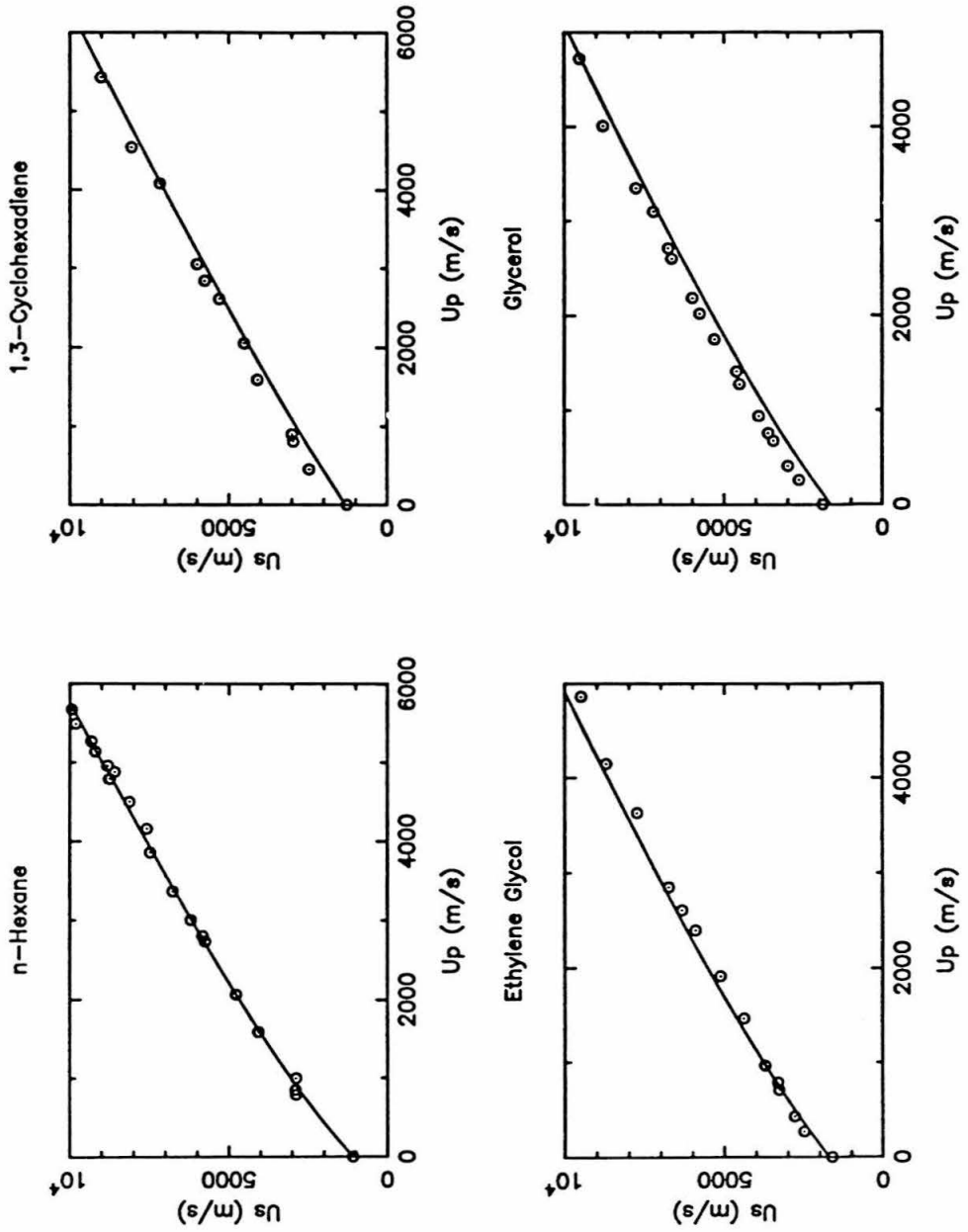


Figure 6. The predicted Hugoniot curves and experimental data shown in figure 5, but now projected on the particle velocity - shock velocity plane.





exception to this can be seen in benzene (figure 7), where there is a pronounced change in the slopes of both projections at 12-13 GPa, where the benzene ring breaks down.

As can be seen in figures 8 and 9, the method works somewhat less well for polymers, generally underestimating the pressures and shock velocities. This is to be expected, given the errors evident in table 7 for the predicted properties. Some insight can be gained, however, by examination of the way in which the errors are manifested in the data. Examination of figure 5 shows that the slopes of the predicted curves are similar to the slopes of the data, but that the predicted intercepts are generally lower than shown by the data. This indicates that, although the values of  $K_{S0}$ , which primarily affect the intercepts, are in error, the values of  $K'$  and  $K''$ , which affect only the slopes, are reasonably correct. One interesting note is that the data for polystyrene exhibit a behavior very similar to the data for benzene at the onset of breaking the aromatic ring. We suggest this implies that future efforts may lead to a method of transforming the results for low molecular liquids to predict the behavior of corresponding polymers.

## CONCLUSION

We have shown here that the properties of organic liquids can be accurately estimated from a set of empirical rules. This technique should also be applicable to polymers, although the existing tabulations of functional group contributions to equation of state properties for polymers may need revision. A new result from our work is the

Figure 7. Predicted Hugoniot curve for benzene, with the data from Marsh (1980). Note that the predicted curve follows the data up to about 12 GPa ( $u_p \approx 2500$  m/s). Above this point, breakdown of the benzene ring causes the data to diverge from the predicted curve.

## Benzene

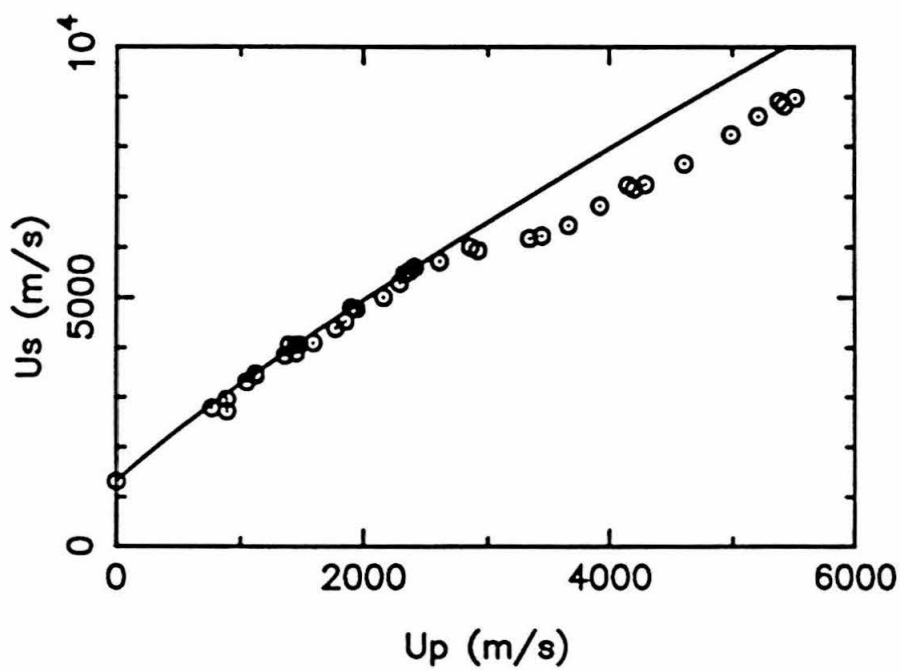
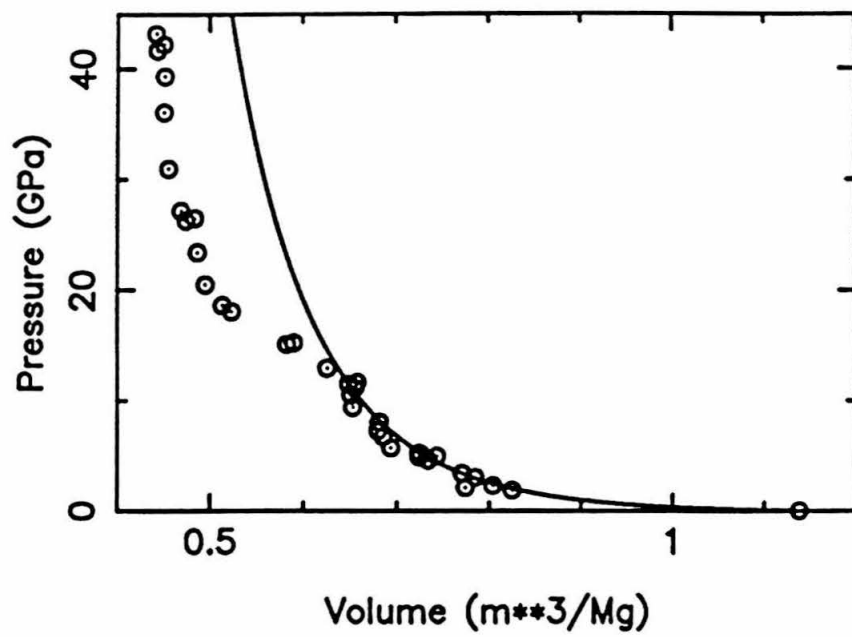


Figure 8. Pressure-volume projections of the predicted shock Hugoniot curves of four polymers, along with the data from Marsh (1980). Note that the predicted curves consistently shown greater compressions than the data. Also note the break in slope of the polystyrene Hugoniot, due to the breakdown of the styrene benzene ring, and similar to that break observed in the benzene Hugoniot curve (figure 7).

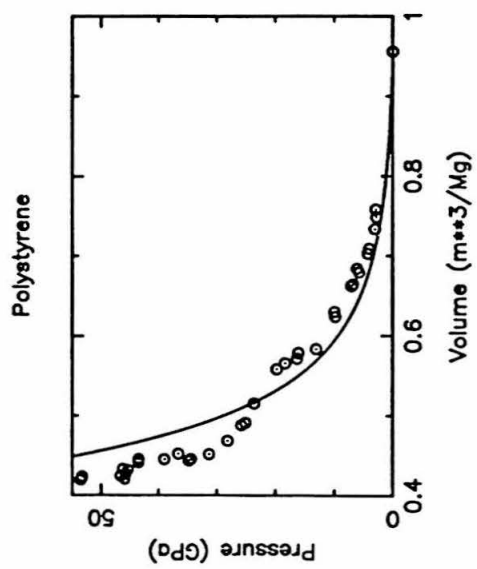
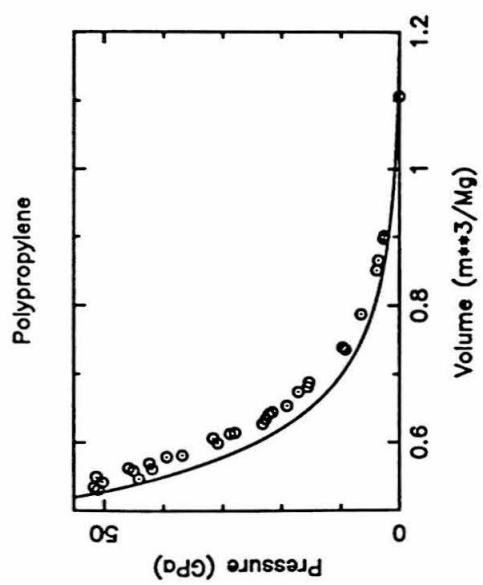
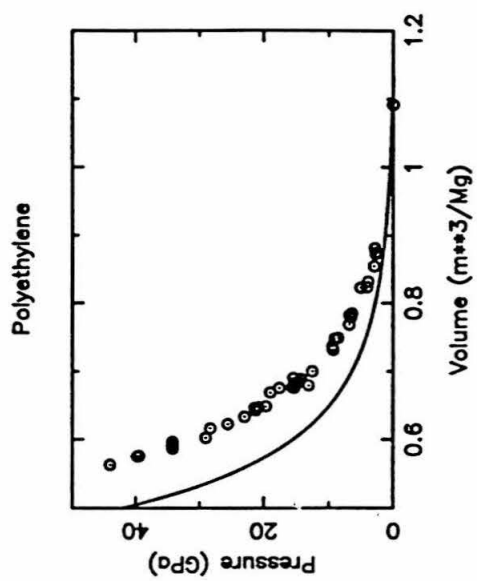
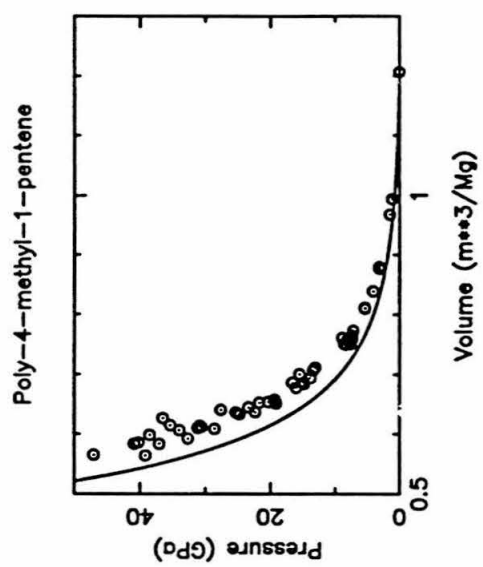
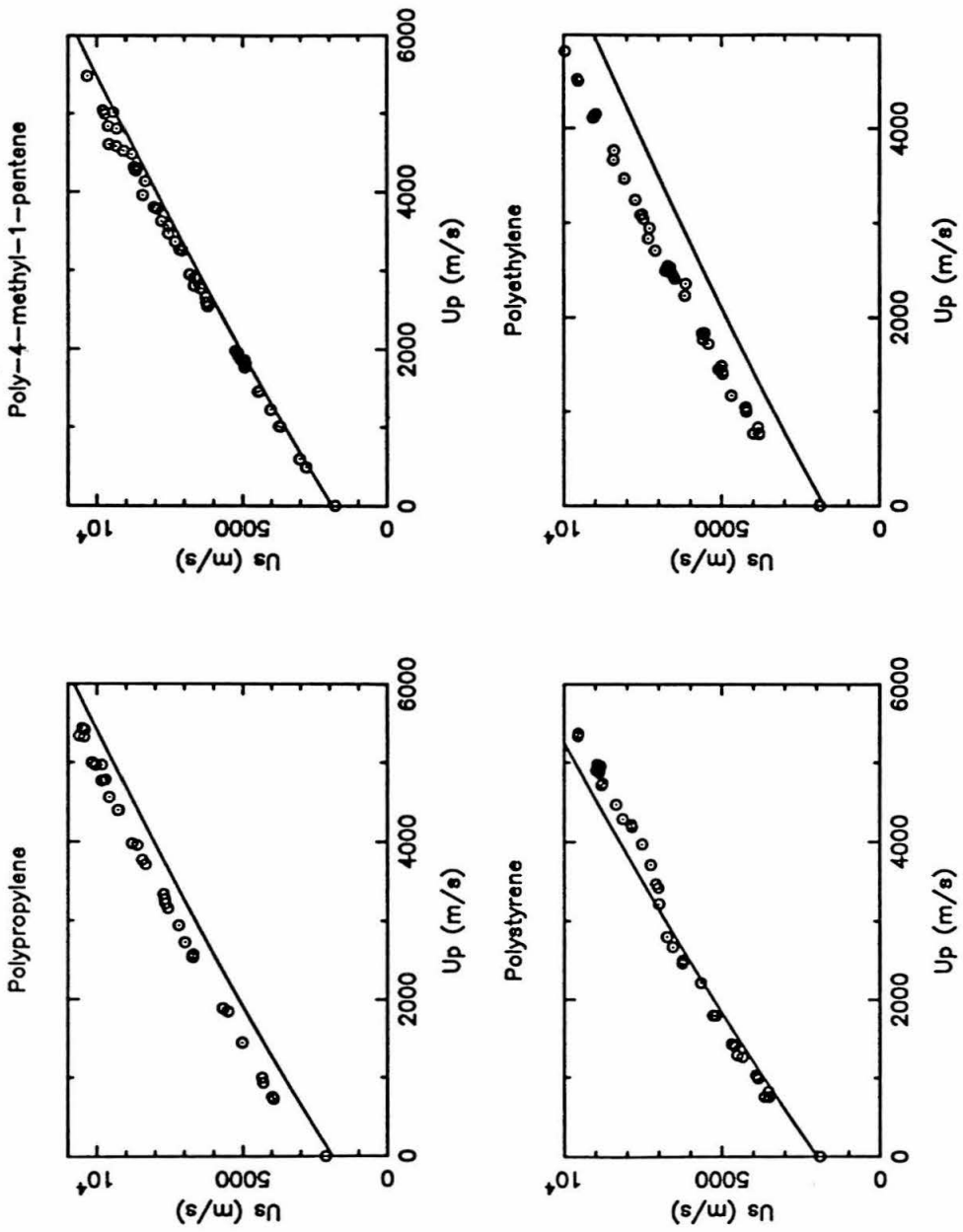


Figure 9.  $U_s$ - $u_p$  projection of the curves and data presented in figure 8.



determination that the sound speeds of organic liquids depend only on the density and that the temperature derivatives, through the thermal expansion coefficients, may be used to predict the first and second pressure derivatives of the bulk modulus. Application to crystalline low molecular compounds may be complicated by the effects of crystal structure, but this remains to be demonstrated. We find that shock wave data to high pressures for many low molecular organic liquids can be accurately predicted, suggesting that determination of a similarly accurate set of group contributions for polymers will allow the tailoring of "designer" materials for specific applications involving high pressures. We also note that similarities between the shock compression behaviors of liquids and polymers may lead to the development of a method for transforming the compression curves of low molecular liquids to corresponding polymers.



**REFERENCES.**

- Anderson, W. W., and T. J. Ahrens (1990). A liquid iron equation of state for geophysical applications. To be submitted to *Geophys. J. Int.*
- Dean, J. A. (ed.) (1985). *Lange's Handbook of Chemistry*, 13th ed. San Francisco, McGraw-Hill.
- Egloff, G. (1939). *Physical Constants of Hydrocarbons*, vol. 1-4. New York, Reinhold.
- Forsythe, W. E. (1954). *Smithsonian Physical Tables*, 9th ed., Smithsonian Institution, Washington, D. C., 827 pp.
- Gray, D. E. (ed.) (1957). *American Institute of Physics Handbook*. New York, McGraw-Hill.
- Marsh, S. P. (1980). *LASL Shock Hugoniot Data*. Los Angeles, U. C. Press. 658 pp.
- Rao, M. R. (1940). A relation between velocity of sound in liquids and molecular volume. *Ind. J. Phys.* 14: 109-116.
- Rao, M. R. (1941). Velocity of sound in liquids and chemical constitution. *J. Chem. Phys.* 9: 682-685.

Ree, F. H. (1979). Systematics of high-pressure and high-temperature behavior of hydrocarbons. *J. Chem. Phys.* 70: 974-983.

Sette, D. (1961). Dispersion and absorption of sound waves in liquids and mixtures of liquids, in: *Handbuch der Physik; Akustik I, Vol. XI*, (S. Flügge, ed.), 275-360.

Van Krevelen, D. W. (1972). *Properties of Polymers; Correlations with Chemical Structure*. New York, Elsevier, 427 pp.

Weast, R. C. (ed.) (1977). *CRC Handbook of Chemistry and Physics*, 58th ed. Cleveland, CRC Press.